

**PREPARATION OF POLY (VINYLIDENE FLUORIDE-CO-
HEXAFLUOROPROPYLENE) COMPOSITE MEMBRANES FOR TREATMENT OF
WATER HARDNESS**

by

Khaleke Veronicah Ramollo

DISSERTATION

Submitted in fulfilment of the requirements for the degree of

MASTER OF SCIENCE

in

Chemistry

in the

FACULTY OF SCIENCE AND AGRICULTURE

(School of Physical and Mineral Sciences)

at the

UNIVERSITY OF LIMPOPO

SUPERVISOR: Prof T Magadzu

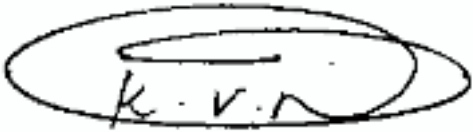
CO-SUPERVISORS: Dr A.A Ambushe (UJ)

Dr L.E Macevele

2022

DECLARATION

I declare that this dissertation is my own work and that all the sources that I have used or quoted have been indicated and acknowledged by means of complete references and that this work has not been submitted before for any other degree at any institution.



Surname, Initials

31/03/2022

Date

DEDICATION

I dedicated this work to my parents, Phineas and Melita Ramollo and my siblings, Eunice, Yulendah and Jan Ramollo.

ACKNOWLEDGEMENTS

Above all, I would like to thank God for everything that he has done for me, Hebrews 12 verse 22-28.

I would like to extend my gratitude and appreciation to my supervisors, Prof T Magadzu, Dr A.A Ambushe and Dr L.E Macevele for their remarkable support, guidance, and encouragement throughout my master's degree. Thank you for believing in me, I really appreciate your precious time that you have invested in my academics to make this project a success.

Thank you, Dr A.A Ambushe for funding my studies with the WRC bursary and for carrying out the TEM, SEM, TGA, and XRD analysis at the University of Johannesburg (chemistry department).

I would also like to thank Dr D.E Motaung for carrying out the SEM, TGA and XRD analysis at CSIR.

A special thanks goes to Dr T.C Leboho, NRF and Sasol Inzalo foundation for financial assistance.

To my mentor from Sasol Inzalo foundation, Mr M.J Coombes, I would like to thank you for the constructive critics and discussions we had.

To my lab-mates, Thole D and Thobakgale R.D, thank you guys for your wonderful patience, continual support, and warm humour. There was never a dull moment with you, I am lucky to have made such great friends.

Lastly, I would like to thank my family, my parents (Phineas and Melita Ramollo), my beautiful sisters (Eunice and Yulendah), my brother (Jan Ramollo), my nephews (Gerald and Junior Ramollo) and my favourite uncle in the whole world (Eric Ramollo "Spoiler") for their unconditional love, support, patience and for being the best family ever.

PUBLICATIONS AND PRESENTATIONS

PUBLICATIONS

1. **K.V Ramollo**, L.E Macevele, T Magadzu and A.A Ambushe. Calcium hardness removal aqueous solution by Poly (vinylidene fluoride-co-hexafluoropropylene) doped cellulose acetate composite membrane. To be submitted for publication to Journal of membranes.

CONFERENCE PRESENTATIONS

1. **K.V Ramollo**, L.E Macevele, T Magadzu and A.A Ambushe. Calcium hardness removal aqueous solution by Poly (vinylidene fluoride-co-hexafluoropropylene) doped cellulose acetate composite membrane. Presented at the 11th FSA Postgraduate Research Day, Polokwane, Bolivia Lodge, October,2021.
2. **K.V Ramollo**, L.E Macevele, T Magadzu and A.A Ambushe. Calcium hardness removal aqueous solution by Poly (vinylidene fluoride-co-hexafluoropropylene) doped cellulose acetate composite membrane. Presented at the 10th Annual Nanosciences Young Researchers' Symposium (NYRS-2020/2021)-National, University of the Witwatersrand, Johannesburg, October,2021.

ABSTRACT

Calcium and magnesium are two dominant species that contribute to water hardness. The aim of this study was to develop a poly (vinylidene fluoride-co-hexafluoropropylene) (PVDF-HFP) composite membrane for treatment of water hardness. The synthesis of PVDF-HFP composite membranes was confirmed by X-ray diffraction (XRD), scanning electron microscopy (SEM), thermogravimetric analysis (TGA) and Fourier transform infrared (FTIR) spectroscopy. The concentrations of the hardness causing agents in both the simulated and real hard water samples were investigated in batch studies wherein parameters such as pH, contact time, temperature, and adsorbent were optimised. The maximum adsorption efficiency of 56 and 45 mg/g (evaluated by Langmuir isotherm) for Ca(II) and Mg(II) ions were obtained. These were achieved at an optimum pH of 7 and adsorption dosage of 0.5 mg/L using the 3% PVDF-HFP/cellulose acetate (CA) and 1% nitrogen doped multiwalled carbon nanotubes (N-MWCNTs)/CA composite membranes respectively. The adsorption kinetics and isotherm models were all consistent with the pseudo-second order and Freundlich isotherm models for all the membranes suggesting that the sorption process met heterogeneous adsorption. Furthermore, the thermodynamic parameters indicated that the adsorption is physical and endothermic in nature. Reusability studies showed that all the PVDF-HFP based membranes can be recycled at least 3 times and for Ca(II) ions an adsorption loss of only 0.35 % was recorded while using a 3% PVDF-HFP/CA composite membrane. These results were further confirmed by XRD, TGA and inductively coupled plasma mass (ICP-MS) spectrometry. Thus, the findings from this study have shown that the PVDF-HFP based membranes could provide valuable material for hardness removal to acceptable level.

TABLE OF CONTENTS

DECLARATION.....	i
DEDICATION	iii
ACKNOWLEDGEMENTS	iv
PUBLICATIONS AND PRESENTATIONS.....	v
ABSTRACT	vi
LIST OF FIGURES.....	xii
LIST OF TABLES	xvi
LIST OF ABBREVIATIONS	xvii
CHAPTER 1	1
1.1 BACKGROUND	1
1.2 PROBLEM STATEMENT	2
1.3 MOTIVATION.....	2
1.4 AIMS AND OBJECTIVES	3
1.4.1 AMS.....	3
1.4.2 OBJECTIVES	3
1.5 DISSERTATION OUTLINE	4
REFERENCES.....	5
CHAPTER 2.....	8
LITERATURE REVIEW.....	8
.....	8
2.1 DESALINATION OF SEAWATER AND BRACKISH GROUNDWATER.....	8
2.2 WATER HARDNESS	9
2.2.1 Hard water	9
2.2.2 Sources of hardness.....	9
2.2.3 Types of hardness	10

2.2.4 Challenges associated with hard water usage.....	11
2.2.5 Other groundwater contaminants.....	12
2.3 Water quality standards	12
2.4 Water softening technologies.....	13
2.4.1 Ion-exchange method	14
2.4.2 Membrane filtration	14
2.4.3 Adsorption.....	15
2.4.3.1. Polymeric membranes	15
2.4.3.1.1. Polyvinylidene-co-hexafluoropropylene	15
2.4.3.1.2. Cellulose acetate	16
2.4.3.2. Carbon-based adsorbents	17
2.4.3.2.1 Nitrogen doped carbon nanotubes.....	17
2.5 Membrane fabrication methods.....	18
2.5.1 Phase inversion	18
2.6 Membrane additives and solvents.....	19
2.7 Comparison of Ca (II) and Mg (II) ions removal with other studies	20
REFERENCES	23
CHAPTER 3.....	31
RESEARCH METHODOLOGY	31
3.1 MATERIALS.....	31
3.2. PREPARATION OF PVDF-HFP COMPOSITE MEMBRANES	31
3.2.1. Preparation of PVDF-HFP membrane.....	31
3.2.2 Preparation of CA membrane	31
3.2.3 Preparation of 3% PVDF-HFP/CA composite membrane.....	32
3.2.4 Preparation of 1% N-MWCNTs/PVDF-HFP composite membranes.....	32
3.2.5 Preparation of 1% N-MWCNTs/CA composite membranes.....	33

3.3 CHARACTERISATION OF PVDF-HFP COMPOSITE MEMBRANES AND N-MWCNTs	33
3.3.1 X-ray diffraction.....	33
3.3.2 Scanning electron microscopy	33
3.3.3 Transmission Electron Microscope	34
3.3.4 Fourier-transform infrared spectroscopy	34
3.3.5 Thermogravimetric analysis	34
3.4 ADSORPTION STUDIES	35
3.4.1 Effect of pH.....	35
3.4.2 Effect of membrane dosage.....	35
3.4.3 Effect of contact time	35
3.4.4 Effect of concentration	36
3.4.5 Effect of temperature	36
3.4.6 Effect of counterions	36
3.4.7 Effect of binary system	37
3.4.7.1 Kinetics of adsorption	37
3.4.7.2 Adsorption isotherm models	38
3.4.7.3 Thermodynamics of adsorption.....	39
3.4.8 Reusability studies.....	40
3.5 REAL WATER APPLICATIONS.....	40
3.5.1 Water sampling.....	40
3.5.2 Analysis of borehole water samples	42
REFERENCES	42
CHAPTER 4	44
RESULTS AND DISCUSSION.....	44
4.1 CHARACTERISATION OF PVDF-HFP COMPOSITE MEMBRANES AND N-MWCNTs	44

4.1.1 Fourier transform infrared (FTIR) results of PVDF-HFP composite membranes and N-MWCNTs.....	44
4.1.2 XRD patterns of N-MWCNTs and polymeric membranes	46
4.1.3 Thermogravimetric analysis (TGA) results of PVDF-HFP blended membranes and N-MWCNTs.....	47
4.1.4 TEM images of pristine N-MWCNTs	49
4.1.5 SEM images of PVDF-HFP based membranes and N-MWCNTs	50
.....	50
4.2 ADSORPTION STUDIES	53
4.2.1 Batch adsorption studies of Ca (II) metal ions.....	53
4.2.1.1 Effect of acid treated and non-treated N-MWCNTs doped CA composite membranes on the hardness removal.....	53
4.2.1.2 Effect of pH on Ca (II) metal ions removal onto PVDF-HFP membrane....	54
4.2.1.3 Effect of membrane adsorbent dosage	55
4.2.1.4 Effect of contact time on adsorption of Ca (II) onto polymeric membranes	56
4.2.1.5 Kinetics of adsorption for Ca (II) metal ions removal by polymeric membranes	58
.....	58
4.2.1.6 Effect of concentration on the adsorption of Ca (II) by various polymeric membranes	60
4.2.1.7 Effect of temperature.....	61
4.2.1.8 Adsorption isotherm models	62
4.2.1.9 Thermodynamics of adsorption	66
4.2.1.10 Effect of counterions.....	68
4.2.1.11 Effect of binary system on the adsorption of Ca (II).....	69
4.2.1.12 Recycling of polymeric membranes.....	70
4.2.2 Batch adsorption studies of Magnesium (II) ions.....	75
4.2.2.1 Effect of pH on Mg (II) ions removal by PVDF-HFP membrane.....	75
.....	75

4.2.2.2	Effect of adsorbent dosage.....	76
4.2.2.3	Effects of contact time on adsorption efficiency of Mg (II) by composite membranes.....	77
4.2.2.4	Adsorption kinetics of Mg (II) metal ions removal by polymeric membranes.....	78
4.2.2.5	Effect of initial metal ion concentration on the adsorption of Mg (II) by PVDF-HFP based membranes.....	80
4.2.2.6	Effect of temperature.....	81
4.2.2.7	Adsorption isotherm models.....	82
4.2.2.8	Thermodynamics of adsorption.....	85
4.2.2.9	Effect of counterions.....	87
4.2.2.10	Effect of binary system.....	88
4.2.2.11	Recycling of the PVDF-HFP composite membranes.....	89
4.3	REAL WATER APPLICATIONS.....	90
4.3.1	Effect of membrane reusability on real hard water samples.....	92
	REFERENCES.....	95
	CHAPTER 5.....	100
	CONCLUSION AND RECOMMENDATIONS.....	101
5.1	CONCLUSION.....	101
5.2	RECOMMENDATIONS.....	103
5.3	APPENDICES.....	103

LIST OF FIGURES

Figure 3.1:Collection of borehole water samples at (a) Sekonye, (b) Mokomene, (c) Ga-Phasha, (d) My Darling (e) Bergendal and (f) Ga-Machaba in summer season.	41
Figure 4.1: FTIR spectra of (a) N-MWCNTs, (b) PVDF-HFP, (c) 1% N-MWCNTs/PVDF-HFP, (d) CA, (e) 3% PVDF-HFP/CA, (f) 1% N-MWCNTs/CA, (g) 1% N-MWCNTs/3 % PVDF-HFP/CA membranes	45
Figure 4.2: XRD patterns of (a) N-MWCNTs, (b) PVDF-HFP/CA, (c) CA, (d) 3% PVDF-HFP/CA, (e) 1% N-MWCNTs/CA, (f) 1% N-MWCNTs/PVDF-HFP/CA.....	46
Figure 4.3: TGA curves of (a) N-MWCNTs, (b) PVDF-HFP, (c) 1% N-MWCNTs/PVDF-HFP, (d) CA, (e) 3% PVDF-HFP/CA, (f) 1% N-MWCNTs/CA, and (g) 1% N-MWCNTs/3% PVDF-HFP/CA membranes.....	48
Figure 4.4: TEM images of pure N-MWCNTs(a-d) at different magnifications	50
Figure 4.5: SEM images of (a) N-MWCNTs, (b) PVDF-HFP, (c) CA, (d) 1% N-MWCNTs/PVDF-HFP (e) 3% PVDF-HFP/CA, (f) 1% N-MWCNTs/CA, and (g) 1% N-MWCNTs/3% PVDF-HFP/CA membranes.....	52
Figure 4.6: Effect of acid treated and non-treated N-MWCNTs/CA composite membranes on the removal of hardness constituents.....	53
Figure 4.7: Effect of pH on the adsorption of Ca (II) metal ions onto PVDF-HFP membrane	55
Figure 4.8: Effect of membrane adsorbent dosage on Ca (II) ions adsorption onto PVDF-HFP composite membranes	56
Figure 4.9: Effect of contact time on adsorption efficiency of Ca (II) ions onto (a) CA, (b) PVDF-HFP, (c) 3% PVDF-HFP/CA, (d) 1% N-MWCNTs/CA, (e)1% N-MWCNTs/PVDF-HFP and (f) 1% N-MWCNTs/3% PVDF-HFP/CA composite membranes	57
Figure 4.10: Pseudo-first order (A) and Pseudo-second order (B) kinetic model for adsorption of Ca (II) ions on (a) CA, (b) PVDF-HFP, (c) 3% PVDF-HFP/CA, (d) 1% N-MWCNTs/CA, (e) 1% N-MWCNTs/PVDF-HFP and (f) 1% N-MWCNTs/3% PVDF-HFP/CA composite membranes.....	60
Figure 4.11: Effect of initial metal ion concentration on the adsorption efficiency of Ca (II) ions onto (a) 3% PVDF-HFP/CA, (b) 1% N-MWCNTs/CA, (c) 1% N-	

MWCNTs/PVDF-HFP and (d) 1 % N-MWCNTs/3% PVDF-HFP/CA composite membranes	61
Figure 4.12: Effect of temperature on adsorption efficiency of Ca (II) ions on (a) 3 % PVDF-HFP/CA, (b) 1 % N-MWCNTs/CA, and (c) 1 % N-MWCNTs/3 % PVDF-HFP/CA based membrane.	62
Figure 4.13: (i) Langmuir isotherm and (ii) Freundlich isotherm for the adsorption of Ca (II) ions onto (a) 3% PVDF-HFP/CA, (b) 1% N-MWCNTs/CA, and (c) 1% N-MWCNTs/3 % PVDF-HFP/CA composite membranes.....	65
Figure 4.14: Thermodynamic parameters of Ca (II) ions onto, (a) 3 % PVDF-HFP/CA, (b) 1% N-MWCNTs/CA, and (c) 1% N-MWCNTs/3% PVDF-HFP/CA composite membranes.	67
Figure 4.15: Effect of counterions on the adsorption of Ca (II) by (a) 3 % PVDF-HFP/CA, (b) 1 % N-MWCNTs/CA, (c) 1 % N-MWCNTs/3 % PVDF-HFP/CA composite membranes.	69
Figure 4.16: Effect of the binary system on the adsorption of Ca (II) by PVDF-HFP blend membranes	70
Figure 4.17: Effect of recycling of (a) 3% PVDF-HFP/CA, (b) 1% N-MWCNTs/CA, and (c) 1% N-MWCNTs/3% PVDF-HFP/CA composite membranes on the adsorption efficiency of Ca (II) metal ions.	71
Figure 4.18: XRD of 3 % PVDF-HFP/CA after recycling the composite membrane at least 3 times for Ca (II) ions	72
Figure 4.19: TGA profile of 3% PVDF-HFP/CA after recycling the composite membrane at least 3 times for Ca (II) ions	73
Figure 4.20: Effect of pH on the removal of Mg (II) ions using PVDF-HFP membrane	75
Figure 4.21: Effect of membrane adsorbent dosage on Mg (II) ions adsorption onto PVDF-HFP composite membranes	77
Figure 4.22: Effect of contact time on adsorption efficiency of Mg (II) ions on (a) 3% PVDF-HFP/CA, (b) 1% N-MWCNTs/CA, and (c) 1% N-MWCNTs/PVDF-HFP composite membranes	78
Figure 4.23: Pseudo-first order (A) and Pseudo-second order (B) kinetic model for adsorption of Mg (II) ions onto (a) 3% PVDF-HFP/CA, (b) 1% N-MWCNTs/CA, and (c) 1% N-MWCNTs/PVDF-HFP composite membranes.....	79

Figure 4.24: Effect of initial metal ion concentration on the adsorption efficiency of Mg (II) ions on (a) 3% PVDF-HFP/CA, (b) 1% N-MWCNTs/CA, and (c) 1% N-MWCNTs/PVDF-HFP composite membranes.....	81
Figure 4.25: Effect of temperature on adsorption efficiency of Mg (II) ions on (a) CA, (b) 3% PVDF-HFP/CA, (c) 1% N-MWCNTs/CA membranes.	82
Figure 4.26: Effect of the Langmuir and Freundlich isotherm on adsorption efficiency of Mg (II) ions on (a) CA, (b) 3% PVDF-HFP/CA, (c) 1% N-MWCNTs/CA, composite membrane.	84
Figure 4.27: Thermodynamic parameters of Mg (II) ions onto (a) CA, (b) 3% PVDF-HFP/CA, (c) 1% N-MWCNTs/CA, composite membranes.	86
Figure 4.28: Effect of counterions on the adsorption of Mg (II) by (a) 3% PVDF-HFP/CA, (b) 1% N-MWCNTs/CA, (c) 1% N-MWCNTs/PVDF-HFP composite membranes	87
Figure 4.29: Effect of the binary system on the adsorption of Mg (II) by (a) 3% PVDF-HFP/CA, (b) 1% N-MWCNTs/CA, (c) % N-MWCNTs/PVDF-HFP composite membranes	88
Figure 4.30: Effect of reusability on the adsorption of Mg (II) ions onto (a) 3% PVDF-HFP/CA, (b) 1% N-MWCNTs/CA, and (c) 1% N-MWCNTs/PVDF-HFP composite membranes.	89
Figure 4.31: Effect of membrane reusability on the removal of calcium hardness using 3% PVDF-HFP/CA and 1% N-MWCNTs/CA from Sekonye water samples. (Concentration 73.99 mg/L, dosage 0.5 mg/L, pH 7, time 90 minutes, temperature = 30 °C, 200 rpm agitation speed).....	93
Figure 4.32: Effect of membrane reusability on the removal of calcium hardness using 3% PVDF-HFP/CA and 1% N-MWCNTs/CA from Bergendal water samples. (Concentration 91.49 mg/L, dosage 0.5 mg/L, pH 7, time 90 minutes, temperature = 30 °C, 200 rpm agitation speed).....	94
Figure 4.33: Effect of membrane reusability on the removal of magnesium hardness using 3% PVDF-HFP/CA and 1% N-MWCNTs/CA from Sekonye water samples. (Concentration 12.535 mg/L, dosage 0.5 mg/L, pH 7.00, time 90 minutes, temperature = 30 °C, 200 rpm agitation speed).....	94
Figure 4.34: Effect of membrane reusability on the removal of magnesium hardness using 3% PVDF-HFP/CA and 1% N-MWCNTs/CA from Bergendal water samples.	

(Concentration 13.145 mg/L dosage 0.5 mg/L, pH 7.00, time 90 minutes, temperature = 30 °C, 200 rpm agitation speed. 95

LIST OF TABLES

Table 2. 1: The degree of water hardness chart.....	9
Table 2. 2: Permanent vs temporary hardness	10
Table 2. 3: Water quality indicators [15]	13
Table 4.1: Kinetics parameters for Ca (II) ions adsorption onto PVDF-HFP composite membranes.....	60
Table 4.2: Langmuir and Freundlich isotherm parameters for Ca (II) ions adsorption onto PVDF-HFP composite membranes.	65
Table 4.3: Comparison of Ca (II) adsorption capacity by various materials.....	65
Table 4.4: Thermodynamic parameters for Ca (II) (120 ppm) adsorption by PVDF-HFP composite membranes	68
Table 4.5: ICP-MS spectrometry results of 3% PVDF-HFP composite membranes	73
Table 4.6: Kinetic parameters for Mg (II) adsorption onto PVDF-HFP based membrane.....	79
Table 4.7: Langmuir and Freundlich isotherm parameters for Mg (II) ions adsorption onto PVDF-HFP composite membranes	84
Table 4.8: Comparison of Mg (II) adsorption capacity by various materials	84
Table 4.9: Thermodynamic parameters for Mg (II) (120 ppm) adsorption by PVDF-HFP composite membranes	86
Table 4.10: Physicochemical analysis of real water samples before membrane adsorption process at 25 °C.....	91
Table 4.11: Physicochemical analysis of real water samples before membrane adsorption process at 30 °C.	91
Table 4.12: Chemical analysis of real water samples after membrane adsorption process at 25 °C.....	92
Table 4.13: Chemical analysis of real water samples after membrane adsorption process at 30 °C.....	92

LIST OF ABBREVIATIONS

AAS: Atomic absorption spectrometry

CA: Cellulose acetate

DMF: Dimethylformamide

EC: Electrical conductivity

FTIR: Fourier transform infrared

ICP-MS: Inductively coupled plasma mass spectrometry

MF: Microfiltration

MWCNTs: Multiwalled carbon nanotubes

NF: Nanofiltration

N-MWCNTs: Nitrogen doped multi walled carbon nanotubes

PEG: Polyethylene glycol

PVDF: Poly (vinylidene fluoride)

PVDF-HFP: Poly (vinylidene fluoride-co-hexafluoropropylene)

RO: Reverse Osmosis

SANS: South African national standards

SEM: Scanning electron microscopy

SWCNTs: Single walled carbon nanotubes

TEM: Transmission electron microscopy

TGA: Thermogravimetric analysis

UF: Ultrafiltration

WHO: World health organisation

XRD: X-ray diffraction

CHAPTER 1

1.1 BACKGROUND

Water is important to sustain life; an adequate, accessible, and safe supply must be available to all [1]. Drinking water is a basic human right and a basic need for good health [2]. Fresh water constitutes a very small part (2.5%) of all the water on planet Earth, while almost 70% of the world is covered by water. The rest is salty and comes from the ocean, even then only 1% of our fresh water is easily accessible, and much of it is trapped in glaciers and snowfields. Fresh water is already a finite resource in many parts of the world due to climate change, increased population growth, and urbanization.

Purification of ground, river and tap water is required for both industrial activities and drinking purposes [3]. Groundwater is utilised in many developing countries as a source of drinking water. In some cases, the levels of contaminants do not meet the acceptable levels regarding their chemical properties such as heavy metals, soluble iron, nitrate contamination, hardness, etc. Among these properties, water hardness can be problematic, and it can be considered as an essential aesthetic parameter (induces a bitter taste), as well as cause health problems such as diarrhoea and tooth decay. Water hardness affects the electrical appliances, and plumbing system due to the salt deposits on pipes which can cause blockages [4]. Hardness of water is caused by carbon dioxide and moisture reacting with magnesium (Mg(II)) and calcium (Ca(II)) ions present on the earth surface. There are two types of water hardness, temporary hardness can be removed by boiling, however permanent hardness requires specific purification methods [5].

Currently, different methods and materials are employed commercially to remove the two hardness causing agents: which are Mg(II) and Ca(II) ions from water streams. These methods include reverse osmosis, electrocoagulation, ion exchange, lime-soda softening, adsorption and activated carbon, modified cellulose, modified pumice,

Glycidyl methacrylate-divinyl-benzene, methyl methacrylate, poly p-phenylene-diamine-thiourea-formaldehyde, and coconut shell [3, 4, 5, 6].

1.2 PROBLEM STATEMENT

Groundwater and river water contribute a high percentage of water supplies in the rural areas. However, groundwater contains high concentrations of dissolved ions such as Ca(II) and Mg(II) ions [7]. Water hardness is associated with Ca(II) and Mg(II) ions concentrations of above 120 mg/L [8]; which has an impact on economic and human health [9]. For example, water hardness causes scale accumulation in the industrial and household electrical appliances, which acts like an insulator and prolong the heating process [10].

Besides altering the taste of water, high hardness in drinking water can cause health hazards such as diarrhoea, dental problems, and vomiting [7, 11, 12]. In the industries, water hardness is monitored regularly to avoid costly breakdowns such as cooling towers, scaling in boilers and other industrial equipment [13]. Recent studies have shown that most communities use ground and river water containing high levels of Ca(II) and Mg(II) content for their daily needs [14]. A long-term sustainability is a drawback associated with a variety of methods [15, 16, 17], used to soften hard water. Although methods such as ion-exchange and adsorption are preferred, due to their cost effectiveness [18], a low adsorption capacity and certain characteristics of ion-exchange materials pose challenge. Despite an impressive amount of scientific investigation on removal of contaminants in water, very few studies were conducted to reduce water hardness, particularly applying a composite of polyvinylidene-co-hexafluoropropylene (PVDF-HFP) and cellulose acetate (CA) combined with multi-walled carbon nanotubes (MWCNTs) as fillers [19]. For example, electrocoagulation prior to reverse osmosis membranes has been used to reduce water hardness [20].

1.3 MOTIVATION

The study is motivated by high demands of clean potable water which can be solved by a feasible option of desalination. This practice has long been used to provide clean drinking water in many deserted, remote, and coastal areas [21]. Carbon nanotube

(CNT) -based membranes have been used in a variety of separation applications [22]. In the literature it has been shown that the incorporation of CNT into the membrane matrix allows manipulating the properties of the membrane such as the improvement of the hydrophilicity of the surface, the permeability, the rejection of solutes, the tendency to fouling, the resistance to traction and electrical conductivity along with controlled surface chemistry and polymer crystallinity [23].

CNTs are well known for their extraordinary adsorption properties. According to a range of research studies, these carbon nanomaterials possess a high porous hollow structure, a large surface area and as a result these properties could enhance the ability of Ca (II) and Mg (II) removal from water [24]. Furthermore, CA derivatives are among the most widely used polymers in membrane preparation for water purification because they are easily available, possess good mechanical strength and are thermally stable [25].

Incorporation of CA into polymeric membranes has been reported to significantly increase the hydrophilicity and mechanical properties of many hybrid membranes such as polyvinylidene fluoride (PVDF) and PVDF-HFFP polymeric membranes [26]. PVDF-HFP is a polymer membrane with good mechanical properties, high dielectric constant, and lower crystallinity compared to PVDF [27]. Therefore, the study envisions that a composite membrane consisting of a combination of MWCNTs, and CA mixed in a PVDFHFFP polymer membrane could be an efficient and economical compound for treating water hardness.

1.4 AIM AND OBJECTIVES

1.4.1 AIM

The aim of the study is to develop a PVDF-HFP composite membrane for treatment of water hardness

1.4.2 OBJECTIVES

The objectives of the study are to:

- i. prepare PVDF-HFP composite membranes using various dosages of CA and N-MWCNTs,
- ii. characterise prepared composite membranes using X-ray diffraction (XRD), scanning electron microscopy (SEM), Fourier transform infrared (FTIR) and thermogravimetric analysis (TGA),
- iii. optimise suitable conditions for removal of Ca and Mg ions from simulated solutions,
- iv. analyse Ca and Mg ions in water before and after treatment in both simulated solutions and real water samples using flame atomic absorption spectrometry (FAAS),
- v. investigate the adsorption capability of the PVDF-HFP composite membranes.

1.5 DISSERTATION OUTLINE

This dissertation attempts to investigate the efficiency of adsorption of the hardness causing constituents onto the PVDF-HFP composite membranes. The four chapters are organised as follows: Literature review is reported in chapter 2 as follows: (a) Desalination of brackish groundwater and seawater, (b) types of water hardness, challenges associated with hard water usage and other groundwater contaminants, (c) water quality standards, (d) water softening technologies, (e) membrane fabrication methods, (f) membrane additives and solvents, (g) comparison of Ca(II) and Mg(II) ion removal with other studies. This chapter briefly discusses the contents which are of paramount importance in this research project.

Chapter 3 describes the methodologies which were followed throughout the research project: this includes the preparation of PVDF-HFP composite membranes using the phase inversion method, characterisation of the prepared membranes, and finally the batch adsorption experiments. The results of this study are reported in chapter 4. The results show that the PVDF-HFP composite membranes are convenient and low-cost adsorbents to soften hard water to acceptable levels. Chapter 5 gives the overall conclusions drawn from the research project and the recommendations for future

work. Finally, tables and figures are integrated within the texts followed by a listing of references at the end of each chapter.

REFERENCES

- [1] Khan, S., Zheng, H., Sun, Q., Liu, Y., Li, H., Ding, W. and Navarro, A., 2020. Analysis of Influencing Factors for Leaching of Acrylamide Monomer from Polyacrylamide-Based Flocculants Used in the Treatment of Sludge Dewatering. *Sensor Letters*, 18(2), pp.128-132.
- [2] Mohsin, M., Safdar, S., Asghar, F. and Jamal, F., 2013. Assessment of drinking water quality and its impact on resident's health in Bahawalpur city. *International Journal of Humanities and Social Science*, 3(15), pp.114-128.
- [3] Seo, S.J., Jeon, H., Lee, J.K., Kim, G.Y., Park, D., Nojima, H., Lee, J. and Moon, S.H., 2010. Investigation on removal of hardness ions by capacitive deionization (CDI) for water softening applications. *Water research*, 44(7), pp.2267-2275.
- [4] Sepehr, M.N., Zarrabi, M., Kazemian, H., Amrane, A., Yaghmaian, K. and Ghaffari, H.R., 2013. Removal of hardness agents, calcium and magnesium, by natural and alkaline modified pumice stones in single and binary systems. *Applied Surface Science*, 274, pp.295-305.
- [5] Hailu, Y., Tilahun, E., Brhane, A., Resky, H. and Sahu, O., 2019. Ion exchanges process for calcium, magnesium and total hardness from ground water with natural zeolite. *Groundwater for Sustainable Development*, 8, pp.457-467.
- [6] Muqeet, M., Khaliq, A., Qureshi, U.A., Mahar, R.B., Ahmed, F., Khatri, Z., Kim, I.S. and Brohi, K.M., 2018. Aqueous hardness removal by anionic functionalized electrospun cellulose nanofibers. *Cellulose*, 25(10), pp.5985-5997.
- [7] Cotruvo, J., 2011. Hardness in Drinking-water background document for development of WHO guidelines for drinking water quality. *World Health Organisation*, 1, pp 1-19.
- [8] World Health Organization., 2003. Background document for development of WHO guidelines for drinking-water quality. *World Health Organization*, 20, pp 4-6.

- [9] Sengupta, P., 2013. Potential health impacts of hard water. *International Journal of Preventative Medicine*, 4, pp 866-875.
- [10] Ferreira, D., Barros, M., Oliveira, C.M., and da Silva, R.J.B., 2019. Quantitative of the uncertainty of visual detection of the endpoint of a titration: Determination of total hardness in water. *Microchemical Journal*, 146, pp 856-863.
- [11] Campbell, J., and Peterson, D., 2010. Determination of water hardness from common water sources using flame atomic absorbance spectrometry. *Concordia College Journal of Analytical Chemistry*, 1, pp 4-8.
- [12] Rygaard, M., Arvin, E., Bath, A., and Binning, P.J., 2011. Designing water supplies: optimizing drinking water composition for maximum economic benefit. *Water Residence*, 45, pp 3712-3722.
- [13] Ali, S., Rehman, S.A.U., Luan, H.Y., Farid, M.U., and Huang, H., 2018. Challenges and opportunities in functional carbon nanotubes for membrane-based water treatment and desalination. *Science of the Total Environment*, 646, pp 1126-1139.
- [14] Calow, R.C., MacDonald, A.M., Nicol, A.L., and Robins, N.S. 2010. Ground water security and drought in Africa: linking availability, access and demand. *Groundwater*, 48, pp 246-256.
- [15] Apell, J.N., and Boyer, T.H., 2010. Combined ion exchange treatment for removal of dissolved organic matter and hardness. *Water Residence*, 44, pp 249-260.
- [16] Izadpanah, A.A., and Javidnia, A., 2012. The ability of a nanofiltration membrane to remove hardness and ions from diluted seawater. *Water*, 4, pp 283.
- [17] Mustapha, S., Ndamitso, M., Mohammad, N., Adeosun, N., and Idris, M. 2016. Study of activated from melon (*Citrullus lunates*) husk as natural adsorbent for removal of hardness in water. *Advanced Analytical Chemistry*, 6, pp 1-9.
- [18] Rao, G.P., Lu, C., and Su, F., 2007. Sorption of divalent metal ions from aqueous solution by carbon nanotubes: a review. *Separation, Purification and Technology*, 58, pp 224-231.

- [19] Lv, J., Zhang, G., Zhang, H., Zhao, C., and Yang, F. 2018. Improvement of antifouling performances for modified PVDF ultrafiltration membrane with hydrophilic cellulose acetate nanocrystal. *Applied Surface Science*, 440, pp 1091-1100.
- [20] Goh, P.S., Ishmail, A.F., and Ng, B.C., 2013. Carbon nanotubes for desalination: Performance evaluation and current hurdles. *Desalination*, 308, pp 15-33.
- [21] Ihsanulah. I, 2019. Carbon nanotubes membranes for water purification: Developments, challenges, and prospects for the future. *Separation and Purification Technology*, 209, pp 307-337.
- [22] Liu, F., Hashim, N.A., Liu, Y., Abed, M.M., and Li, K., 2011. Progress in the production and modification of PVDF membranes. *Journal of Membrane Science*, 375, pp 1-27.
- [23] Wongchitphimon, S., Wang, R., Jiraratananon, R., Shi, L. and Loh, C.H., 2011. Effect of polyethylene glycol (PEG) as an additive on the fabrication of polyvinylidene fluoride-co-hexafluoropropylene (PVDF-HFP) asymmetric microporous hollow fiber membranes. *Journal of Membrane Science*, 369, pp 329-338.
- [24] Stephan, A.M., Kumar, S.G., Renganathan, N.G., and Kulandainathan, M.A., 2005. Characterization of poly (vinylidene fluoride–hexafluoropropylene) (PVDF–HFP) electrolytes complexed with different lithium salts. *European Polymer Journal*, 41, pp15-21.
- [25] Phao, N., Nxumalo, E.N., Mamba, B.B., and Mhlanga, S.D., 2013. A nitrogen-doped carbon nanotube enhanced polyethersulfone membrane system for water treatment. *Physics and Chemistry of the Earth, Parts A/B/C*, 66, pp.148-156.
- [26] Kožíšek, F., 2003. Health significance of drinking water calcium and magnesium. *National Institute of Public Health*, 1, pp 219-227.
- [27] Liu, F., Hashim, N.A., Liu, Y., Abed, M.M., and Li, K., 2011. Progress in the production and modification of PVDF membranes. *Journal of Membrane Science*, 375, pp 1-27.

CHAPTER 2

LITERATURE REVIEW

2.1 DESALINATION OF SEAWATER AND BRACKISH GROUNDWATER.

The lack of potable water has led to the discovery of water treatment technologies. Rapid changes in the human way of living over the years have repeatedly brought various anthropogenic pollutants into the water. Treating these emerging nano, macro, or micro pollutants is difficult or impossible with traditional treatment methods, and they have been reported to cause various diseases such as cancer, heart problems, diarrhoea, etc. [1]. These purification methods should not only remove nano-, macro- or micro-pollutants, but also desalinate saline water to acceptable levels. Climate change and global warming are environmental factors that have been reported to increase the salinity level of both sea and land water resources, reducing the accessibility of existing fresh water for industrial, agricultural, and domestic activities [2]. Brackish and sea water desalination could offer solutions to water scarcity of freshwater resources throughout the world. The process of removing salts and mineral contents from saline water (i.e., seawater or brackish water) to generate pure water is referred to as desalination [3].

Salinity of brackish water is between sea and fresh water. Total dissolved solids (TDS) in undiluted sea water are 35,000 mg/L, while TDS in brackish water is between 1,000 to 15,000 mg/L. The mixing of fresh and sea water results in brackish water, as in estuaries, or it can also be generated through a dike. The exact area which comprises of brackish water is not easily spotted, it can be found in lakes, rivers, estuaries, and underground water in most cases. The biggest supply of brackish water is underground. In many parts of the world such as North and Western Africa, Southern and Western Europe, Australia, Canada, United States and South America, brackish groundwater reserves are also present. Treatment of brackish water before any usage is important to increase the health and environmental concerns [4].

2.2 WATER HARDNESS

Calcium and magnesium are two dominant species that contribute to water hardness. Water can be divided into two groups: soft or hard water, depending on the amount of Ca (II) and Mg (II) metal ions present [5].

Table 2. 1: The degree of water hardness chart [5]

CaCO ₃ concentrations (mg/L) or ppm	Indication
0 - 60 mg/L	Soft water
60 - 120 mg/L	Moderately hard water
120 - 180 mg/L	Hard water
180 mg/L and over	Very hard water

2.2.1 Hard water

Water hardness is measured in terms of carbonate concentration in parts per million (ppm) or milligrams per litre (mg / L) using calcium carbonate (CaCO₃²⁻), which is an expression of all hardness ions present in water [7]. If the concentration of calcium and magnesium in the water exceeds the permissible limit of 120 mg / L, this water is called hard water [8].

Hard water can easily be spotted by the appearance of mineral deposits (scale) on the surfaces of bathroom faucets, soap scums in bathtubs, electrical appliances (e.g., kettles) etc. Different methods have been developed to reduce the concentration of the hardness causing agents from water samples because these mineral deposits make hard water to be unsuitable for various applications such as drinking, cooking, washing, etc [9].

2.2.2 Sources of hardness

The principal natural source of hardness are minerals like dolomite (CaMgCO_3) and limestone (CaCO_3) which introduces Ca (II) and Mg (II) metal ions into water, respectively. $\text{H}_2\text{O} (\text{l}) + \text{CO}_2 (\text{g}) \rightarrow \text{H}_2\text{CO}_3 (\text{l})$, which mostly exists as bicarbonate (HCO_3^-) ion at environmental pH. Aquatic microorganisms consume carbonic acid as carbonate (CO_3^{2-}) to form calcite skeletons. These calcite skeletons undergo various environmental changes in the earth surface over a period of millions of years that build up extensive limestone deposits [10].

The partial acidity of ground water is caused by the absorbed CO_2 from the air and respiration of soil bacteria. When this water diffuses in the limestone, calcium and bicarbonate ions are released into water thus making ground water to be hard. The extent of hardness increases when ground water percolates through rocks, which contain dolomite and limestone [10]. Furthermore, water hardness has also been reported to be caused by dissolved divalent metal ions such as zinc, strontium, iron and manganese[11].

2.2.3 Types of hardness

There are two types of water hardness: permanent and temporary hardness, which are sometimes called non-carbonate or carbonate hardness respectively. It is well known that water hardness is caused by various divalent metal ions in water, which can combine with other negatively charged ions (anions) to form stable salts. Temporary and permanent hardness can be differentiated based on the type of anions found in the salts. As shown in table 2.2, permanent hardness forms when the hardness constituents react with either SO_4^- or Cl^- , while temporary hardness forms from a reaction of Mg (II) and Ca (II) with OH^- or HCO_3^- or CO_3^{2-} anions to form stable salts [10].

Table 2.2: Permanent vs temporary hardness

Permanent hardness	Temporary hardness
---------------------------	---------------------------

Calcium chloride (CaCl ₂)	Calcium hydroxide (Ca(OH) ₂)
Magnesium chloride (MgCl ₂)	Magnesium hydroxide (Mg(OH) ₂)
Calcium sulfate (CaSO ₄)	Magnesium bicarbonate (Mg(HCO ₃) ₂)
Magnesium sulfate (MgSO ₄)	Magnesium carbonate (MgCO ₃)
	Calcium carbonate (CaCO ₃)

Temporary hardness can be removed by boiling water in an open container or by addition of lime (calcium hydroxide). Heating water in an open chamber facilitates the decomposition of bicarbonate into carbonates. The cooled leaving water is softened after the precipitation of calcium carbonate. Permanent hardness cannot be reduced by boiling because boiling causes only the temperature to increase. High temperature causes the solubility of calcium and magnesium salts in water to increase, hence permanent hardness requires specific treatment methods like membrane filtration to soften hard water to acceptable limit [6].

2.2.4 Challenges associated with hard water usage

Hard water forms a precipitate known as a lime scale (i.e mineral deposit), which can easily be noticed as a white, flaky buildup found on household and industrial items. Scale accumulation in electrical appliances acts like an insulator, causing a prolonged heating of water, which results in consumption of more energy than what is required. In the industries, hard water is monitored regularly because the buildup of scale in the industrial sized water boilers can cause a drastic effect on the power bills. The potential health impacts of drinking hard water excessively causes diseases such as kidney stones, skin dermatitis, pancreatic cancer, atopic dermatitis, reproductive health issues and chronic inflammatory diseases [8]. Hard water causes the clogging of pipes resulting in reduced flow of water in the piping system [12]. Furthermore, washing

clothes and utensils will require more soap and detergents as well as bathing to produce a lather [11].

2.2.5 Other groundwater contaminants

There are other groundwater contaminants apart from water hardness. Groundwater is mainly used as a source of drinking water because of its perceived good microbial quality in its natural state. The geological set up of the aquifer, anthropogenic activities and climate are factors that have been reported to influence the quality of groundwater [13]. Improper disposal of wastewater generated from industrial practices like combustion and extraction contain heavy metals that can pollute surface water, soil, and groundwater. There are certain heavy metals which are needed for the proper functioning of the body, but excessive amounts of those metals may lead to health risks [14]. Apart from the heavy metals (arsenic and lead) which have been reported to contribute to groundwater pollutions, there are other chemical ions such as phosphates, nitrates, chlorides, and manganese which are also found in groundwater due to various human activities. The permissible limits of drinking water contaminants are provided by the environmental protection agencies like the World Health Organisation (WHO) [15]. Real water samples contain various ionic species which might affect the adsorption uptake of the hardness causing agents. The chloride, nitrate, and sulfate ions, as well as Ca(II) or Mg(II) were selected in this study to prepare a synthetic water sample simulating a real water sample [16].

2.3 Water quality standards

Most rural communities rely on groundwater resources of unknown water quality, and they are therefore at a high risk of getting water borne diseases if they consume groundwater with unknown water quality. The locations of boreholes in most rural communities are close to a dumping site or near a pit toilet, which could contribute to further health effects. In 2009, Bessong et al., [13] conducted a study of high levels of faecal contamination in Vhembe District of South Africa. Water pollution is caused by

an imbalance of microbial and physicochemical contamination in water resources. Diseases that are commonly associated with poor water quality are cholera, Tetanus, Typhoid, and diarrhoea [17]. Table 2.3 below shows the physico-chemical indicators of water quality as indicated by the World Health Organisation (WHO). The pH value of a water source measures the amount of hydrogen ions concentration and can indicate the acidity or basicity of a water sample. The acceptable limit of pH is 6.5 to 8.5 [15] at room temperature. Electrical conductivity (EC) measures the ability of water to conduct electricity and is directly proportional to TDS. TDS measures the amounts of all dissolved ions (organic and inorganic substances) in a water source.

Table 2.3: Water quality indicators [15]

Parameters	Units	Permissible limits
Physical indicators		
pH at 25 °C	pH units	6.5 to 8.5
Total dissolved solids (TDS)	mg/L	≤ 1200
Conductivity at 25 °C	mS/m	≤ 170
Chemical indicators		
Sulfate as SO ₄ ²⁻	mg/L	≤ 500
Nitrate as NO ₃ ⁻	mg/L	≤ 11
Chloride as Cl ⁻	mg/L	≤ 300
Sodium as Na	mg/L	≤ 200

2.4 Water softening technologies

2.4.1 Ion-exchange method

Water softening refers to technologies that remove the metal ions that causes water to be hard, particularly calcium and magnesium [18]. Although there are many methods that are currently used to soften hard water, ion-exchange is the commonly used method. Ion-exchange is a reversible-interchange of ions in an aqueous solution with similarly charged ion attached to the ion exchange media [4]. The mostly used ion-exchangers that exchange the hardness constituents (Ca(II) and Mg(II) metal ions) from solution are zeolites, Amberlite, titanate nanotube (TiNTs) and sodium chloride (NaCl) salts [8]. Apart from water hardness, these materials can also remove a wide range of water pollutants. The ion-exchange method requires the replacement of zeolites regularly, its slightly expensive and the fate of zeolites is unknown [10]. In addition, the application of the ion exchange process to the batch application of drinking water is negligible, but it is mainly used in industrial water desalination. This is because the ion exchange resins used in this process are a brittle organic material that is used to remove material and has been reported to pose a threat when applied to drinking water. Zeolites are mainly used for adsorption of organic, ionic and ammonium nitrogen in water treatment because they are good ion exchangers [19].

2.4.2 Membrane filtration

Membrane provides a physical barrier which allows certain transportation of chemical species such as liquids, ions, and gases [20]. Membrane filtration is a physical separation method that rejects solute fluids, gases, and different particles that are present in contaminated water bodies but allows only water to pass through. Reverse osmosis (RO), nanofiltration (NF), ultrafiltration (UF), microfiltration (MF), dialysis, electrodialysis and distillation are membrane separation technologies that are currently available [21]. These membrane processes can either be dependent on concentration gradients, electrical gradients, pressure driven or other driving forces [22].

UF and MF can be distinguished by their ability to remove colloidal and suspended particles through a sieving mechanism based on the size of the membrane pores relative to that of the particulate matter. RO and NF are characterised by their ability to remove ionic contaminants, these membrane separation technologies are mostly applied in desalination or water softening processes [22]. The benefits of using these membrane filtration processes include low chemical sludge effluent, smaller bulk chemical storage tanks and feed facilities, compact modular construction, smaller footprint, easy operation, monitoring, and maintenance. Although these processes have been reported to remove a variety of water pollutants, most of them are prone to fouling during their long-term operation. Fouling results in premature membrane replacement, reduced service time, feed water loss, and permeate quality deterioration costs due to limited recoveries [23].

2.4.3 Adsorption

Different water-treatment technologies have been presented and implemented in the industrial and experimental level to address the unquestionable need of pure water for various purposes [21]. Adsorption is among the technologies which have been reported to effectively soften hard water [8]. It is simple to operate, cheap and yields higher removal capacities as compared to other conventional technologies which have been reported thus far [24].

2.4.3.1. Polymeric membranes

2.4.3.1.1. Polyvinylidene-co-hexafluoropropylene

Among the polymeric membranes, (polyvinylidene fluoride) PVDF is a semi-crystalline membrane which has attracted much interest in research due to its outstanding chemical and physical properties [25, 26, 27]. It is an ideal membrane material used to fabricate PV, MF, UF, and NF membranes. Its application in wastewater and water treatment is hindered by its hydrophobic nature, causing permeability decline due to severe membrane fouling. Different methods have been investigated to enhance the

hydrophilicity of PVDF membranes to overcome membrane fouling problem [28]. PVDF and its copolymers can be easily processed using techniques such as electrospinning, melt pressing, injection molding, melt pressing, solution casting, phase inversion etc [29, 30, 31].

PVDF-HFP is more hydrophobic than PVDF, with higher solubility, lower degree of crystallinity and lower glass transition than PVDF, and this is due to the addition of the hexafluoropropylene group to the main vinylidene fluoride blocks, which increases the content of fluorine [32]. Amorphous hexafluoropropylene (HFP) groups improve their plasticity and ionic conductivity, while the crystalline phase of vinylidene fluoride (VdF) groups offers excellent mechanical and chemical stability [29]. Furthermore, PVDF-HFP polymer can also be used to fabricate membranes for a variety of applications ranging from simple condensers to high-tech sensors and actuators, including water treatment [29].

2.4.3.1.2. Cellulose acetate

Loeb and Sourirajan [33] reported the first membrane structure made from cellulose acetate (CA) using the phase inversion process. Feron et al., [34] described CA as the promising membrane material when compared to other polymeric materials because it has the highest CO₂/N₂ selectivity. CA is a renewable polymer which can be obtained by introduction of acetyl groups on cellulose. It is hydrophilic, it is cost-effective, it has moderate chlorine resistance, it possesses good fouling resistance and good biocompatibility making it to be an ideal membrane which is mostly used in separation processes. The disadvantages of using this polymer are that it has low oxidation, thermal and chemical resistance, and poor mechanical strength, which demands efficient modification [35]. Blending polymers in membrane preparation has been studied to develop new membranes with envisaged properties and performance. The significance of polymer blending is to enhance hydrophilicity and decrease membrane fouling [36]. The focus of hydrophilicity is to attain high water flux with reduced resistance to fouling, this is due to the hydration layer on membrane surface that may inhibit the nonspecific interaction between membrane surface and foulants [37].

2.4.3.2. Carbon-based adsorbents

2.4.3.2.1 Nitrogen doped carbon nanotubes

CNTs are allotropes of carbon which comprises of cylindrical graphite sheets rolled in a tubular form. There are two types of CNTs, MWCNTs and single walled carbon nanotubes (SWCNTs) [38]. SWCNTs are made up of a single graphene sheet while MWCNTs consists of multilayers of graphene sheets. They were invented by Sumio Iijima in 1991 at the NEC Laboratory in Tsukuba, Japan, using an arc-discharge technique [38]. There are different methods which are used to synthesise CNTs such as chemical vapor deposition (CVD), laser ablation, arc-discharge, etc. These nanomaterials have unique electrical, chemical, thermal, and mechanical properties which make them useful materials to eliminate different pollutants from aqueous solutions [38]. As compared to conventional technologies (e.g chemical oxidation, physical separation etc), membrane-based technologies have been reported to require less energy and space, as well as their simplicity to operate which render them appropriate for use in separation processes. The only problem with the conventional membranes is fouling. Mixed matrix membranes (MMM) are an appropriate way to overcome the limitations of conventional membranes. MMM are membranes, which consist of inorganic nanomaterials like carbon nanostructures, zeolites, metal oxides, graphite, etc. Amongst these nanomaterials, CNTs have received great attention owing to their outstanding physicochemical properties. The only challenge of preparing CNTs/MMM membranes is agglomeration of the CNTs into membrane matrix [39].

Agglomeration results in an uneven distribution of CNTs into the polymer matrix, this causes poor mechanical strength and formation of non-selective voids in the membrane. A satisfactory interfacial adhesion between the polymer matrix and the CNTs to form an even dispersion is significant. There are two approaches which have been reported to address the issue of agglomeration namely, chemical, and mechanical modification. Chemical modification involves the use of surfactants to change the surface properties of CNTs and/or acid functionalisation. While the mechanical modification involves grinding and/or sonication of the CNTs before being

immersed into the membrane matrix, functionalisation also reduced agglomeration [39].

Doping of CNTs with heteroatoms alters the chemical and physical properties of CNTs by producing new conditions that improves their electronic structure. The most effectively used dopants are nitrogen and boron, the reason is because they have a smaller atomic size like the carbon atom, which makes it easier for them to enter a nanotube lattice. The substitutional doping of CNTs with nitrogen has received great attention, the lone pairs of electrons on the nitrogen (N atom) enhances the electronic properties of the carbon material. Studies have shown that N-CNTs have a smaller energy gap, which increases their storage capacity and offers the chances of greater electrical conductivity as compared with the undoped CNTs [40]. The method of introducing N into the CNTs serves as an alternative method of functionalisation, usually using nitric acid to modify the surface of CNTs. For example, the N in N-CNTs has been reported to bind strongly to metals leading to an excellent metal dispersion in metal/N-CNTs materials. In many catalytic applications, modification of CNTs surface by N-doping increases the selectivity and reactivity of carbon supported catalysts [41].

2.5 Membrane fabrication methods

2.5.1 Phase inversion

Membranes are categorised into two groups, namely polymeric or inorganic membranes depending on the membrane raw material. Fabrication of polymeric membranes require only organic polymers which are either rubbery or glassy and either amorphous or crystalline. Polymer membranes are mainly used in desalination and water purification. Its manufacture involves one of the following techniques, namely, phase inversion, interfacial polymerization, stretching, and casting. Most commercial membranes are manufactured using the phase inversion process and comprise the following steps: mixing, casting, coagulation, and membrane formation, as well as annealing of the produced membrane [42]. Phase inversion is the most common method for membrane production, in which a homogeneous polymer solution is converted from a liquid to a solid state in a controlled manner. A thin film of the

polymer solution is poured onto a glass plate (an inert substrate) with a casting knife and then immersed in a solvent-free coagulation bath. A membrane will form after a de-mixing phase whereby the solvent diffuses and exchange with the non-solvent [43].

Interfacial polymerization (IP) is a process used to produce thick and thin active layers for thin film composite membranes (TFC), for example pressure driven membranes such as nanofiltration (NF) and reverse osmosis (RO) [44]. The TFC design was discovered by Cadotte in 1978 and is now the widely used commercial desalination membrane [43]. IP is based on the polycondensation reaction between two monomers (e.g, polyacyl chlorides and polyamines) that dissolve in an immiscible solvent, one of which the aqueous polyamide solution first permeates the substrate. An ultra-thin film is created on the interface that adheres to the substrate. This technique can produce nano/micro composites membranes and structure, which play a pivotal role in technological implications for microencapsulation for drug delivery, as well as chemical and biological sensors [44].

Apart from phase inversion and interfacial polymerization, polymeric membranes can be modified by nanomaterials by using surface grafting, coating, and other methods. In this regard, the membrane surface is grafted or coated with functional groups to enhance membrane durability and stability. The setbacks of using this approach are the reduced membrane permeability, which occurs because of the trade-off between the membrane durability and flux [43].

2.6 Membrane additives and solvents

Hydrophilic polymer additives like polyethylene glycol (PEG), polyvinylpyrrolidone (PVP), and poly (methyl methacrylate) (PMMA) are commonly used to fabricate polymeric membranes such as PVDF. Their role is to enhance the formation of pores because they are water soluble, and they can easily be washed out during the membrane preparation and operation. Furthermore, introduction of these additives into the polymer solution is to modify the thermodynamics and kinetics in spinning/casting solution to control the pore sizes, pore size distribution and membrane morphology [45]. PEG is a linear polyether compound, with a general formula, $H(OCH_2CH_2)_nOH$, where n is the average number of repeating oxyethylene

groups. It is water soluble and soluble in numerous organic solvents like aromatic hydrocarbons. Hence, studies have reported PEG as a pore former to enhance membrane permeation properties for both hydrophilic and hydrophobic membranes [46]. Solvents also play a pivotal role in determining the membrane's morphology and performance. These include, N, N-dimethylformamide (DMF), N, N-dimethylacetamide (DMAc), N-methyl-2-pyrrolidone (NMP), dimethylsulfoxide (DMSO), tetramethylurea (TMU), hexamethylphosphoramide (HMPA), triethylphosphate (TEP), and trimethyl phosphate (TMP). The commonly used solvents among these are DMF, DMSO, DMAc, and NMP because they have been used as high boiling point strong solvents in casting polymeric membranes like PVDF [45].

2.7 Comparison of Ca (II) and Mg (II) ions removal with other studies

Rolence et al., [47] reported on the use of coconut shell activated carbon (CSAC) for hardness removal. The equilibrium isotherms were analysed using the Langmuir and Freundlich isotherm model, all the isotherm models fitted to explain the adsorption behaviour of the hardness causing agents onto the CSAC adsorbent. Their results showed a maximum adsorption capacity (q_{max}) of 48.5 mg/g for Ca (II) at pH 7. The removal efficiencies for both the field and synthetic water samples were 55% and 60 %, respectively [47].

In 2015, Werkneh et al., [48] synthesized and employed alkali modified sugarcane bagasse and coffee husk for removal of water hardness causing constituents. They have observed a maximum adsorption capacity of 46.8 and 37.35 mg/g for Ca (II) ions using a 2 g/L adsorbent dosage and a pH of 6.5 at room temperature. Furthermore, their results have shown that the alkaline modified sugarcane bagasse and coffee husk are considered as effective low-cost adsorbents because after treating synthetic water solution simulating an actual water stream the total hardness of the treated water samples met the required standard for drinking water, below 60 mg/L of $CaCO_3$ [48]

In 2016, Bibiano-Cruz et al., [49] have prepared the natural and homoionic clinoptilolite for hardness removal in batch and column test analyses. Their optimum pH of 6.5 yielded Ca (II) removal of 33% and 42% for natural and homoionic clinoptilolite adsorbents using a 1 g/100 mL dosage at constant temperature of 298 K. The kinetic

studies fitted well with the pseudo-second order kinetic model. The Langmuir and Freundlich isotherm models fitted well with the equilibrium data, even though it was fitted better by the Langmuir isotherm with a maximum adsorption capacity of 10.5 and 9.68 mg/g for homoionic and natural clinoptilolite adsorbents [49].

Ab et al., [50] studied the adsorption capacity of adsorbent surfactant coatings by sodium dodecylbenzene sulfonate (SDBS) modified bentonite (SMB) for removal of Ca (II) and Mg (II) ions from the hard water samples. Testing of adsorbent was conducted in terms of surfactant: binder ration and the best formulation of SMB were obtained by using polyvinyl acetate (PVAc) and bentonite in the ration of 0.7:1.0 (w/w). The optimum adsorption uptake of Ca (II) and Mg (II) ions onto the SMB was adsorbent coating were carried out using the Temkin, Langmuir and Freundlich isotherm models. Adsorption thermodynamics and kinetic parameters were conducted to study the adsorption behaviour of the hardness causing agents at various temperature intervals. The highest removal efficiency for both Ca (II) and Mg (II) was 29.27 mg/g in 90 min using a concentration of 120 ppm hardness [50].

In 2018, Lestari et al., [51] modified *Amorphophallus campanulatus* skin as a low-cost adsorbent for the removal of Ca (II) and Mg (II) ions from hard water samples. Their results revealed the adsorption capacity for Ca (II) and Mg (II) ions onto KB and KM in 100 ppm aqueous solutions are 10.85 mg/g, 27.64 mg/g, 1.79 mg/g, 20.1 mg/g respectively using a 1.5 g/25 mL dosage. Experimental data then fitted with Temkin, Dubinin Radushkevich, Langmuir and Freundlich isotherm models and the adsorption follows the Dubinin isotherm model as compared to the other models [51].

Çalgan and Ozmetin [52] investigated the removal of hardness using response surface methodology from wastewater containing high boron using Bigadic clinoptilolite. Their findings recorded high values of adsorption efficiency and adsorption capacity by NaOH-modified clinoptilolite, and its maximum values were above 99% and 12.30 mg/g using a 20 g/L adsorbent dosage at a temperature of 299 K [52]. Soliman et.al [53] prepared novel magnetic nanocomposite adsorbents based on functionalisation of wood sawdust for fast removal of calcium hardness from water samples. Their results showed adsorption capacity of 18.4 mg/g and 27.2 mg/g, as well as removal

efficiency of 84.4 -100% and 98.29 -100% using dosage of 0.4 g /50 mL and 0.2 g/50 mL at pH of 7 and temp=298 K [53].

Cetin [54] employed an ion exchange method as an approach to remove the hardness causing agents from the simulated hard water solutions. The adsorption uptake of Mg (II) ions in artificial solutions of hard water was studied at pH 3, agitation speed of the solution was 115 rpm, amount of the resin was found to be 10 g, and the ration of resin/solution was 1 g/100 mL. The maximum ion exchange capacity and removal efficiency for Mg (II) was found to be 12.0 mg/g and 70%. Furthermore, the results have shown that the ion exchange capacity and rate of the resin are higher for Ca (II) than Mg (II) ions. This could be attributed to the competition of adsorption of Ca (II) and Mg (II) ions and hydrogen ions on the resin sites and exchange of Ca (II) ions was formed in preference to ions of Mg (II) and hydrogen ions. The difference of selectivity of the resin for sorption of Ca (II) and Mg (II) ions has a great effect on removal of Ca (II) hardness with the pH range higher than 2.0 [54].

In 2015, Pratomo et al., [55] studied the softening of hard water using *Pistacia vera* shell as an adsorbent for calcium and magnesium removal. Batch adsorption experiments were investigated to optimise the removal of the hardness causing agents from artificial hard water samples. The adsorption capacity of Mg(II) ions was found to be 2.19 mg/g at pH 8 using 1.5 g of *Pistacia vera* shell. The adsorption isotherm data fitted well for both metal ions, the curve model for Mg(II) ions was found to be Freundlich isotherm while Ca(II) ions fitted well with the Langmuir isotherm model. It was concluded that the *Pistacia vera* shell is biodegradable, easy, inexpensive bio adsorbent to adsorb the hardness causing agents [55].

Mustapha et al., [54] studied the hardness removal from water samples using melon (*Citrullus lanatus*) husk as a natural adsorbent. Batch adsorption tests were conducted to optimise the removal of the hardness constituents by varying the solution pH, adsorbent dose, contact time, and solution temperature. Thermodynamic parameters such as ΔS° , ΔH° , ΔG° and E_a have been computed and the results revealed that higher solution temperature favours the hardness removal by the activated melon husk using the solution pH of 7 and 0.5 g/0.04 dm³ dose. Higher temperatures enhance the

sorption of the hardness causing agents due to the increased surface activities and kinetic energy of the solute [56].

In 2019, Aragaw et al.,[57] reported on the hardness removal using zeolites synthesized from Ethiopian kaolin by hydrothermal method. The kaolin was utilised for zeolite synthesis using the hydrothermal method. The solution pH, temperature, and the contact time were optimised in the batch adsorption tests to enhance the removal of the hardness causing constituents from water samples. The removal rate of Mg(II) ions increased from 22.5 to 81.4%, and the maximum adsorption capacity of 15.7 mg/g was achieved at pH 6.5 using a 2.5 g/50 mL dose. In addition, the removal of Ca(II) ions onto zeolites showed higher affinity compared to Mg(II) ions [57].

In 2020, Elwakeel [58] investigated the sorption of Mg (II) ions using a titan yellow supported on classic thiourea-formaldehyde resin. The results revealed that the adsorption kinetics was consistent with the pseudo-second order kinetics model (PSORE). The maximum adsorption capacity was found to be 19.45 mg/g at pH 10.5, and 0.05 g/20 mL at 298 K. From the batch adsorption tests, it was found that the Titan yellow (TY) supported on thiourea-formaldehyde resin (TF) resin has good adsorption effect on Mg (II) ions, indicating that the TF-TY could be used as the best and available material for reduction of the hardness causing agents [58].

In 2020, Pourshadlou et al., [59] reported on bentonite/ γ -alumina nanocomposite for adsorption of Mg(II) ions from aqueous solutions. Effect of process parameter including γ -alumina content, adsorbent dosage, initial ion concentration, contact time and solution pH were investigated to enhance the adsorption uptake of Mg (II) ions. Adsorption isotherms were used to describe the way the Mg(II) ions distribute themselves between the liquid and solid phase when the adsorption process reaches equilibrium level. The Langmuir isotherm model was found to be a perfect model with a higher correlation coefficient value of ($R^2 = 0.9955$). The highest adsorption capacity was found to be 3.478 mg/g at pH of 7.8, using 20 g/L dose at 293 K.

REFERENCES

- [1] Das, R., Ali, M.E., Abd Hamid, S.B., Ramakrishna, S. and Chowdhury, Z.Z., 2014. Carbon nanotube membranes for water purification: A bright future in water desalination. *Desalination*, 336, pp.97-109.
- [2] Sahle-Demessie, E., Hassan, A.A. and El Badawy, A., 2019. Bio-desalination of brackish and seawater using halophytic algae. *Desalination*, 465, pp.104-113.
- [3] Vatanpour, V. and Safarpour, M., 2018. Carbon-based polymer nanocomposite membranes for desalination. *Carbon-based polymer nanocomposites for environmental and energy applications*, pp.281-304.
- [4] Dietz, K. and Kulinkina, A., 2009. The design of a desalination pretreatment system for brackish groundwater. *Worcester Polytechnic Institute*, pp.0802.
- [5] Tiangco, K.A.A., de Luna, M.D.G., Vilando, A.C. and Lu, M.C., 2019. Removal and recovery of calcium from aqueous solutions by fluidized-bed homogeneous crystallization. *Process Safety and Environmental Protection*, 128, pp.307-315.
- [6] Tofighy, M.A. and Mohammadi, T., 2011. Permanent hard water softening using carbon nanotube sheets. *Desalination*, 268(1-3), pp.208-213.
- [7] Campbell, J., and Peterson, D., 2010. Determination of water hardness from common water sources using flame atomic absorbance spectrometry. *Concordia College Journal of Analytical Chemistry*, 1, pp 4-8.
- [8] Ab Kadir, N.N., Shahadat, M. and Ismail, S., 2017. Formulation study for softening of hard water using surfactant modified bentonite adsorbent coating. *Applied Clay Science*, 137, pp.168-175.
- [9] Ferreira, D., Barros, M., Oliveira, C.M. and da Silva, R.J.B., 2019. Quantification of the uncertainty of the visual detection of the endpoint of a titration: Determination of total hardness in water. *Microchemical Journal*, 146, pp.856-863.
- [10] Hiji, M.F. and Ntalikwa, J.W., 2014. Investigations of Dodoma municipal hard water:(Part 1): Review of hard water treatment processes and identification of contaminants. *Journal of Environmental Monitoring and Protection*, pp.1-56.
- [11] Akram, S. and Rehman, F., 2018. Hardness in drinking-water, its sources, its effects on humans and its household treatment. *Journal of Chemistry and Applications*, 4(1), pp.1-4.

- [12] Lerga, T.M. and O'Sullivan, C.K., 2008. Rapid determination of total hardness in water using fluorescent molecular aptamer beacon. *Analytica Chimica Acta*, 610(1), pp.105-111.
- [13] Edokpayi, J.N., Enitan, A.M., Mutileni, N. and Odiyo, J.O., 2018. Evaluation of water quality and human risk assessment due to heavy metals in groundwater around Muledane area of Vhembe District, Limpopo Province, South Africa. *Chemistry Central Journal*, 12(1), pp.1-16.
- [14] Elumalai, V., Brindha, K. and Lakshmanan, E., 2017. Human exposure risk assessment due to heavy metals in groundwater by pollution index and multivariate statistical methods: a case study from South Africa. *Water*, 9(4), p.234.
- [15] WHO., 2018. Water health and human rights, World water day 2001. Available online at <http://www.worldwaterday.org/thematic/hmnrights.html#n4>. (accessed 10 June 2021)
- [16] Sepehr, M.N., Zarrabi, M., Kazemian, H., Amrane, A., Yaghmaian, K. and Ghaffari, H.R., 2013. Removal of hardness agents, calcium and magnesium, by natural and alkaline modified pumice stones in single and binary systems. *Applied Surface Science*, 274, pp.295-305.
- [17] Alsalmeh, A., Al-Zaqri, N., Ullah, R. and Yaqub, S., 2021. Approximation of ground water quality for microbial and chemical contamination. *Saudi Journal of Biological Sciences*, 28(3), pp.1757-1762.
- [18] Lazar, L., Bandrabur, B., Tataru-Fărmuș, R.E., Droboță, M., Bulgariu, L. and Gutt, G., 2014. FTIR analysis of ion exchange resins with application in permanent hard water softening. *Environmental Engineering & Management Journal (EEMJ)*, 13(9), pp.2145-2152.
- [19] Liu, W., Singh, R.P., Jothivel, S. and Fu, D., 2019. Evaluation of groundwater hardness removal using activated clinoptilolite. *Environmental Science and Pollution Research*, pp.1-9.
- [20] Julbe, A., Drobek, M. and Ayrat, A., 2019. About the role of adsorption in inorganic and composite membranes. *Current Opinion in Chemical Engineering*, 24, pp.88-97.

- [21] Das, R., Ali, M.E., Abd Hamid, S.B., Ramakrishna, S. and Chowdhury, Z.Z., 2014. Carbon nanotube membranes for water purification: A bright future in water desalination. *Desalination*, 336, pp.97-109.
- [22] Tansel, B., 2008. New technologies for water and wastewater treatment: A survey of recent patents. *Recent Patents on Chemical Engineering*, 1(1), pp.17-26.
- [23] Esfahani, M.R., Aktij, S.A., Dabaghian, Z., Firouzjaei, M.D., Rahimpour, A., Eke, J., Escobar, I.C., Abolhassani, M., Greenlee, L.F., Esfahani, A.R. and Sadmani, A., 2019. Nanocomposite membranes for water separation and purification: Fabrication, modification, and applications. *Separation and Purification Technology*, 213, pp.465-499.
- [24] Khalfa, L., Sdiri, A., Bagane, M. and Cervera, M.L., 2021. A calcined clay fixed bed adsorption studies for the removal of heavy metals from aqueous solutions. *Journal of Cleaner Production*, 278, pp.123935.
- [25] Li, N., Xiao, C., An, S. and Hu, X., 2010. Preparation and properties of PVDF/PVA hollow fiber membranes. *Desalination*, 250(2), pp.530-537.
- [26] Huo, R., Gu, Z., Zuo, K. and Zhao, G., 2009. Preparation and properties of PVDF-fabric composite membrane for membrane distillation. *Desalination*, 249(3), pp.910-913.
- [27] Wang, Q., Wang, Z. and Wu, Z., 2012. Effects of solvent compositions on physicochemical properties and anti-fouling ability of PVDF microfiltration membranes for wastewater treatment. *Desalination*, 297, pp.79-86.
- [28] Lalia, B.S., Kochkodan, V., Hashaikeh, R. and Hilal, N., 2013. A review on membrane fabrication: Structure, properties, and performance relationship. *Desalination*, 326, pp.77-95.
- [29] Purkait, M.K., Sinha, M.K., Mondal, P. and Singh, R., 2018. Introduction to membranes. In *Interface Science and Technology* (Vol. 25, pp. 1-37). Elsevier.
- [30] Safarpour, M., Khataee, A. and Vatanpour, V., 2014. Preparation of a novel polyvinylidene fluoride (PVDF) ultrafiltration membrane modified with reduced graphene oxide/titanium dioxide (TiO₂) nanocomposite with enhanced hydrophilicity and antifouling properties. *Industrial & Engineering Chemistry Research*, 53(34), pp.13370-13382.

- [31] Prabakaran, K., Mohanty, S. and Nayak, S.K., 2014. Influence of surface modified TiO₂ nanoparticles on dielectric properties of PVdF–HFP nanocomposites. *Journal of Materials Science: Materials in Electronics*, 25(10), pp.4590-4602.
- [32] Salazar, H., Nunes-Pereira, J., Correia, D.M., Cardoso, V.F., Gonçalves, R., Martins, P.M., Ferdov, S., Martins, M.D., Botelho, G. and Lanceros-Méndez, S., 2016. Poly (vinylidene fluoride-hexafluoropropylene)/bayerite composite membranes for efficient arsenic removal from water. *Materials Chemistry and Physics*, 183, pp.430-438.
- [33] Haddada, R., Ferjani, E., Roudesli, M.S. and Deratani, A., 2004. Properties of cellulose acetate nanofiltration membranes. Application to brackish water desalination. *Desalination*, 167, pp.403-409.
- [34] Jin, R.P.W.X., Jawad, Z.A., Tan, P.C., Chin, B.L.F., Chew, T.L. and Saptorio, A., 2020. Preparation and Characterisation of Blend Cellulose Acetate Membrane for CO₂/N₂ Separation. *Journal of Physical Science*, 31(2), pp.15-31.
- [35] Rasool, M.A., Van Goethem, C. and Vankelecom, I.F., 2020. Green preparation process using methyl lactate for cellulose-acetate-based nanofiltration membranes. *Separation and Purification Technology*, 232, p.115903.
- [36] Madaeni, S.S., Ghaemi, N. and Rajabi, H., 2015. Advances in polymeric membranes for water treatment. In *Advances in membrane technologies for water treatment*. Woodhead Publishing, pp.3-41.
- [37] Shen, S.S., Chen, H., Wang, R.H., Ji, W., Zhang, Y. and Bai, R., 2019. Preparation of antifouling cellulose acetate membranes with good hydrophilic and oleophobic surface properties. *Materials Letters*, 252, pp.1-4.
- [38] Ihsanullah, 2019. Carbon nanotube membranes for water purification: Developments, challenges, and prospects for the future. *Separation and Purification Technology*, 209, pp.307-337.
- [39] Phao, N., Nxumalo, E.N., Mamba, B.B. and Mhlanga, S.D., 2013. A nitrogen-doped carbon nanotube enhanced polyethersulfone membrane system for water treatment. *Physics and Chemistry of the Earth, Parts A/B/C*, 66, pp.148-156.

- [40] Mabena, L.F., Ray, S.S., Mhlanga, S.D. and Coville, N.J., 2011. Nitrogen-doped carbon nanotubes as a metal catalyst support. *Applied Nanoscience*, 1(2), pp.67-77.
- [41] Nxumalo, E.N. and Coville, N.J., 2010. Nitrogen doped carbon nanotubes from organometallic compounds: a review. *Materials*, 3(3), pp.2141-2171.
- [42] El-Gendi, A., Abdallah, H., Amin, A. and Amin, S.K., 2017. Investigation of polyvinylchloride and cellulose acetate blend membranes for desalination. *Journal of Molecular Structure*, 1146, pp.14-22.
- [43] Vatanpour, V., and Safarpour, M., 2018. Carbon-based polymer nanocomposite membranes for desalination. *Carbon-based Polymer Nanocomposites for Environmental and Energy Applications*, pp.281-304.
- [44] Song, Y., Sun, P., Henry, L.L. and Sun, B., 2005. Mechanisms of structure and performance controlled thin film composite membrane formation via interfacial polymerization process. *Journal of Membrane Science*, 251(1-2), pp.67-79.
- [45] Liu, F., Hashim, N.A., Liu, Y., Abed, M.M. and Li, K., 2011. Progress in the production and modification of PVDF membranes. *Journal of Membrane Science*, 375(1-2), pp.1-27.
- [46] Wongchitphimon, S., Wang, R., Jiraratananon, R., Shi, L. and Loh, C.H., 2011. Effect of polyethylene glycol (PEG) as an additive on the fabrication of polyvinylidene fluoride-co-hexafluoropropylene (PVDF-HFP) asymmetric microporous hollow fiber membranes. *Journal of Membrane Science*, 369(1-2), pp.329-338.
- [47] Rolence, C., Machunda, R., and Njau, K.N., 2014. Water hardness removal by coconut shell activated carbon. *International Journal of Science, Technology and Society*, 2(5), pp.97-102.
- [48] Werkneh, A.A., Abay, A.K. and Senbeta, A.M., 2015. Removal of water hardness causing constituents using alkali modified sugarcane bagasse and coffee husk at Jigjiga city, Ethiopia: A comparative study. *World*, 1, pp.2.
- [49] Bibiano-Cruz, L., Garfias, J., Salas-García, J., Martel, R., and Llanos, H., 2016. Batch and column test analyses for hardness removal using natural and homoionic

clinoptilolite: breakthrough experiments and modeling. *Sustainable Water Resources Management*, 2(2), pp.183-197.

[50] Ab Kadir, N.N., Shahadat, M. and Ismail, S., 2017. Formulation study for softening of hard water using surfactant modified bentonite adsorbent coating. *Applied Clay Science*, 137, pp.168-175.

[51] Lestari, A.Y.D., Malik, A., Ilmi, M.I., and Sidiq, M., 2018. Removal of calcium and magnesium ions from hard water using modified *Amorphophallus campanulatus* skin as a low-cost adsorbent. In *MATEC Web of Conferences* (Vol. 154, pp. 01020). EDP Sciences.

[52] Çalgan, E., and Ozmetin, E., 2019. Optimization of hardness removal using response surface methodology from wastewater containing high boron by Bigadic clinoptilolite. *Desalination and Water Treatment*, 172, pp.281-291.

[53] Soliman, E.M., Ahmed, S.A., and Fadl, A.A., 2020. Microwave-enforced green synthesis of novel magnetic nano composite adsorbents based on functionalization of wood sawdust for fast removal of calcium hardness from water samples. *Water Environment Research*, 92(12), pp.2112-2128.

[54] Cetin, G., 2014. Removal of hardness of earth alkaline metals from aqueous solutions by ion exchange method. *International Scholarly Research Notices*, 2014, pp.7.

[55] Pratomo, U., Anggraeni, A., Lubis, R.A., Pramudya, A., Farida, I.N., 2015. Study of softening hardwater using *Pistacia vera* shell as adsorbent for calcium and magnesium removal. *Procedia Chem.* 16, pp. 400–406.

[56] Mustapha, S., Ndamitso, M.M., UM, M., NO, A. and Idris, M., 2016. Study on activated from melon (*Citrullus lanatus*) husk as natural adsorbent for removal of hardness in water. *Advances in Analytical Chemistry*, 6(1), pp.1-9.

[57] Aragaw, T.A., and Ayalew, A.A., 2019. Removal of water hardness using zeolite synthesized from Ethiopian kaolin by hydrothermal method. *Water Practice and Technology*, 14(1), pp.145-159.

[58] Elwakeel, K.Z., 2020. Magnesium sorption onto titan yellow supported on classic thiourea-formaldehyde resin. *Aswan University Journal of Environmental Studies*, 1(2), pp.125-136.

[59] Pourshadlou, S., Mobasherpour, I., Majidian, H., Salahi, E., Bidabadi, F.S., Mei, C.T. and Ebrahimi, M., 2020. Adsorption system for Mg²⁺ removal from aqueous solutions using bentonite/ γ -alumina nanocomposite. *Journal of Colloid and Interface Science*, 568, pp.245-254.

CHAPTER 3

RESEARCH METHODOLOGY

3.1 MATERIALS

All chemicals were of analytical reagent grade and were used as received unless otherwise stated. Dimethylformamide (DMF), poly (vinylidene fluoride-co-hexafluoropropylene) (PVDF-HFP), cellulose acetate (CA), calcium and magnesium sulphate, nitric acid, sodium hydroxide, polyethylene glycol (PEG), were all purchased from Sigma Aldrich. Nitrogen doped multi-walled carbon nanotubes (N-MWCNTs, > 98% carbon purity, 3-5 wt. % N) were purchased from SabiNano (Pty) Ltd.

3.2. PREPARATION OF PVDF-HFP COMPOSITE MEMBRANES

3.2.1. Preparation of PVDF-HFP membrane

The PVDF-HFP composite membranes were prepared via a phase inversion method as reported elsewhere [1]. PVDF-HFP (1.00 g) and PEG (0.2 g) were dissolved in DMF (10 mL) in a round bottom flask and the polymer solution was vigorously stirred at 80 °C for 2 h. The reaction was allowed to settle in a silica gel desiccator overnight and then casted onto a glass plate using a casting knife (Elcometer 3580 adjustable bird film applicator) of 180 µm thickness. The prepared membranes were dried in a vacuum oven at 80 °C for 30 s to pre-evaporate the solvent and then immersed in a coagulation bath (deionized water at 5 °C) to induce phase inversion. The resultant membranes were rinsed with de-ionised water and air dried in plain sheets of papers at room temperature.

3.2.2 Preparation of CA membrane

Cellulose acetate membranes were also prepared via a phase inversion method as described elsewhere [1]. The polymer solution was prepared from a mixture of CA

(0.900 g) and PEG (0.2 g) in DMF (10 mL) in a round bottom flask and the polymer solution was vigorously stirred at 80 °C for 2 h. The polymer solution was kept in a silica gel desiccator overnight and then casted onto a glass plate using a casting knife (Elcometer 3580 adjustable bird film applicator) of 180 µm thickness. The resultant membranes were rinsed with de-ionised water and air dried in plain sheets of papers at room temperature.

3.2.3 Preparation of 3% PVDF-HFP/CA composite membrane

A blend of PVDF-HFP/CA was prepared by the phase inversion method, [2]. Firstly, a CA (0.97 g) was added in 9 mL of DMF, together with 1 mL of PEG (pore forming agent) under constant stirring (600 rpm) at 60 °C. Approximately, 0.03 g of PVDF-HFP was added to a solution of CA (so as to achieve 3% PVDF-HFP/CA composite membrane) and while stirring at 60 °C, the reaction was allowed to stir for a further 24 hours. After 24 hours, the reaction mixture was kept in a silica gel desiccator overnight and then casted onto a glass plate using a casting knife (Elcometer 3580 adjustable bird film applicator) of 180 µm thickness. The prepared membranes were dried in a vacuum oven at 80 °C for 30 s to pre-evaporate solvent and then immersed in a coagulation bath (deionized water at 5 °C) to induce phase inversion. The resultant membranes were rinsed with de-ionised water and air dried in plain sheets of papers at room temperature.

3.2.4 Preparation of 1% N-MWCNTs/PVDF-HFP composite membranes

N-MWCNTs/PVDF-HFP composite membranes were prepared by the phase inversion method, [1]. PVDF-HFP (0.99 g) was dissolved in 9 mL of DMF together with 1 mL of PEG (pore forming agent) in a round bottomed flask. The polymer solution was vigorously stirred at 80 °C for 2 h. On a separate flask, a 0.010g of N-MWCNTs were sonicated in 5 mL DMF at room temperature for 30 minutes. The final mixture was prepared by adding N-MWCNTs to a solution of PVDF-HFP. The mixture was stirred for another 1 h and hand casted onto a glass plate using a casting knife (Elcometer 3580 adjustable bird film applicator) of 180 µm thickness. The prepared membranes were dried in a vacuum oven at 80 °C for 30 s to pre-evaporate solvent and then immersed in a coagulation bath (deionized water at 5 °C) to induce phase inversion.

The resultant membranes were rinsed with de-ionised water and air dried in plain sheets of papers at room temperature.

3.2.5 Preparation of 1% N-MWCNTs/CA composite membranes

The N-MWCNTs/CA composite membranes were prepared by the phase inversion method, [1]. Approximately, 0.99 g of cellulose acetate was dissolved in 9 mL of DMF with 1 mL of PEG (pore forming agent) in a round bottomed flask. The polymer solution was vigorously stirred at 80 °C for 2 h. In a separate beaker, approximately 0.010 g of N-MWCNTs were sonicated in 5 mL DMF at room temperature for 30 minutes. The final mixture was prepared by adding N-MWCNTs into a solution of CA (to achieve 1% N-MWCNTs/CA) and the final mixture was stirred for an additional 1 h at 80 °C. Thereafter, a composite membrane was casted onto a glass plate using a casting knife (Elcometer 3580 adjustable bird film applicator) of 180 µm thickness. The prepared membranes were dried in a vacuum oven at 80 °C for 30 s to pre-evaporate solvent and then immersed in a coagulation bath (deionized water at 5 °C) to induce phase inversion. The resultant membranes were rinsed with de-ionised water and air dried in plain sheets of papers at room temperature. The same procedure was repeated to prepare 1% N-MWCNTs/3% PVDF-HFP/CA based membrane, wherein 0.03 g of PVDF-HFP was used.

3.3 CHARACTERISATION OF PVDF-HFP COMPOSITE MEMBRANES AND N-MWCNTs

3.3.1 X-ray diffraction

The structural properties of the polymeric membranes and the pristine N-MWCNTs were measured using X-ray diffraction (XRD), fitted with a $\text{CuK}\alpha$ (1.5405Å) radiation. The scanning rate of the graphite monochromator was 0.02 s^{-1} ranging from 5 to 65° 2-theta (2θ), where θ is the diffraction angle.

3.3.2 Scanning electron microscopy

Surface morphology of the sample specimen was examined using the scanning electron microscopy (SEM) (JSM 5910, JEOL 5910/Japan). The membranes were placed on a carbon tape, stuck to an aluminium stud, and coated with palladium and gold in the ratio (1:1) to produce a reflective surface for the SEM imaging. The SEM was operated at accelerating velocities of 15 kV and 17 kV.

3.3.3 Transmission Electron Microscope

Transmission Electron Microscope (TEM) (JM 2100, JEOL, Japan) was used to study the internal structure of the pristine N-MWCNTs operating at an accelerating voltage of 200 Kv. Preparation of sample specimen for TEM studies used ultrasonic dispersion of a small quantity of the N-MWCNTs in alcohol (i.e ethanol). The suspensions were coated onto a holey carbon grid by dipping the carbon grid inside the N-MWCNTs/ethanol suspension. The carbon grids were allowed to dry at 25 °C and loaded onto sample holders for analysis.

3.3.4 Fourier-transform infrared spectroscopy

Fourier Transform Infrared spectroscopy (FTIR) studies were carried out using a BRUKER-FTIR-ATR spectrometer in the intervals of 650 to 4000 cm^{-1} with a 4 cm^{-1} resolution and 4 scan numbers at 25 °C. Calibration of the instrument was performed by running the background correction, followed by cleaning the crystal area of the instrument with acetone/alcohol. A small portion of the sample specimen was placed on the crystal area and was analysed thereafter.

3.3.5 Thermogravimetric analysis

Thermogravimetric analysis (TGA) was performed using a Perkin Elmer STA 6000 analyser to monitor the thermal stability of the sample specimen. Approximately 5-10 mg of the sample was placed inside a ceramic pan and inserted in the instrument furnace. The sample temperature was raised from 25 to 900 °C at 10 °C/min under an oxidative atmosphere (air, 50 mL/min). The resulting TGA profile provide information of the sample composition, thermal stability (under a specific atmosphere) and the purity.

3.4 ADSORPTION STUDIES

The methods described below were used to study Ca(II) and Mg(II) adsorption.

3.4.1 Effect of pH

The pH studies were examined by varying the initial pH of the solution. Approximately, 35 mg/L solution was prepared from the analytical grade Ca(II) and Mg(II) sulfate in de-ionised water. The pH of the solution was varied in the interval (5, 5.5, 6, 6.5, and 7). In all the experiments, 25 mg of the membranes were soaked into 50 mL of the prepared solutions. The pH = 7 of the solutions was adjusted using 0.1 M nitric acid (HNO₃) and 0.1 M sodium hydroxide (NaOH) while vigorously stirring for 90 minutes, at room temperature (25 °C) [3]. Flame atomic absorption spectroscopy (F-AAS) was used to measure the concentration of Ca(II) and Mg(II) after adsorption. All the experiments were repeated in triplicates and the mean values were reported. The equation below was used to obtain the amount of the adsorbed salts:

$$\% \text{ Removal} = \frac{(C_o - C_e)}{C_o} \times 100$$

where C_o and C_e are the initial and final concentrations of either Mg (II) or Ca (II) ions in mg/L [3].

3.4.2 Effect of membrane dosage

The effect of membrane adsorbent dosage on the hardness removal (120 mg/L) was studied by varying the membrane dosage from 0.1 to 0.9 mg/L (at an interval of 0.2 mg/L) at pH of 7 for 90 minutes [4]. All the experiments were repeated in triplicates and the average of the two measured values was recorded

3.4.3 Effect of contact time

The effect of contact time on the adsorption of Ca(II) and Mg(II) ions was carried out using 120 mg/L solutions prepared from analytical grade calcium and magnesium

sulfates in de-ionised water. All the experiments were performed by immersing 25 mg of the polymeric membranes in 50 mL of the prepared hard water samples at various time intervals from 30 to 180 minutes (at an interval of 30 minutes). At predetermined time intervals, the flasks were removed from the shaker and the residual metal concentrations were analysed using F-AAS [4]. All the experiments were performed in triplicates and the mean values were recorded.

3.4.4 Effect of initial metal ion concentration

The PVDF-HFP composite membranes (25 mg) were immersed in 100 mL conical flasks containing Ca(II) or Mg(II) solutions (50 mL) with different initial concentrations (100, 300, 600, 900 and 1200 mg/L). The membrane dosage was 0.5 mg/L, and the pH of the aqueous solutions were adjusted to 7 using 0.1 M HNO₃ or 0.1 M NaOH solutions for 90 minutes [5]. All the experiments were repeated in triplicates and the mean values were reported.

3.4.5 Effect of temperature

The temperature effect was studied from 25 to 35 °C (at an interval of 5 °C). The PVDF-HFP membranes (25 mg) were immersed in 50 mL solution prepared from 120 ppm of analytical grade calcium and magnesium sulfate. The pH of the prepared water samples was adjusted to 7, using 0.1 M HNO₃ and 0.1 M NaOH and vigorously stirred for 90 minute. At the end of 90 minutes, the final concentrations of the metals were analysed using F-AAS [4]. All the experiments were repeated in triplicates and the mean values were reported.

3.4.6 Effect of counterions

Real water samples contain various ionic species which might influence the adsorption of the hardness causing agents (Ca (II) and Mg (II)). To study the performance of the PVDF-HFP based membranes in actual field trials, a simulated water sample containing sulfate (325 mg/L), nitrate (25 mg/L), and chloride (450 mg/L) with 120 mg/L calcium or magnesium were prepared. These solutions were prepared from sodium sulfate, potassium nitrate, sodium chloride and analytical grade calcium and

magnesium sulphate. From each prepared solution, 12.5 mL was transferred into a 100 mL conical flask giving a total volume of 50 mL. All the experiments were performed by immersing 25 mg of the polymeric membranes into 50 mL of the prepared water samples. The pH of 7 was adjusted using 0.1 M HNO₃ and 0.1 M NaOH and vigorously stirred for 90 minutes, at room temperature (25 °C) [6]. All the experiments were repeated in triplicates and the average of the two measured values was recorded.

3.4.7 Effect of binary system

Ca(II) and Mg(II) coexist together in real water samples. To investigate the effect of one another, 25 mg of the PVDF-HFP based membrane was added into 50 mL solution containing Ca(II) and Mg(II) (25 mL each) prepared from 120 mg/L analytical grade calcium and magnesium sulfates in de-ionised water. The pH of 7 of the prepared solutions was adjusted using 0.1 M HNO₃ and 0.1 M NaOH and vigorously stirred for 90 minutes, at room temperature (25 °C) [6]. All the experiments were repeated in triplicates and the mean values were reported.

3.4.7.1 Kinetics of adsorption

The adsorption kinetic modelling of the hardness constituents on the PVDF-HFP composite membranes was performed by placing 25 mg of the membranes into 50 mL of the prepared metal (120 mg/L) solutions at various time intervals of 0-180 minutes. At predetermined times, the conical flasks were removed from the shaker and the water samples were analysed using F-AAS. The kinetic parameters of each systems were obtained by nonlinear regression analysis to fit the experimental data with the empirical kinetic models (i.e Lagergren pseudo-first and second-order kinetic model) [3].

Lagergren's pseudo-first-order model and its linearised form are expressed in the equations below [7].

$$q_t = q_t(1 - e^{-k_1 t})$$

$$\ln(q_e - q_t) = \ln q_e - k_1 t$$

Langergren's pseudo-second-order model is as follows:

$$\frac{t}{q_t} = \frac{1}{k_2 q_e^2} + \frac{t}{q_e}$$

where q_t and q_e are the concentrations of Ca(II) and Mg(II) ions adsorbed at equilibrium and at time t respectively in mg/g. k_1 (min^{-1}) and k_2 (g/mg.min) are the pseudo-first and second-order rate constants, respectively.

3.4.7.2 Adsorption isotherm models

The concentrations of the hardness causing agents present in water varies, and this mainly depends on the geological set-up of the aquifer. It is essential to investigate the adsorption capacity of the initial metal ion concentration present in the solutions. The theoretical adsorption capacity of the PVDF-HFP membranes were determined using the nonlinear Langmuir and Freundlich isotherm models [8].

The non-linear equation for the Langmuir isotherm may be expressed as [8]:

$$q_e = \frac{q_{\max} b C_e}{1 + b C_e}$$

$$\frac{1}{q_e} = \frac{1}{q_{\max}} + \frac{1}{b q_{\max} C_e}$$

where q_e and q_{\max} represents the equilibrium adsorption amount and maximum adsorption capacity both in (mg/g) respectively, C_e (mg/L) is the equilibrium concentration of metal adsorbed in the solution, and b (L/mg) is the Langmuir equilibrium constant.

The dimensionless factor R_L , is an important term of Langmuir adsorption isotherm model and can be calculated using the equation below:

$$R_L = \frac{1}{1 + b C_o}$$

where C_o (mg/L) represents the initial concentration of the metal and the Langmuir equilibrium constant for adsorption can be expressed as b (L/mg). The value of R_L indicates the type of Langmuir isotherm to either be unfavourable adsorption ($R_L > 1$), linear ($R_L = 1$), favourable ($0 < R_L < 1$) or irreversible ($R_L = 0$).

Another well-known adsorption model namely Freundlich isotherm can be expressed as [7]:

$$q_e = K_f C_e^{1/n}$$

$$\ln q_e = \ln K_f + \frac{1}{n} \ln C_e$$

where q_e is the equilibrium adsorption amount (mg/g), C_e (mg/L) represents the solute concentration at equilibrium. The Freundlich constants, K_f ($\text{mg}^{1-1/n} \text{L}^{1/n} \text{g}^{-1}$) and n (dimensionless) corresponds to the adsorption capacity and adsorption intensity, respectively.

3.4.7.3 Thermodynamics of adsorption

Thermodynamic analysis was carried out using the equations below [7]:

$$\Delta G^\circ = -RT \ln K_c$$

$$\ln K_c = \frac{\Delta S^\circ}{R} - \frac{\Delta H^\circ}{RT}$$

$$K_c = \frac{C_{ad}}{C_e}$$

where C_e (mg/L) and C_{ad} (mg/L) represents the equilibrium concentration of metal adsorbed in the solution and the concentration of the metal in the adsorbent at equilibrium, respectively. R represents the universal gas constant (8.314 J/mol. K). ΔS° , ΔH° and ΔG° represents changes in standard entropy (J/mol/K), standard enthalpy (kJ/mol) and the standard Gibbs free energy (kJ/mol), respectively. The

values of ΔS° and ΔH° represents the intercept and slope from the plot of $\ln K_c$ versus $1/T$.

3.4.8 Reusability studies

Recycling of the polymeric membranes were carried out by following the Ca(II) and Mg(II) ions adsorption-desorption for three (3) cycles. The spent PVDF-HFP based membranes (25 mg) were immersed in 50 mL of the Ca(II) or Mg(II) solution (120 mg/L) for 90 minutes at room temperature. After 90 minutes, the final concentration of Ca(II) and Mg (II) ions was determined by F-AAS. The saturated PVDF-HFP based membranes were cleaned by air-drying and immersed in 50 mL of 0.1 M NaOH solution for 2 h at 25 °C to remove Ca(II) or Mg(II) (desorption process). Finally, the membranes were separated from the solution and washed with deionised water and dried at 60 °C. The recycling of the spent PVDF-HFP based membranes was repeated 3 times for both hardness constituents [3].

3.5 REAL WATER APPLICATIONS

3.5.1 Water sampling

Water samples were collected from six (6) sites in the Limpopo province, in Botlokwa (**Sekonye, Mokomene, and Ga-Phasha**) and Bochum (**My Darling, Bergendal, and Ga-Machaba**). Before the collection of the samples, high density polyethylene sampling bottles of 1000 mL were soaked in 10% (v/v) HNO_3 for 24 h, thoroughly rinsed with deionised water and left to dry. At the sampling sites, bottles were rinsed with borehole water before collection of the water samples to remove any external factor that might have an impact on water sampling [9].

The samples were collected from the boreholes (ground water) into the sampling bottles through a tap. Immediately after sampling, the pH (Mettler Toledo FE20-Kit FiveEasy™ Benchtop pH Meter) of the water samples was measured and 1% (v/v) HNO_3 was added to preserve all the metal ion content. Water samples were stored in a cooler box containing ice and then transported into the laboratory and placed in the refrigerator. The samples were filtered through with 0.45 μm nylon membranes and

the filtered water samples were stored in the refrigerator at 4°C pending the analysis [9].

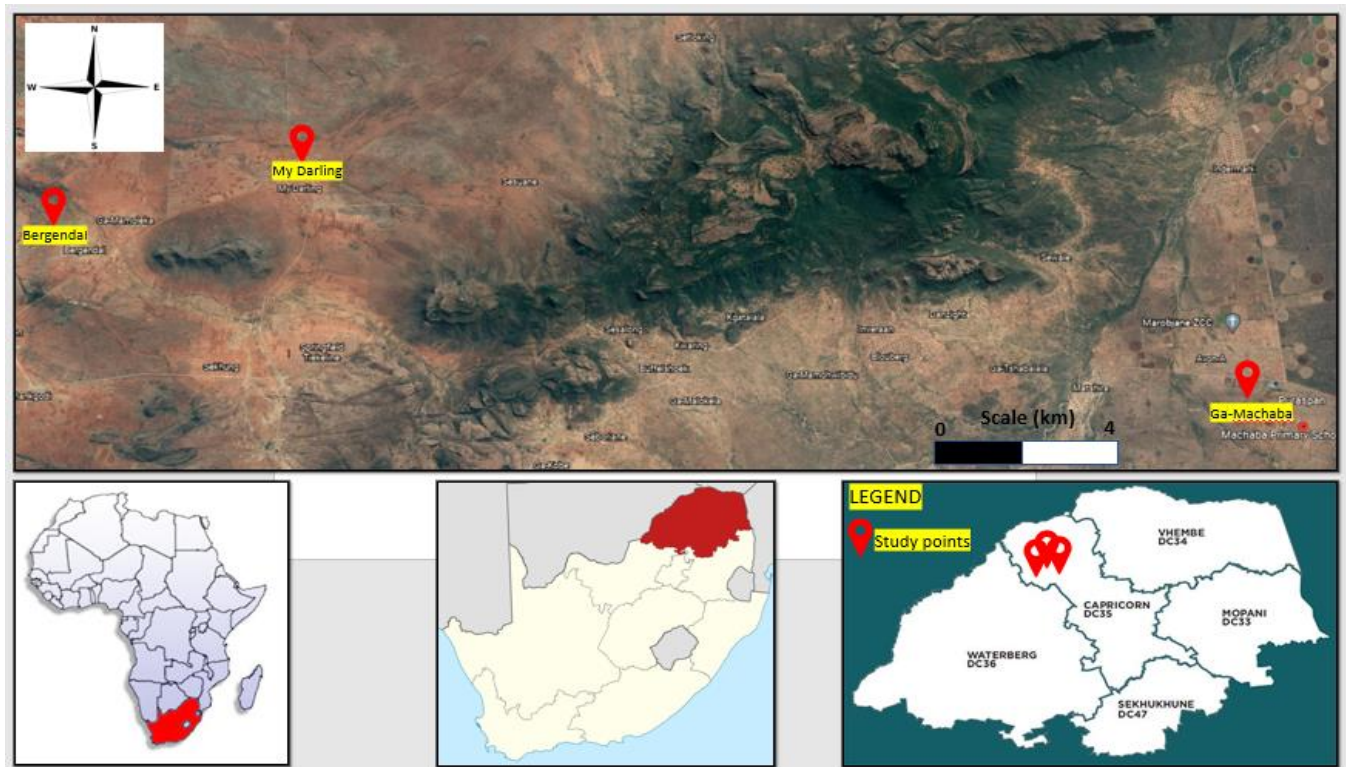
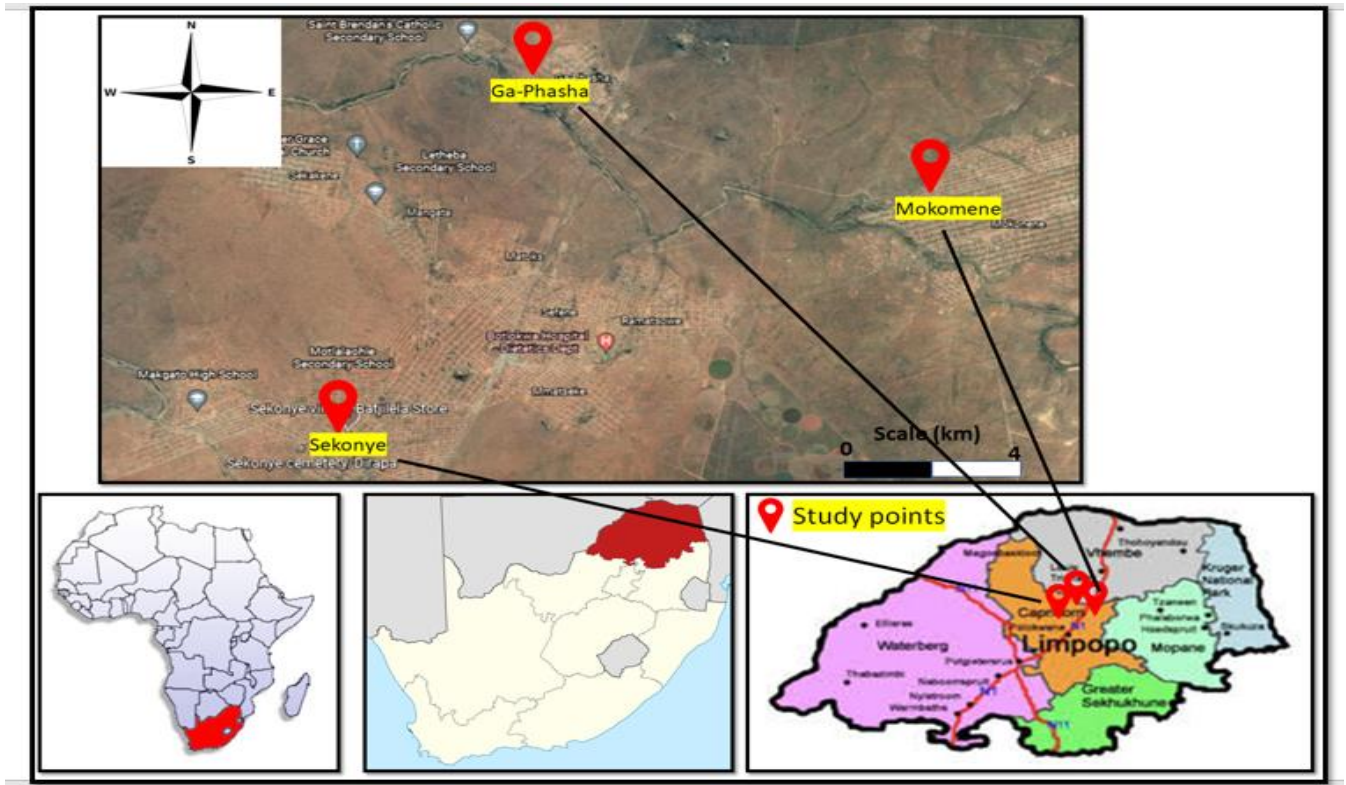


Figure 3.1 [9]: Collection of borehole water samples at (a) Sekonye, (b) Mokomene, (c) Ga-Phasha, (d) My Darling (e) Bergendal and (f) Ga-Machaba in summer season.

3.5.2 Analysis of borehole water samples

Analysis of borehole water samples were carried out before and after membrane adsorption at 25 and 30 °C (i.e optimum temperature). In the first set of analysis, pH of the water samples was not adjusted, and a water bath was used to raise the temperature from 4 to 25 °C. All the water samples at 25 °C, were analysed before and after adsorption process. The second set of analysis was done at 30 °C, firstly a pH meter was used to adjust the pH of 7 using 1 M NaOH and 1 M HNO₃. The temperature was raised from 4 to 30 °C using a water bath. All the water samples at 30 °C, were analysed before and after adsorption process.

The membrane adsorption process was carried out by soaking 25 mg of the 3% PVDF-HFP/CA or 1% N-MWCNTs/CA membranes into 50 mL of the water samples. The pH = 7 of the water samples was adjusted and vigorously stirred for 90 minutes, at 30 °C. The same adsorption method was used to analyse water sample at 25 °C, but the pH was not adjusted. Flame atomic absorption spectroscopy (F-AAS) was used to measure the total concentrations of the analytes of interest, i.e Ca (II) and Mg (II). The samples were analysed in triplicates and the average of the measured values were recorded. The equation below was used to calculate the amount of the adsorbed metal ion.

$$\% \text{ Removal} = \frac{(C_0 - C_e)}{C_0} \times 100'$$

REFERENCES

[1] Macevele, L.E., Moganedi, K.L. and Magadzu, T., 2017. Investigation of antibacterial and fouling resistance of silver and multi-walled carbon nanotubes doped poly (vinylidene fluoride-co-hexafluoropropylene) composite membrane. *Membranes*, 7(3), pp.35.

- [2] Fitri, S.J. and Widiastuti, N., 2017, March. Preparation of polyvinylidene fluoride/cellulose acetate blend membrane with polyethylene glycol additive for apple juice clarification. In *AIP Conference Proceedings* (Vol. 1823, No. 1, pp. 020091). AIP Publishing LLC.
- [3] Muqheet, M., Khaliq, A., Qureshi, U.A., Mahar, R.B., Ahmed, F., Khatri, Z., Kim, I.S. and Brohi, K.M., 2018. Aqueous hardness removal by anionic functionalized electrospun cellulose nanofibers. *Cellulose*, 25(10), pp.5985-5997.
- [4] Werkneh, A.A., Abay, A.K. and Senbeta, A.M., 2015. Removal of water hardness causing constituents using alkali modified sugarcane bagasse and coffee husk at Jijjiga city, Ethiopia: A comparative study. *World*, 1, pp.2.
- [5] Tofighy, M.A. and Mohammadi, T., 2011. Permanent hard water softening using carbon nanotube sheets. *Desalination*, 268(1-3), pp.208-213.
- [6] Sepehr, M.N., Zarrabi, M., Kazemian, H., Amrane, A., Yaghmaian, K. and Ghaffari, H.R., 2013. Removal of hardness agents, calcium, and magnesium, by natural and alkaline modified pumice stones in single and binary systems. *Applied Surface Science*, 274, pp.295-305.
- [7] Ab Kadir, N.N., Shahadat, M. and Ismail, S., 2017. Formulation study for softening of hard water using surfactant modified bentonite adsorbent coating. *Applied Clay Science*, 137, pp.168-175.
- [8] Desta, M.B., 2013. Batch sorption experiments: Langmuir and Freundlich isotherm studies for the adsorption of textile metal ions onto teff straw (*Eragrostis tef*) agricultural waste. *Journal of Thermodynamics*, 2013, pp.6.
- [9] Letsoalo, M.R., Godeto, T.W., Magadzu, T. and Ambushe, A.A., 2018. Quantitative speciation of arsenic in water and sediment samples from the Mokolo River in Limpopo Province, South Africa. *Analytical Letters*, 51(17), pp.2763-2777.

RESULTS AND DISCUSSION

4.1 CHARACTERISATION OF PVDF-HFP COMPOSITE MEMBRANES AND N-MWCNTs

4.1.1 Fourier transform infrared (FTIR) results of PVDF-HFP composite membranes and N-MWCNTs

Figure 4.1 show the FTIR spectra of the pure N-MWCNTs and the membranes made from PVDF-HFP. The FTIR spectrum of the NMWCNTs is shown in Figure 4.1 a. The peak at $1595,1\text{ cm}^{-1}$ is assigned to C = N stretching vibrations, while the other peaks at $1077, 1118,1$ and 1382 cm^{-1} , correspond to the characteristic absorption of the individual CN bonds. The results obtained confirm the presence of nitrogen incorporated in the NTC [1]. The exchange of N atoms instead of C atoms in a carbon lattice with sp^2 bonds has been reported to induce strong IR activity [1]. Consequently, an absorption in the range of $1750 - 1000\text{ cm}^{-1}$ is expected if the N atoms are integrated into the carbon lattice [1]. Several sharp and very strong peaks were observed in the spectrum of the pristine PVDF-HFP membrane. The FTIR spectra of the pure PVDF-HFP membrane showed IR bands at $471, 511, 765, 975, 841, 1278$ and 1401 cm^{-1} , which correspond to the characteristic peaks of (CH_2CF_2) (Figure 4.1 b) [2,3]. The IR bands at $511, 765$ and 975 cm^{-1} can be attributed to the α phase of the PVDF-HFP crystal [2]. The characteristic peaks at 841 cm^{-1} could be attributed to the rocking vibrations of the CH_2 of the β phase of the polymer. The characteristic peak at 471 cm^{-1} confirms the CF wagging vibration of the γ phase of the PVDF-HFP crystals, while the IR bands at 1278 and 511 cm^{-1} are assigned to the bending vibrations and the asymmetric stretching of the CF_2 group [3]. The characteristic peaks of the original PVDF-HFP substrate were obtained in Figure 4.1 c for the 1% NMWCNT / PVDF-HFP based membrane [3]; the introduction of the pure NMWCNTs in the PVDF-HFP casting solution did not give rise to new groups.

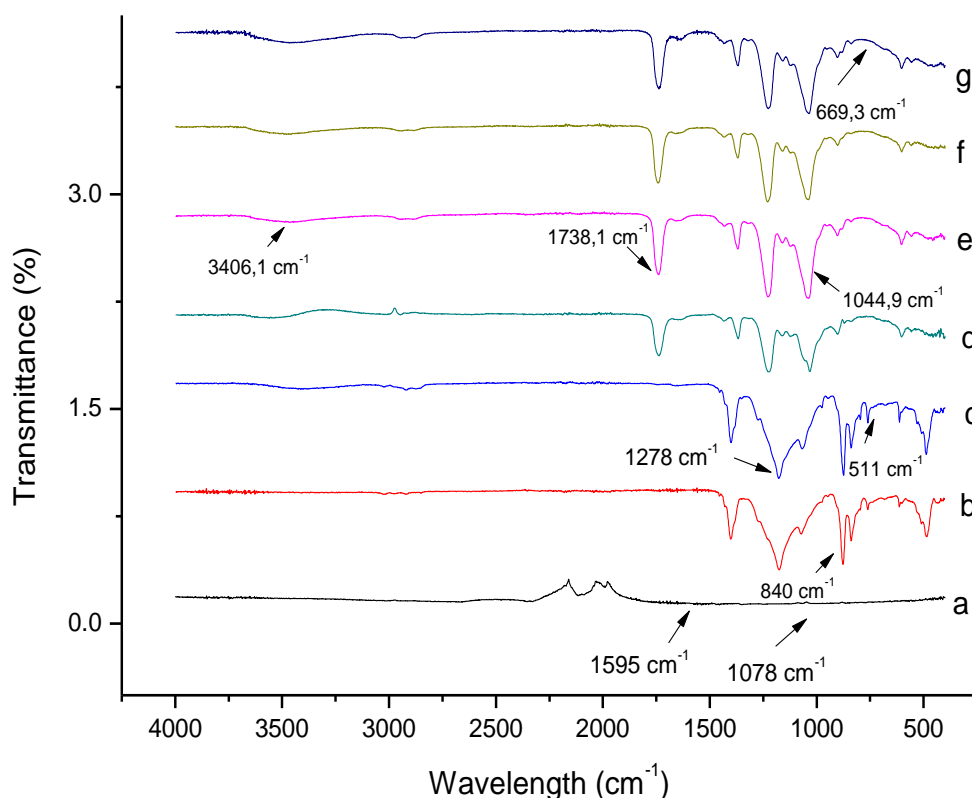


Figure 4.1: FTIR spectra of (a) N-MWCNTs, (b) PVDF-HFP, (c) 1% N-MWCNTs/PVDF-HFP, (d) CA, (e) 3% PVDF-HFP/CA, (f) 1% N-MWCNTs/CA, (g) 1% N-MWCNTs/3 % PVDF-HFP/CA membranes

In figure 4.1 d, there is a weak broad peak at around $3400 - 3000 \text{ cm}^{-1}$ for the CA, this is the representative peak for the cellulose. The IR bands between $1633.3-1738.1 \text{ cm}^{-1}$ from the carbonyl (C=O) vibrational bands, are also observed in the composite membranes presented in figure 4.1 e, f, and g [3]. This is because of high CA content in the membranes. The existence of CA in the composite membranes can further be confirmed by the increased hydroxyl (OH) and the CH_3 stretching between $2918-3406.1 \text{ cm}^{-1}$ and $1370.9-1489.7 \text{ cm}^{-1}$, respectively. The characteristic peaks at 1269.9 , 1044.9 , 669.3 cm^{-1} in figure 4.1 d corresponds to -CH, C-O- ROR' and R-COH groups present in the CA membrane, respectively. The peaks at -CH, C-O-ROR' and R-COH in the CA substrate was also observed in figure 4.1 e, f, and g for (e) 3% PVDF-HFP/CA, (f) 1% N-MWCNTs/CA, (g) 1% N-MWCNTs/3% PVDF-HFP/CA composite membranes, respectively [3]. The blending of the pristine N-MWCNTs and the PVDF-HFP into the CA casting solution did not give rise to new groups in figure 4.1 g for the

1% N-MWCNTs/3% PVDF-HFP/CA composite membrane. All the PVDF-HFP based membranes were prepared successfully. Similar results were also reported in this literature [4,5].

4.1.2 XRD patterns of N-MWCNTs and polymeric membranes

Figure 4.2 demonstrate the XRD patterns of (a) N-MWCNTs, (b) PVDF-HFP/CA, (c) CA, (d) 3% PVDF-HFP/CA, (e) 1% N-MWCNTs/CA, (f) 1% N-MWCNTs/PVDF-HFP/CA. From the XRD patterns, the peak at $2\theta = 26^\circ$ is associated with the (002) diffractions of the hexagonal graphite structures in the pristine N-MWCNTs (figure 4.2 a) [7]. Figure 4.2 b of pure PVDF-HFP membrane show predominant broad peaks at $2\theta = 20$ and 38° which can be attributed to the (020) and (021) crystalline peaks of the polymer. The presence of the broad peaks in figure 4.2 b confirms the semi-crystalline nature of PVDF-HFP in which crystalline phase is mixed with the amorphous region [8].

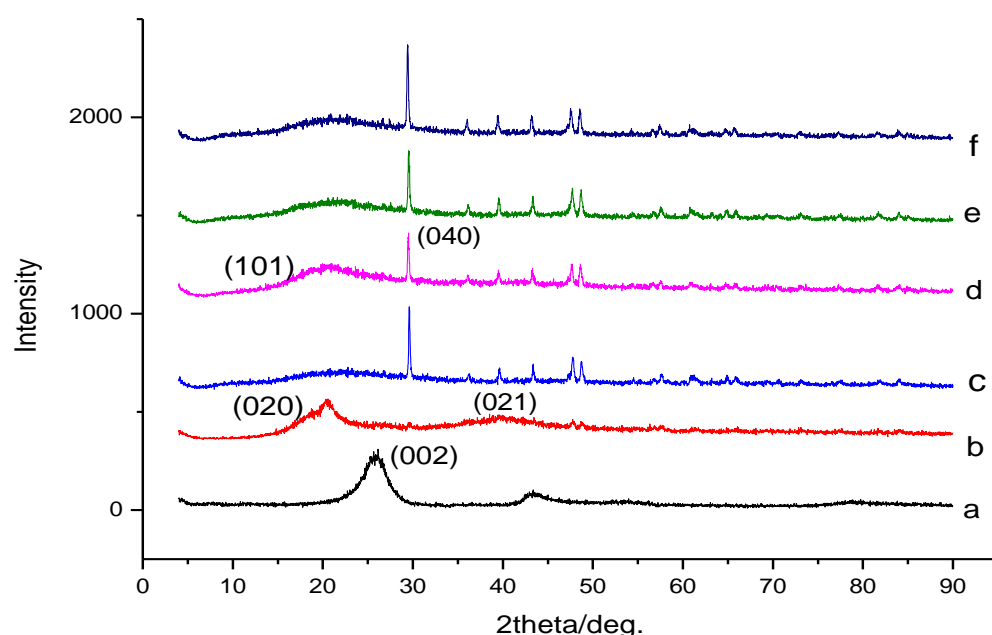


Figure 4.2: XRD patterns of (a) N-MWCNTs, (b) PVDF-HFP, (c) CA, (d) 3% PVDF-HFP/CA, (e) 1% N-MWCNTs/CA, (f) 1% N-MWCNTs/PVDF-HFP/CA.

In figure 4.2 c, CA shows diffraction pattern peaks at $2\theta = 14.9, 16.1, 22.2,$ and 34.8° which are assigned to the diffraction planes 101, 101, 002, and 040, respectively. A

shoulder peak at 16.1 and 34.8° confirms the lignin and hemicellulose groups. The weak diffraction peaks appear at around 10.6°, in the diffraction patterns of CA, which further confirms the crystalline nature of the polymer. Furthermore, the diffraction peak at around $2\theta = 19.7^\circ$, can be attributed to the less ordered or amorphous region of the cellulose chains [9]. The diffraction patterns of the initial CA substrate were also preserved in figure 4.2 d, e, and f for the 3% PVDF-HFP/CA, 1% N-MWCNTs and 1% N-MWCNTs/3% PVDF-HFP/CA composite membranes, respectively. This is because of high CA content in the membranes. Introducing either N-MWCNTs or the PVDF-HFP into the CA casting solution did not introduce new groups in the composite membranes [9].

4.1.3 Thermogravimetric analysis results of PVDF-HFP blended membranes and N-MWCNTs

Figure 4.3 shows the thermal stability of N-MWCNTs and PVDF-HFP composite membranes in terms of weight loss (%) as a function of temperature (° C). The thermal stability of the polymeric membranes over a range of temperature plays a vital role to determine their operational conditions and working temperature limits prior to their use in practical applications e.g industrial applications [10]. As presented in figure 4.3 a, there was no weight loss for the pristine N-MWCNTs, and the results indicates that these nanomaterials are thermally stable up to 800 °C [11]. The TGA thermograms for the membranes presented in figure 4.3 b and c shows a distinct single step weight loss with a high temperature shoulder for PVDF-HFP and 1% N-MWCNTs/PVDF-HFP membranes only. The thermal stability of the PVDF-HFP membranes is strengthened by the repeating CF₂ units. A single weight loss observed at around 420 to 470 °C is attributed to the decomposition of the polymeric backbone units (i.e PVDF matrix) [5, 12]. The extraction of the HFP unit results in carbonization of the polymer and the polymer cross-linking at higher temperatures. It can be observed in figure 4.3 e and g that the thermal stability of PVDF-HFP after CA modification significantly improves, maintaining the structural integrity even at lower temperature (i.e., 200 °C) [5]. Blending the pristine N-MWCNTs into the CA casting solution did not record any significant change to the thermal behaviour of the 1% N-MWCNTs/CA composite membrane (figure 4.3 f). The 3% PVDF-HFP and 1% N-MWCNTs/3% PVDF-HFP/CA composite membranes decompose through three stages: the first stage is the

extraction of moisture (before 200 °C, shown in figure 4.3 e and g); the second stage is the cellulose decomposition which covers temperatures above 350 °C, the third stage corresponds to the decomposition of PVDF-HFP above 464 °C, which contributes the major weight loss of about 60 % [5].

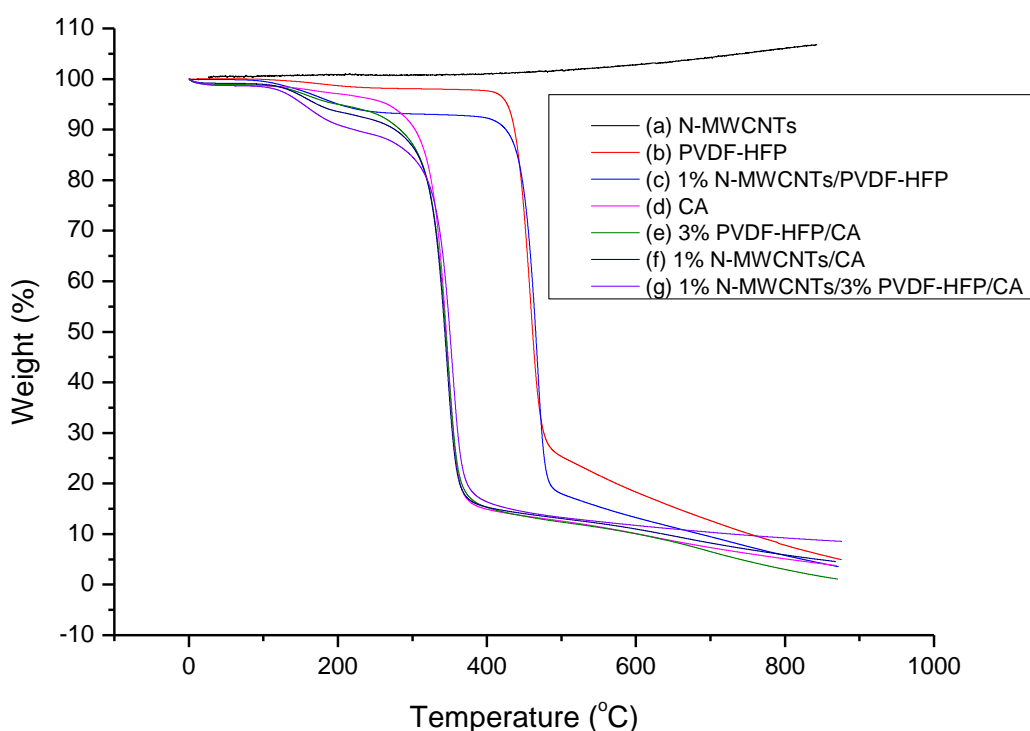


Figure 4.3: TGA curves of (a) N-MWCNTs, (b) PVDF-HFP, (c) 1% N-MWCNTs/PVDF-HFP, (d) CA, (e) 3% PVDF-HFP/CA, (f) 1% N-MWCNTs/CA, and (g) 1% N-MWCNTs/3% PVDF-HFP/CA membranes

The TGA thermograms of CA, 3% PVDF-HFP/CA, 1% N-MWCNTs/CA and 1% N-MWCNTs/3 % PVDF-HFP/CA composite membranes in figure 4.3 d, e, f, and g started to decompose at low temperature between 300 and 400 °C, this could be related to the evaporation of moisture and residual solvents in the membranes [8]. Decomposition of CA in all the membranes occurs in three steps. The first step constitutes the deacetylation and evaporation of residual absorbed water molecules from 30 to 330 °C. The degradation of the pyrose ring in CA results from the exclusion of the secondary acetate groups. The second step represents the volatilization of the volatile matter formed because of the scission of the glycosidic bond of CA and starts from 330 °C to 400 °C. This phase is regarded as the major decomposition step in CA

and this massive degradation results from the extensive loss of carbon oxides and acetic acids. The final step symbolizes the carbonization of the decomposed matter to ash and starts at 400 °C. These three (3) stages may correspond to the steps reported in the literature [9], representing the thermal degradation of CA. Blending the N-MWCNTs into the 3% PVDF-HFP/CA casting solution did not record any significant change to the thermal behaviour of the 1% N-MWCNTs/3% PVDF/CA composite membrane (figure 4.3 g) [11].

4.1.4 TEM images of pristine N-MWCNTs

Figure 4.4 shows typical TEM micrographs of pristine N-MWCNTs at four different magnifications. The micrograms observed in figure 4.4 a, b, and c shows that the N-MWCNTs have a hollow channel morphology and are multi-walled while the micrographs observed in figure 4.4 d clearly shows that these nanomaterials are multi-walled carbon nanotubes and bamboo-shaped as reported and explained in previous works [13,14,15].

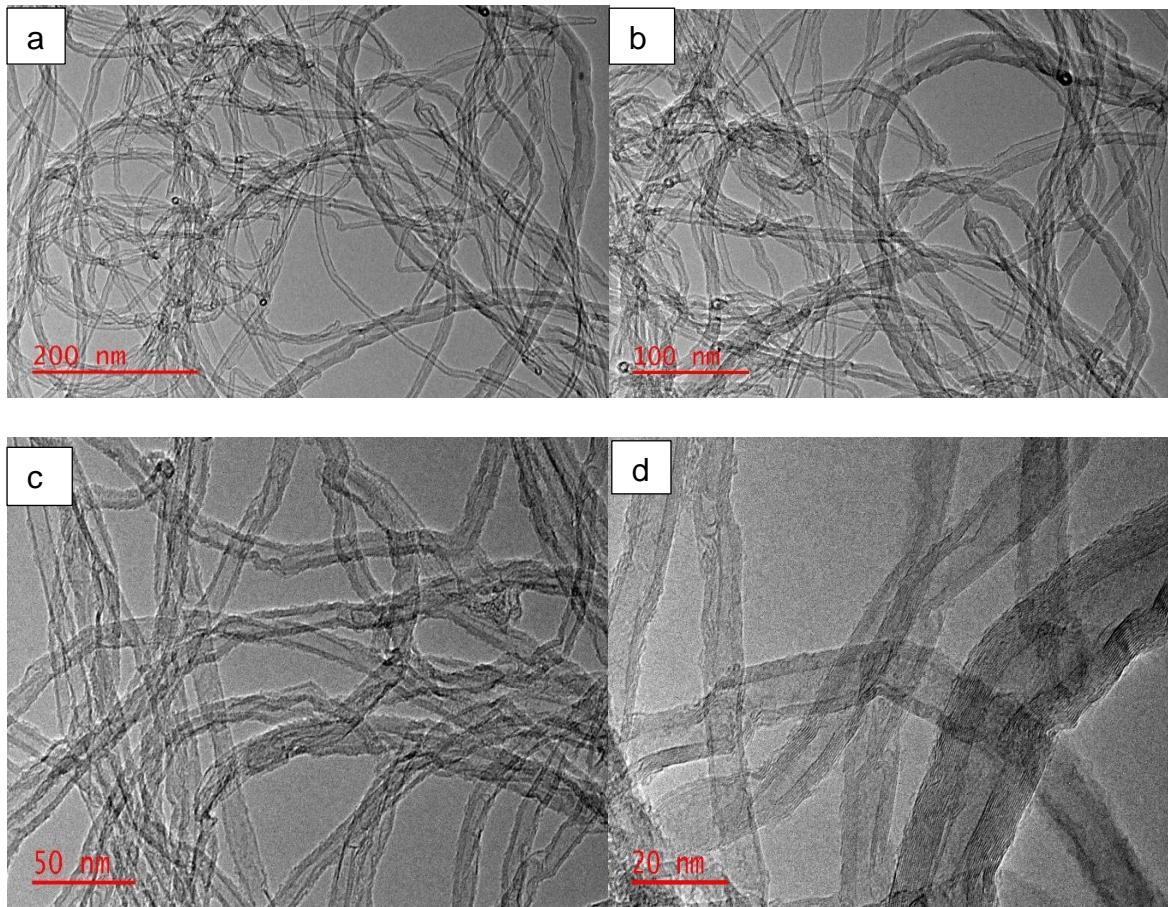


Figure 4.4: TEM images of pure N-MWCNTs(a-d) at different magnifications

In addition, the formation of bamboo-like structure and the presence of very defective and less aligned parts in the walls of N-MWCNTs can be explained by the presence of the nitrogen atoms, bringing about drastic local distortions within the hexagonal graphitic-based structure [15].

4.1.5 SEM images of PVDF-HFP based membranes and N-MWCNTs

The surface morphology of the PVDF-HFP composite membranes and N-MWCNTs was examined by SEM analysis and the images were shown in figure 4.5. SEM images of the pristine N-MCNTs are presented in fig 4.4 a. The surface morphology of these nanomaterials reveals an irregular shape of particles with a low degree of agglomeration [16]. SEM images of the pristine PVDF-HFP membrane presented in figure 4.5 b reveals some small pores distributed uniformly [17], while the SEM images demonstrated in figure 4.5 c shows a porous and dense surface layer of CA membrane, [4] with agglomerates on the surface. This could probably be due to the intermolecular interaction of the hydrogen bonding present in the CA molecules. Figure 4.5 d presents a solidified and dense membrane surface of the 1% N-MWCNTs/PVDF-HFP composite membrane upon the addition of the pristine N-MWCNTs into the PVDF-HFP casting solution. The surface morphology of 3% PVDF-HFP/CA, 1% N-MWCNTs/CA and 1% N-MWCNT/3% PVDF-HFP/CA blended membranes in figure 4.5 e, f and g became irregular, and have appeared to form porous-like holes upon the introduction of PVDF-HFP or N-MWCNTs onto the CA casting solution. This type of morphology has been reported to have a high contact surface, and a greater adsorption performance.

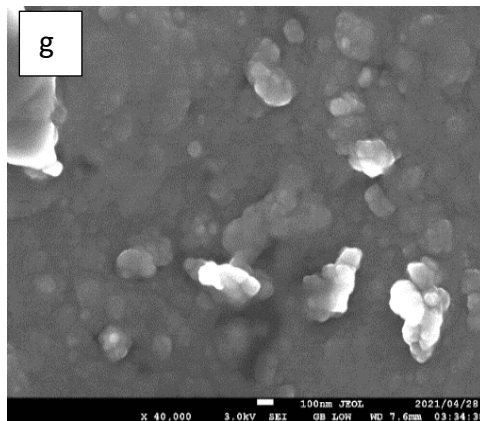
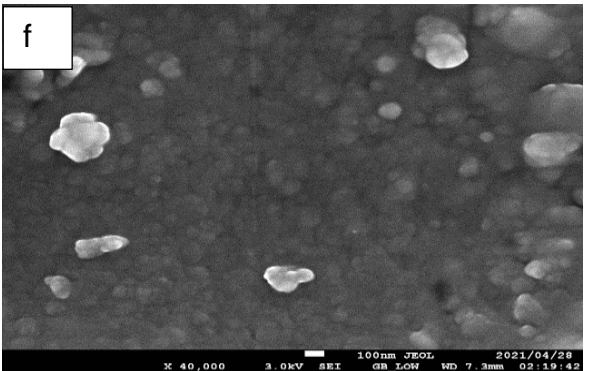
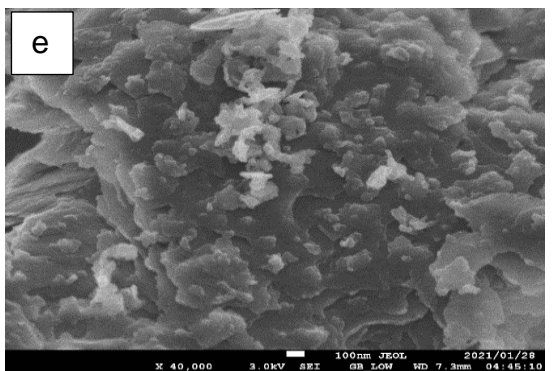
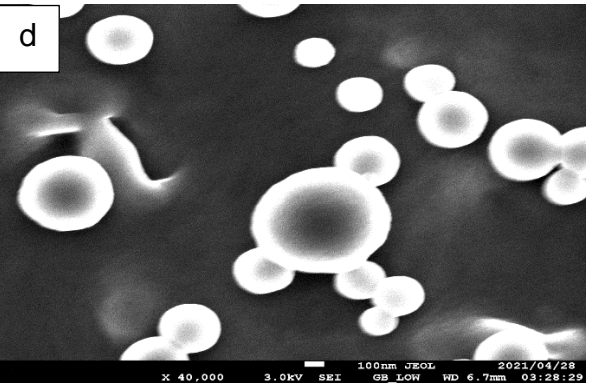
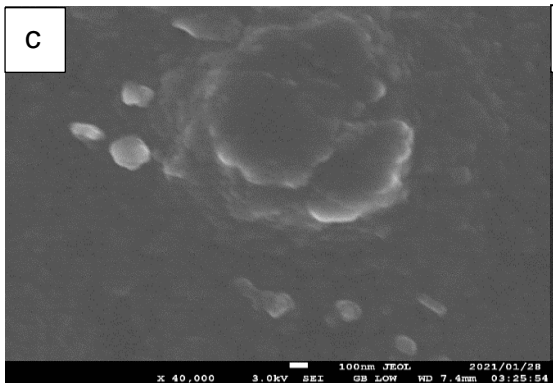
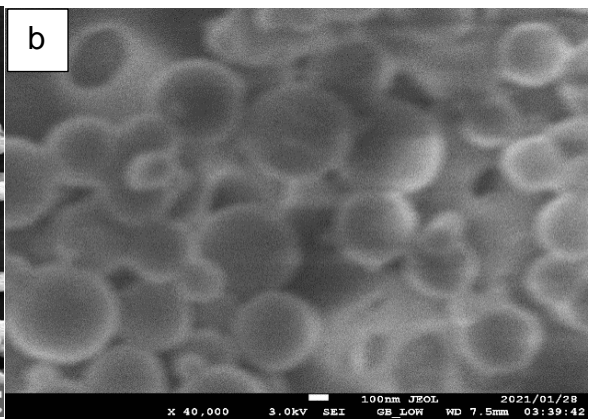
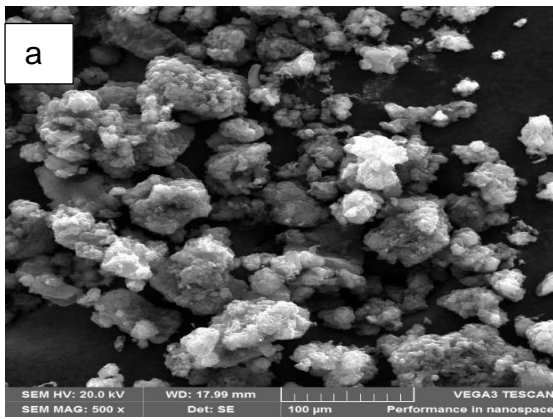


Figure 4.5: SEM images of (a) N-MWCNTs, (b) PVDF-HFP, (c) CA, (d) 1% N-MWCNTs/PVDF-HFP (e) 3% PVDF-HFP/CA, (f) 1% N-MWCNTs/CA, and (g) 1% N-MWCNTs/3% PVDF-HFP/CA membranes.

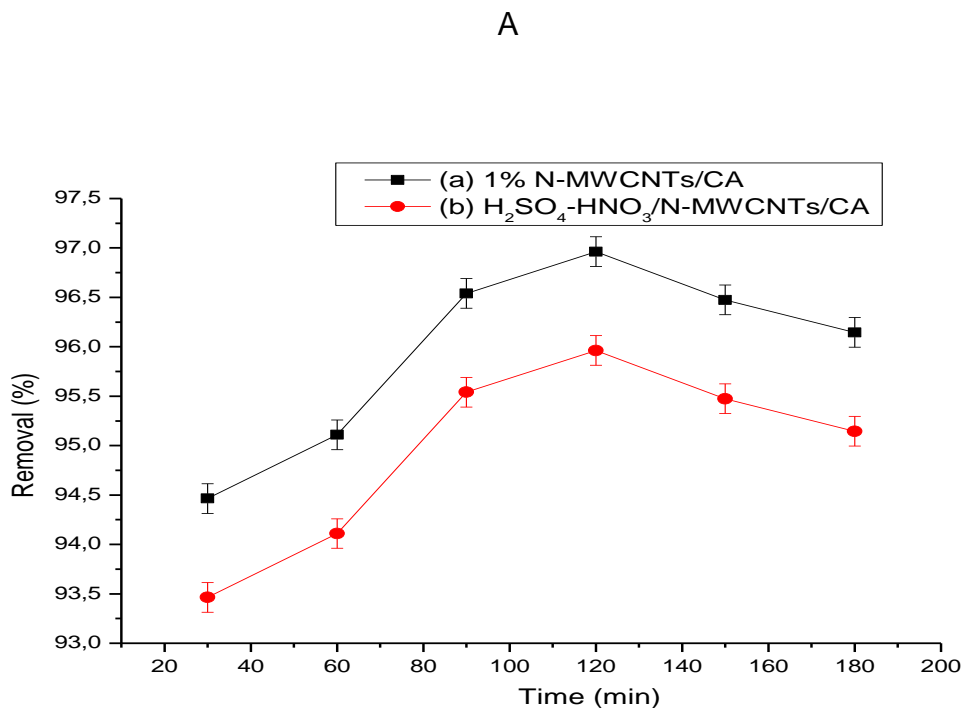
The small active dense layer observed on the surfaces of the polymeric membrane presented in figure 4.5 b, d, e, and g shows that the membranes are asymmetric, and the degree of tortuosity might influence the membranes permeate flux. Nevertheless, in figure 4.5 e, f and g, the heterogeneous layers of CA were observed on the membrane surfaces which indicates the presence of bulk CA molecules onto the 3% PVDF-HFP/CA, 1% N-MWCNTs/CA and 1% N-MWNTs/3% PVDF-HFP/CA based membranes [18]. Furthermore, the blending of CA has been reported to enhance the membrane hydrophilicity which can provide a high permeate flux [3]. These results indicates that all the PVDF-HFP composite membranes were prepared successfully.

4.2 ADSORPTION STUDIES

4.2.1 Batch adsorption studies of Ca (II) metal ions

4.2.1.1 Effect of acid treated and non-treated N-MWCNTs doped CA composite membrane on the hardness removal

Figure 4.6 demonstrates the effect of acid treated and non-treated N-MWCNTs/CA based membranes on the adsorption of A (Ca (II)) and B (Mg (II)) ions. The pristine N-MWCNTs were functionalised using sulfuric and nitric acids in 3:1 ratio. The results show that blending of the functionalised N-MWCNTs into CA did not enhance the adsorption uptake of both metal ions. The H₂SO₄-HNO₃/N-MWCNTs/CA composite membrane yields lower adsorption uptake of approximately 93.50% and 90% for Ca (II) and Mg (II) in 30 minutes, respectively. The removal efficiency for both metal ions using the 1% N-MWCNTs/CA composite membrane are higher as compared to H₂SO₄-HNO₃/N-MWCNTs/CA composite membrane. The non-treated N-MWCNTs were selected for the remaining tests because functionalisation of the pristine N-MWCNTs did not enhance the adsorption efficiency of the metal ions as can be seen in figure 4.6.



B

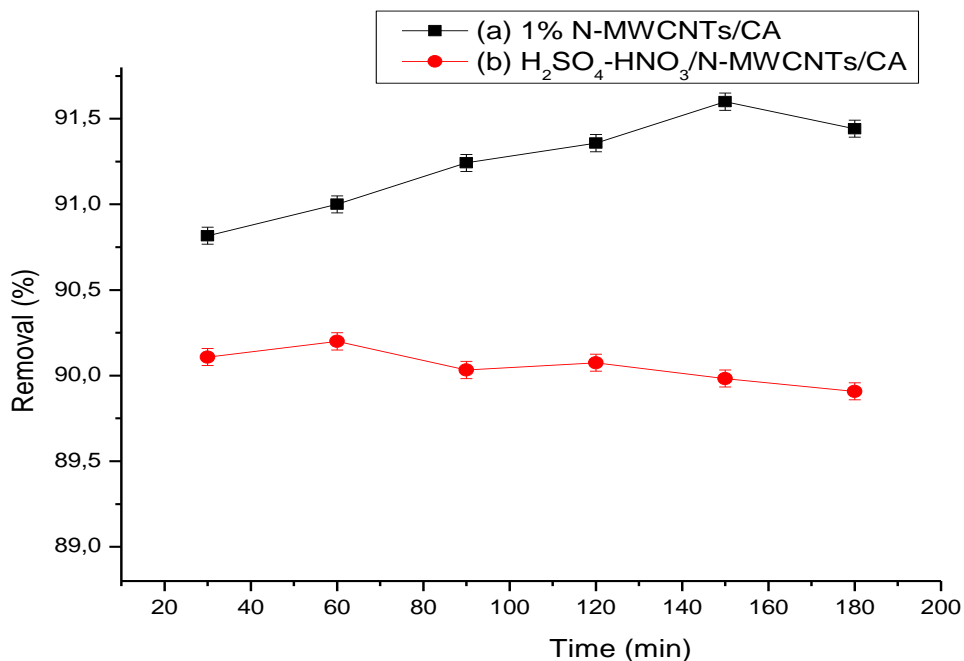


Figure 4.6: Effect of acid treated and non-treated N-MWCNTs/CA composite membranes on the removal of A (Ca (II)) and B (Mg (II)) ions

4.2.1.2 Effect of pH on Ca (II) metal ions removal onto PVDF-HFP membrane

Figure 4.7 demonstrates the effect of pH on the adsorption of Ca(II) metal ions onto PVDF-HFP membrane. The solution pH plays an important role on the sorption of the adsorbate by the adsorbent. The graph shows that the removal of Ca(II) increased from 74.5 to 79.5% as the pH increases from 5 to 7, respectively. At pH beyond 7 (i.e. 7.5) the adsorption of the metal ion starts to decrease. Higher removal efficiency of PVDF-HFP for the metal ion was achieved at neutral pH (6.8-7.0) as compared to the acidic and basic media, which is in agreement with the results shown in figure 4.7 a. The lower removal percentages at the acidic pH ($\text{pH} < 7$) can be attributed to the competition of the H^+ with the hardness agent to bind and occupy the active sites of the membrane or a prolonged protonation of the adsorbent functional groups due to the addition of the 0.1 M HNO_3 to reduce the solution pH. On the other hand, at an alkaline media ($\text{pH} > 7$), the lower removal of Ca(II) can be attributed to the formation of the OH^- group which originates from the addition of 0.1 M NaOH to increase the solution pH. As a result, there is a formation of metal hydroxide to bind and occupy the active sites on the membrane surface hindering the adsorption of Ca(II) metal ions,

hence a lower percentage removal is observed [19]. The pH value of 7.00 was selected for the remaining tests.

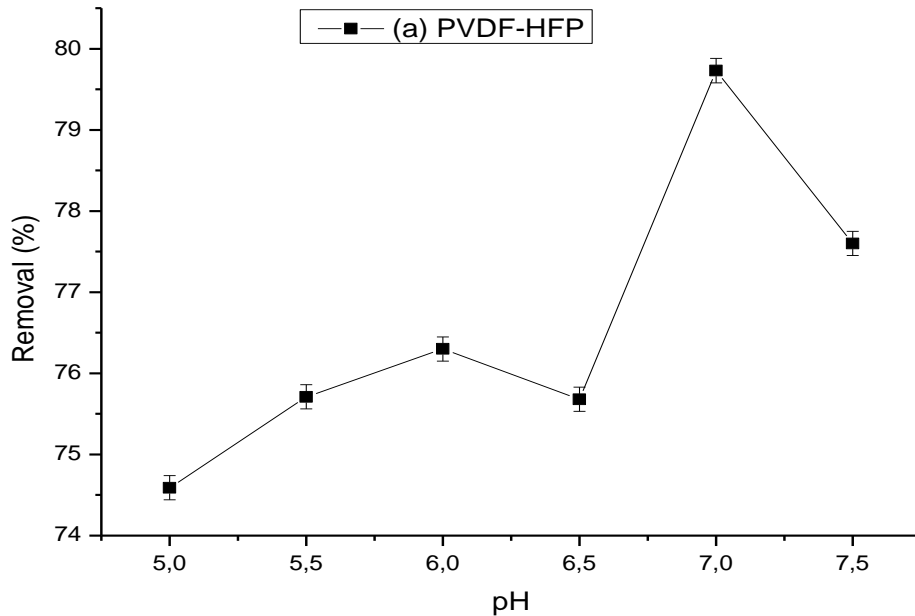


Figure 4.7: Effect of pH on the adsorption of Ca (II) metal ions onto PVDF-HFP membrane

4.2.1.3 Effect of membrane adsorbent dosage

The effect of membrane adsorbent dosage on the softening of Ca(II) hardness was investigated and the results are presented in figure 4.8. The membrane adsorbent dose was varied from 0.1 – 0.9 mg/L and it was observed that the removal efficiency increased with an increase in adsorbent dose up to 0.5 mg/L where further dose increases yielded negligible adsorption of Ca(II) [20]. The maximum adsorption uptake of Ca(II) ions was 70.33, 62.02, and 80.38% for CA, PVDF-HFP and 3% PVDF-HFP/CA membranes using 0.5 mg/L dose respectively. This is because when the sorbent mass increases, the number of active sites on the sorbent material also increases thereby resulting in an increase of Ca(II) adsorption by the polymeric membranes from the aqueous solutions [21]. Interestingly, a slight increase on the Ca(II) removal was observed when CA was added on PVDF-HFP. The highest adsorption of 80.38% was observed on 3% PVDF-HFP/CA composite membrane,

better than the adsorption percentage reported in literature [21]. The selected dose for Ca (II) removal for all the adsorption experiments was 0.5 mg/L, immediately after this optimum dosage the removal efficiency for all the membranes started to decrease. According to Rolence et al., [20] after a certain adsorbent dose, the maximum adsorption is attained and hence the number of ions remain constant with further addition of adsorbent dose. Furthermore, the initially deposited Ca(II) metal ions penetrate to the interior of the membranes through the intra-particle diffusion process which was a slower process hence the removal was lower for all the membranes.

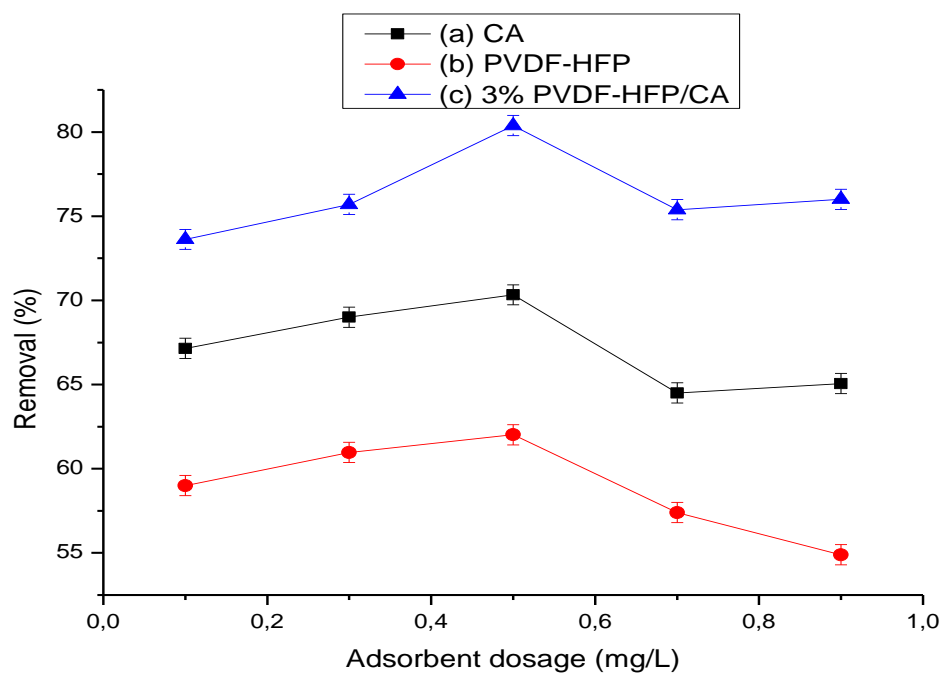


Figure 4.8: Effect of membrane adsorbent dosage on Ca(II) ions adsorption onto PVDF-HFP composite membranes

4.2.1.4 Effect of contact time on adsorption of Ca (II) onto polymeric membranes

Figure 4.9 shows the effect of time on the adsorption of Ca(II) by various polymeric membranes. The data reveals that within the first 30 minutes of adsorption, removal of >90 % was achieved for all the polymeric membranes and these remained almost constant until 180 minutes was reached. This is because, at the beginning of adsorption process there are many vacant adsorption sites which are available for

adsorption, adsorption then slightly reduces, approaching equilibrium as the adsorption sites of the membrane are all covered [21]. These results demonstrate that PVDF-HFP membrane alone gave the lowest Ca (II) ions removal, with approximately 95 % followed by CA, 1% N-MWCNTs/PVDF-HFP, 1% N-MWCNTs/CA and 1% N-MWCNTs/3% PVDF-HFP/CA membranes.

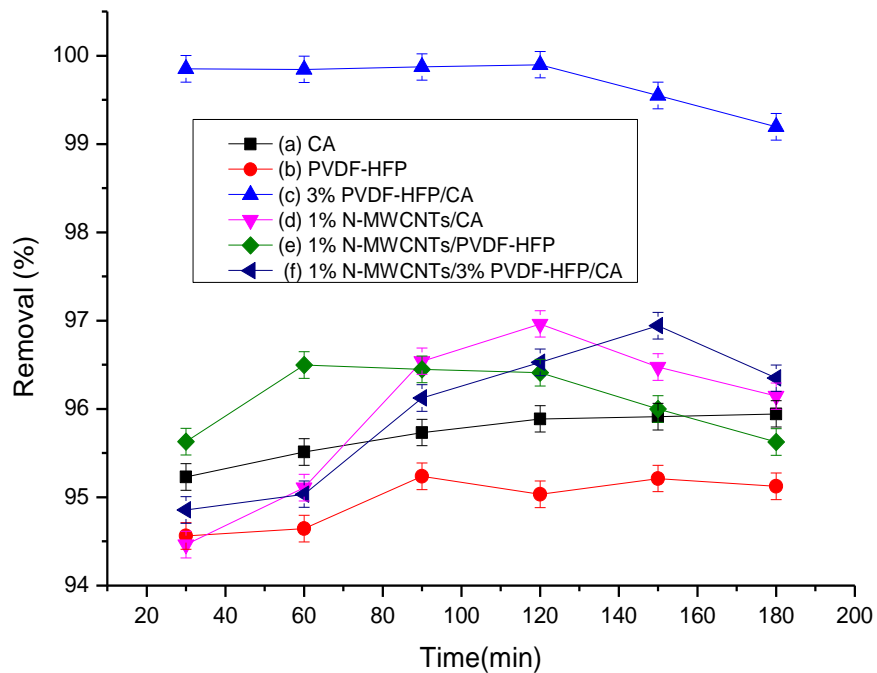


Figure 4.9: Effect of contact time on adsorption efficiency of Ca (II) ions onto (a) CA, (b) PVDF-HFP, (c) 3% PVDF-HFP/CA, (d) 1% N-MWCNTs/CA, (e) 1% N-MWCNTs/PVDF-HFP and (f) 1% N-MWCNTs/3% PVDF-HFP/CA composite membranes.

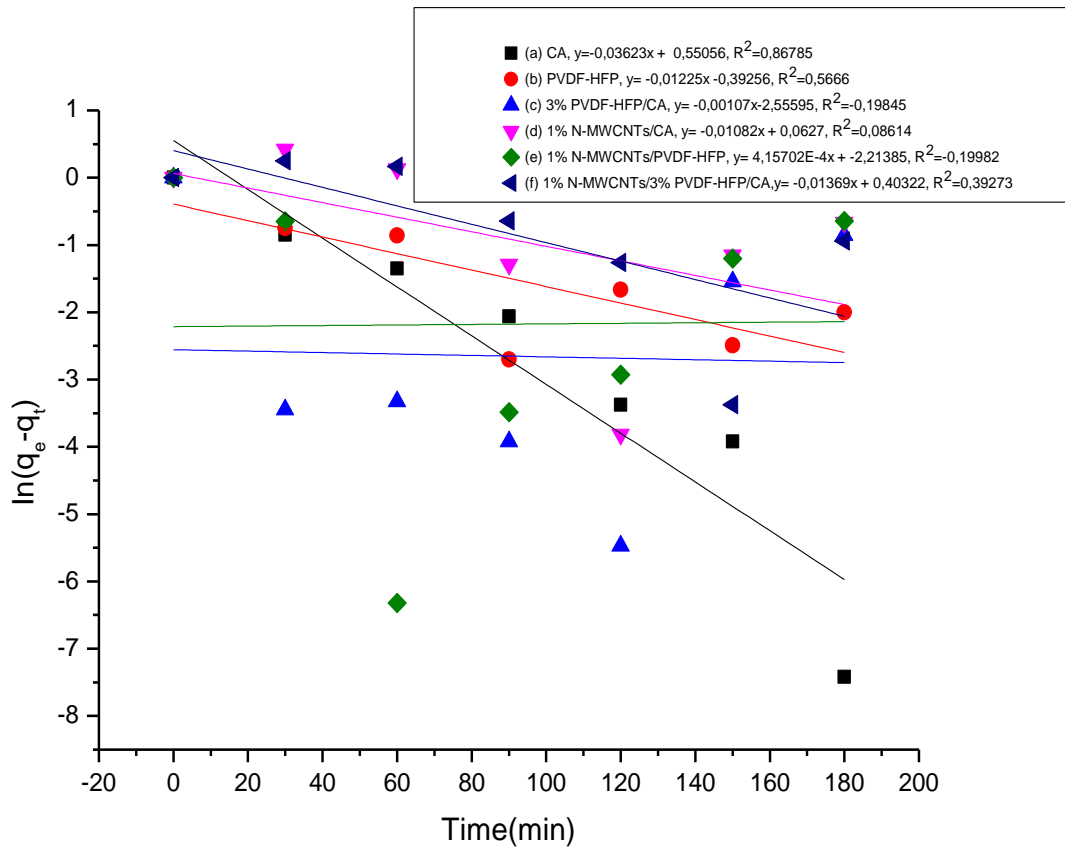
The highest adsorption of approximately 99.00 % was observed on 3% PVDF-HFP/CA composite membrane for Ca(II) ions, which exceeds the rest of the other membranes presented in figure 4.9. Ideally, one would have expected the 1% N-MWCNTs/3% PVDF-HFP/CA composite membrane to give the highest Ca (II) ions removal, because it consists of the CA, PVDF-HFP and the N-MWCNTs as compared to the other membranes. This was not the case; a slight decrease on the Ca (II) ions was observed when the N-MWCNTs were added on 3% PVDF-HFP/CA. The selected optimum time for the removal of Ca(II) was 90 minutes. The results are better as compared to the ones reported in the literature [21]. Furthermore, the results for the effect of contact

time on the removal efficiency of Ca(II) ions using the PVDF-HFP based membranes over a period of 24 and 48 hours are shown in appendix 1.

4.2.1.5 Kinetics of adsorption for Ca(II) metal ions removal by polymeric membranes

Figure 4.10A and 4.10B describes the pseudo-first order and pseudo-second-order kinetic model behaviour for the adsorption of Ca(II) ions onto the polymeric membranes, respectively. Kinetic study is important to estimate the adsorption rate, and this can be described by the two kinetic models [22]. The sorption rate parameters (K_1 , K_2 and q_e) along with correlation coefficients (R^2) for the pseudo-first and pseudo-second order are shown in table 4.1. As can be seen from table 4.1, the rate constant of pseudo-second order, K_2 , values are higher than the pseudo-first order. The theoretical and experimental values of the equilibrium adsorption capacity, q_e , for the pseudo-second order kinetic model are closer to each other for all the polymeric membranes meaning that the adsorption process follows the pseudo-second-order process. The high values of the correlation coefficients (R^2) also confirmed that the adsorption process follows a pseudo-second-order process. It can be observed that the pseudo-second-order kinetic model yields a better fit than the pseudo-first-order kinetic model [22].

A



B

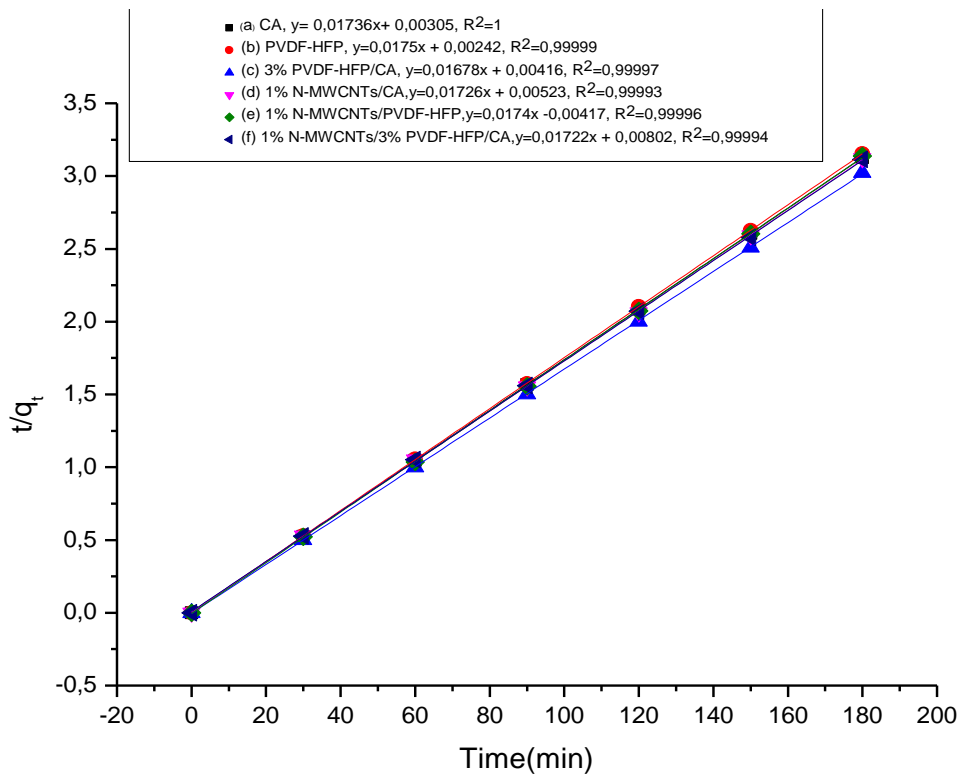


Figure 4.10: Pseudo-first order (A) and Pseudo-second order (B) kinetic model for adsorption of Ca (II) ions on (a) CA, (b) PVDF-HFP, (c) 3% PVDF-HFP/CA, (d) 1% N-MWCNTs/CA, (e) 1% N-MWCNTs/PVDF-HFP and (f) 1% N-MWCNTs/3% PVDF-HFP/CA composite membranes.

Table 4.1: Kinetics parameters for Ca (II) ions adsorption onto PVDF-HFP composite membranes

Membrane	q_e (mg/g)	Pseudo-first order Kinetic model			Pseudo-second order Kinetic model		
		K_1 (min^{-1})	q_e (mg/g)	R^2	K_2 (g/mg. min)	q_e (mg/g)	R^2
CA	57.57	0.04	1.73	0.87	0.10	57.60	1.00
PVDF-HFP	57.21	0.01	0.68	0.57	0.13	57.14	1.00
3% PVDF-HFP/CA	59.94	0.00	0.08	-0.20	0.07	59.60	1.00
1% N-MWCNTs/CA	58.20	0.00	1.06	0.09	0.06	57.94	1.00
1% N-MWCNTs/PVDF-HFP	57.90	4.16E-4	0.11	-0.20	0.07	57.47	1.00
1% N-MWCNTs/3% PVDF-HFP/CA	58.20	0.01	1.50	0.39	0.04	58.07	1.00

4.2.1.6 Effect of concentration on the adsorption of Ca(II) by various polymeric membranes

The data presented in figure 4.11 shows the effect of concentration on the adsorption of Ca(II) metal ion onto PVDF-HFP based membranes. When the concentration increased from 100-1200 mg/L, the removal efficiency of Ca(II) increased significantly for 3% PVDF-HFP/CA and 1 % N-MWCNTs/CA composite membrane (figure 4.11 a and b) as compared to the other two membranes. The stability (surface saturation) for 1% N-MWCNTs/PVDF-HFP and 1% N-MWCNTs/3% PVDF-HFP composite membranes in figure 4.10 c and d was reached faster at approximately 300 ppm, while the surface saturation for 3% PVDF-HFP and 1% N-MWCNTs/CA was reached at around 600 – 1200 ppm. These results demonstrate that 1% N-MWCNTs/PVDF-HFP based membrane gave the lowest Ca(II) ions removal, with approximately 92% followed by 1% N-MWCNTs/3% PVDF-HFP/CA membranes. The highest adsorption of approximately 99.00% was observed on 3% PVDF-HFP/CA composite membrane for Ca(II) ions, which exceeds the rest of the other membranes presented in figure 4.10. Interestingly, the removal efficiency for all the polymeric membranes exceeds 89 % from the lower concentration to higher.

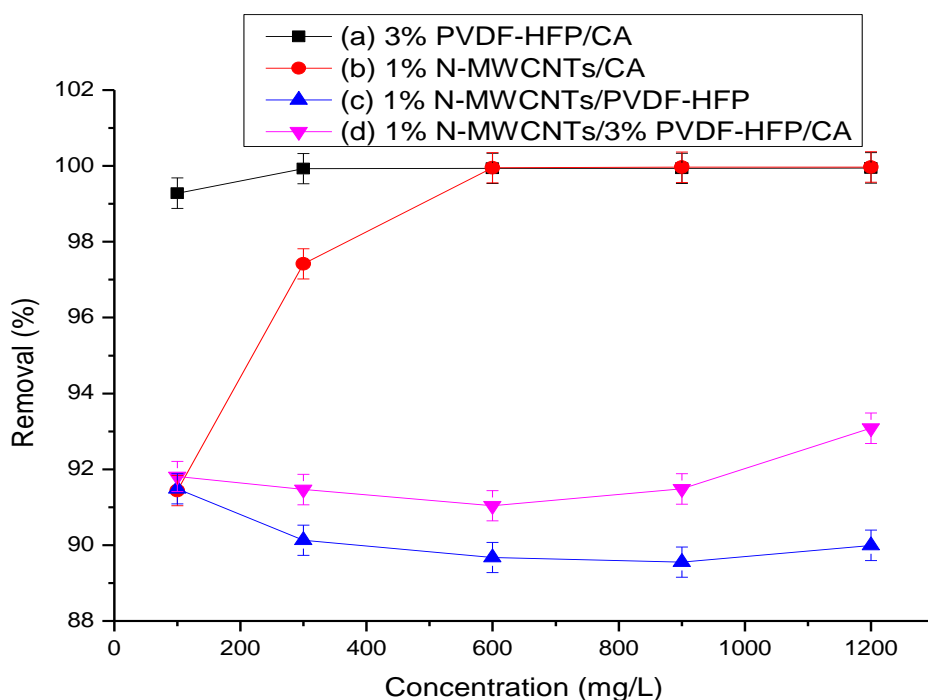


Figure 4.11: Effect of initial metal ion concentration on the adsorption efficiency of Ca (II) ions onto (a) 3% PVDF-HFP/CA, (b) 1% N-MWCNTs/CA, (c) 1% N-MWCNTs/PVDF-HFP and (d) 1 % N-MWCNTs/3% PVDF-HFP/CA composite membranes

These high adsorption results for the composite membranes presented in figure 4.11 are better as compared to a study conducted by Werkneh et al., [21] their study focussed on the synthesis and application of alkali modified sugarcane bagasse and coffee husk for removal of water hardness causing agents. They have observed removal efficiency of 97% and 94.10% for an initial Ca(II) ion concentration of 120 mg/L using a 2 g/L adsorbent dosage and a pH of 6.5 at room temperature [21]. Furthermore, other membranes were also studied, and the results are presented in appendix 2.

4.2.1.7 Effect of temperature

Effect of temperature on the adsorption of Ca(II) metal ions onto various polymeric membranes was studied by conducting different set of experiments at 20, 25, 30 and 35 °C and the results are presented in figure 4.12. It can be observed that increasing the temperature from 20 – 35 °C, increases the removal efficiency of the polymeric

membranes. The higher removal efficiency and adsorption rate results from the increase in thermal energy of the adsorbing material (i.e membranes). Rolence *et.al.* [20] has reported that, an increase in temperature results in swelling of the adsorbent that in turn opens more active sites available for hardness ions adsorption. Furthermore, the adsorption of Ca(II) by the polymeric membranes is endothermic because adsorption increases with the increase in temperature. The highest adsorption of approximately 97.00% was observed on 3% PVDF-HFP/CA composite membrane for Ca (II) ions at 30 °C (figure 4.12 a), which exceeds the rest of the other composite membranes presented in figure 4.12 b and c. Interestingly, the addition of CA increased the thermal energy of PVDF-HFP, hence the adsorption uptake of Ca(II) increased slightly. Similar trend of results was reported elsewhere [22]. The optimum temperature of 30 °C was selected for the remaining adsorption experiments. Furthermore, other membranes were also studied, and the results are presented in appendix 3.

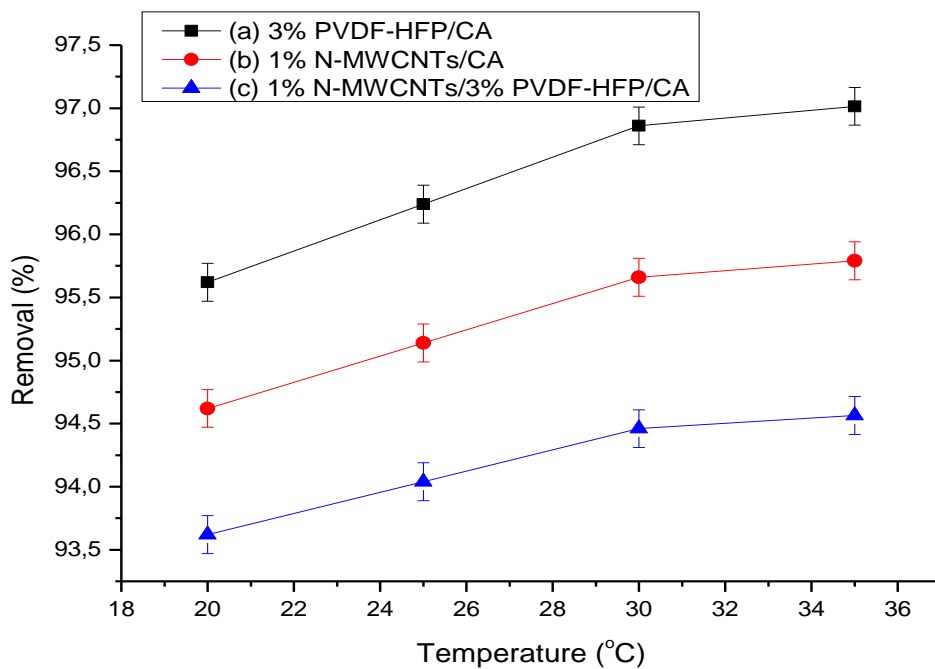
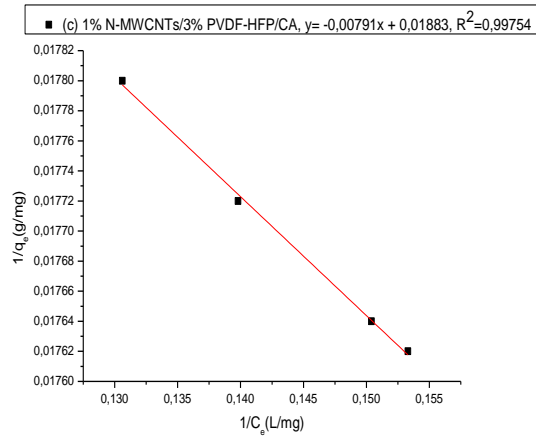
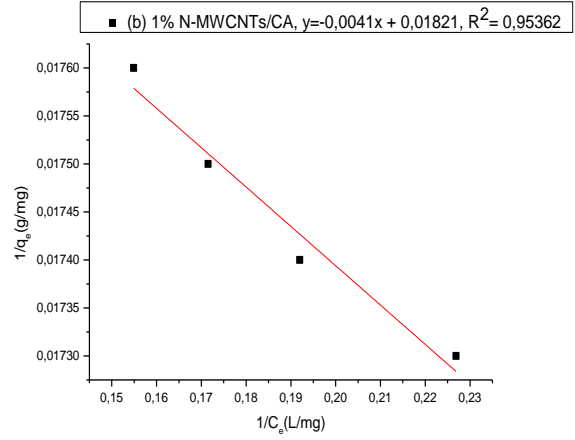
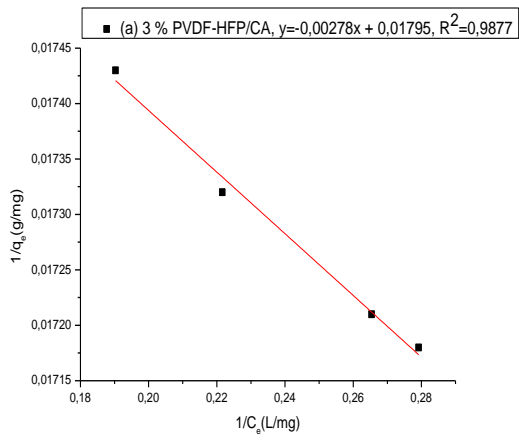


Figure 4.12: Effect of temperature on adsorption efficiency of Ca (II) ions on (a) 3 % PVDF-HFP/CA, (b) 1 % N-MWCNTs/CA, and (c) 1 % N-MWCNTs/3 % PVDF-HFP/CA based membrane.

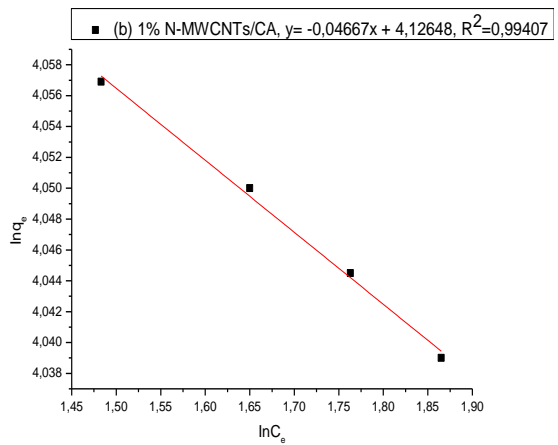
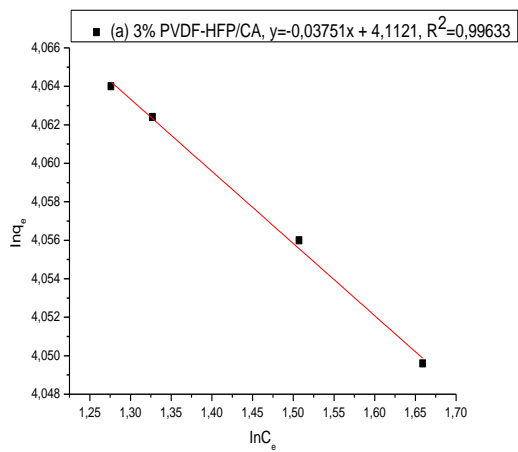
4.2.1.8 Adsorption isotherm models

Adsorption isotherms provides significant data to demonstrate the way the adsorbate molecules (i.e Ca(II)) distribute themselves between the solid and liquid phase when adsorption process reaches an equilibrium level [24]. Figure 4.13 (i) and (ii) presents the Langmuir and Freundlich isotherm models which were used to predict the adsorption capacities (i.e adsorption isotherms) and other important data derived from the parameters e.g surface heterogeneity, adsorption nature etc. Table 4.2 displays the calculated values of Langmuir values (q_{max} , R_L and b) and Freundlich values (K_f and n) along with their corresponding R^2 . The Freundlich isotherm model appears to be a better model as it shows high values of regression correlation coefficients ($R^2 = 0.99407 - 0.99929$) as compared to the Langmuir values ($R^2 = 0.95362 - 0.99754$), which are in good agreement with the isotherm plots at four different temperatures. The Freundlich isotherm model suggests a heterogeneous surface and a multilayer adsorption as reported elsewhere [25]. In addition, the Freundlich isotherm is an empirical model which is widely recommended due to its accuracy [24]. This satisfactory empirical isotherm model can best describe the non-ideal sorption that involves heterogeneous adsorption. It provides more accurate results more than the Langmuir isotherm for various heterogeneous adsorptions. The values of n for the Freundlich constants, denotes the favourability of adsorption and results are less than 1 for all the polymeric membranes, suggesting that the sorption of Ca (II) is a chemical process [25]. The values of the Freundlich constant, K_f , are high for all the polymeric membranes this suggests that the adsorption capacity increased when the temperature increased from 20 - 35 °C, similar trend of results was reported elsewhere [22].

(i) Langmuir isotherm



(ii) Freundlich isotherm



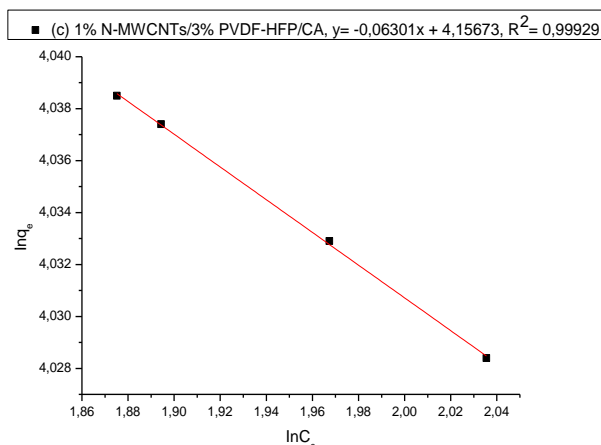


Figure 4.13: (i) Langmuir isotherm and (ii) Freundlich isotherm for the adsorption of Ca (II) ions onto (a) 3% PVDF-HFP/CA, (b) 1% N-MWCNTs/CA, and (c) 1% N-MWCNTs/3 % PVDF-HFP/CA composite membranes.

Table 4.2: Langmuir and Freundlich isotherm parameters for Ca (II) ions adsorption onto PVDF-HFP composite membranes.

Membrane	q_{\max} (mg/g)	Langmuir model			Freundlich model		
		b (L/mg)	R^2	R_L	K_f (mg/g)	n	R^2
3% PVDF-HFP/CA	55.710	-6.457	0.9877	-0.00129	12944.939	-26.660	0.99633
1% N-MWCNTs/CA	54.915	-4.441	0.95362	-0.00188	13380.736	-21.427	0.99407
1% N-MWCNTs/3% PVDF-HFP/CA	53.107	-2.381	0.99754	-0.00351	14345.973	-15.870	0.99929

Based on this results, the Freundlich isotherm yields a better fit compared to the Langmuir isotherm model. The maximum adsorption capacity (i.e q_{\max}), from the Langmuir isotherm model for the 3% PVDF-HFP/CA composite membrane was 56 mg/g at 298.15 K. This value exceeds the ones reported elsewhere, [20, 21, 24, 25, 26, 27, 28]. The equilibrium parameter (i.e R_L) values for all the membranes are below 1, indicating a favourable adsorption as recorded in the literature [22, 20]. Furthermore, other membranes were also studied, and the results are presented in appendix 4.

Table 4.3: Comparison of Ca (II) adsorption capacity by various materials

Table 4.3 summarises the list of previously reported adsorption capacities of Ca(II) ions by some synthetic adsorbents, not only conventional adsorbents but also natural

based adsorbents. The results show that the 3% PVDF-HFP/CA composite membrane has the adsorption ability for Ca (II) ions better than those shown in table 4.3. Another advantage of the 3% PVDF-HFP/CA based membrane is the availability of the raw materials for preparation of the composite membrane, it is easily regenerated, and it is environmentally friendly.

Adsorbent	Experimental Conditions	Metal capacity (mg/g)	% Removal	Reference (s)
3% PVDF-HFP/CA	pH = 7 Temp = 298 K Dosage = 0.5 mg/L	56	99.99	this study
Coconut shell activated carbon	pH = 6.30 Temp = 303 K Dosage = 0.16 g/cm ³	48.50	60	[20]
Alkali modified sugarcane bagasse and coffee husk	pH = 6.50 Temp = 298 K Dosage = 2 g/L	46.80 and 37.37	96 and 79	[21]
Natural and homoionic clinoptilolite	pH = 6.50 Temp = 298 K Dosage = 1 g/100 mL	9.68 and 10.50	33 and 42	[24]
Surfactant modified bentonite adsorbent coating	Adsorbent: Binder (0.75 g: 1.0 g) Hardness=120 mg/L	14.63	66.67	[25]
Modified Amorphophallus campanulatus skin as a low-cost adsorbent	Ca =100 mg/L Dosage=1.5 g/25 mL	10.85 and 27.64	85	[26]
Bigadic clinoptilolite	Temp = 299 K Dosage = 20 g/L Time=93 min	12.30	99	[27]
Novel magnetic nano composite adsorbents based on functionalization of wood sawdust	pH = 7 Temp = 298 K Dosage = 0.4 g/50 mL and 0.2 g/50 mL	18.40 and 27.20	84.40 to 100 98.29 to 100	[28]

4.2.1.9 Thermodynamics of adsorption

The temperature effect in the interval of 20, 25, 30 and 35 °C, was studied and thermodynamic parameters were calculated and displayed in table 4.4. As can be seen in figure 4.14, the linear plot of $\ln K_c$ vs $1/T$ yields a linear plot for Ca (II) adsorption onto the PVDF-HFP based membranes. The Arrhenius equation is helpful

to find the missing parameters, which results from the negative-slope line, the same trend was reported elsewhere [29]. The thermodynamic parameters, ΔG° , ΔH° , ΔS° are important to understand the adsorption mechanism. The ΔS° and ΔH° values were obtained from the intercept and slope of the Van't Hoff ($\ln K_c$ vs $1/T$) as illustrated in figure 4.14. Table 4.4 summarises the results of the thermodynamic parameters as mentioned before. The negative values of ΔG° decreased with an increase in temperature, indicating that the adsorption of Ca(II) onto the membranes was spontaneous in nature and higher temperatures favoured the adsorption process [30]. In addition, the more the negative values of ΔG° , this implies an increased driving force of sorption, resulting in higher sorption capacity [31]. The positive values of ΔS° indicates a higher degree of randomness at the solid-solute interface during the adsorption of Ca(II), whereas the positive values of ΔH° confirmed the endothermic character of the adsorption of Ca(II)/PVDF-HFP based membranes. The data illustrates that the adsorption process of Ca(II) ions by PVDF-HFP composite membrane is spontaneous, endothermic, and mainly physical in nature [29, 32]. Furthermore, other membranes were also studied, and the results are presented on appendix 5.

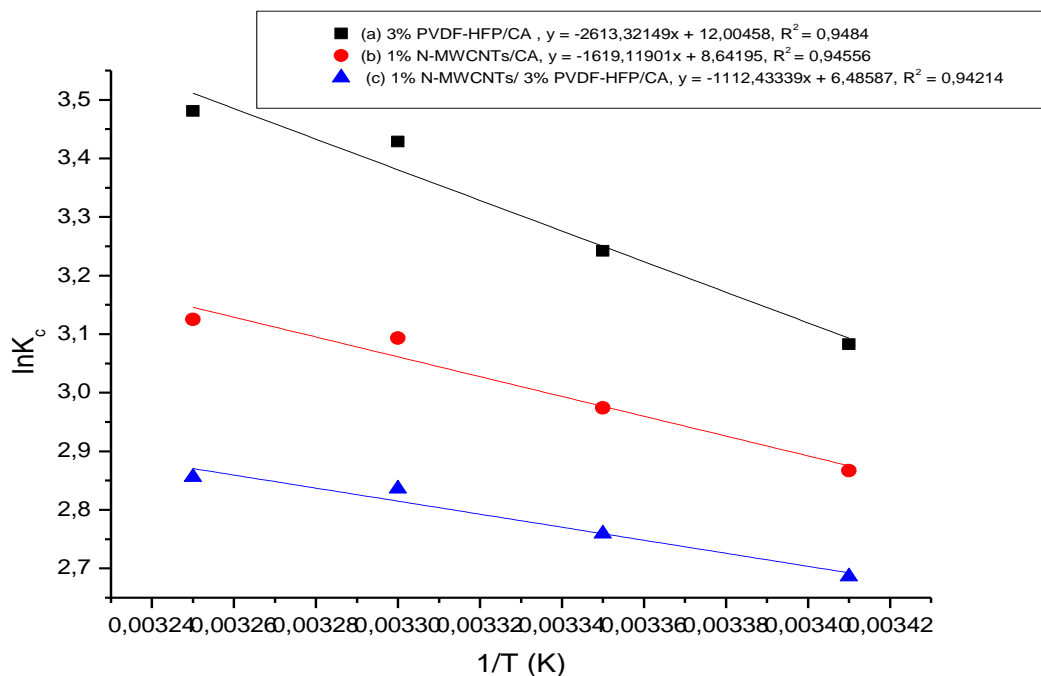


Figure 4.14: Thermodynamic parameters of Ca (II) ions onto, (a) 3 % PVDF-HFP/CA, (b) 1% N-MWCNTs/CA, and (c) 1% N-MWCNTs/3% PVDF-HFP/CA composite membranes.

Table 4.4: Thermodynamic parameters for Ca (II) (120 mg/L) adsorption by PVDF-HFP composite membranes

Membrane	Temperature (K)	Thermodynamic parameters		
		ΔG (KJ/mol)	ΔH (KJ/mol)	ΔS (J.mol/K)
3% PVDF-HFP/CA	293.15	-7514.85	314.33	1.44
	298.15	-8037.39		
	303.15	-8642.53		
	308.15	-8918.86		
1% N-MWCNTs/CA	293.15	-6988.03	203.40	1.04
	298.15	-7372.78		
	303.15	-7795.38		
	308.15	-8005.34		
1% N-MWCNTs/3% PVDF-HFP/CA	293.15	-6546.64	133.80	0.78
	298.15	-6838.19		
	303.15	-7148.28		
	308.15	-7318.05		

4.2.1.10 Effect of counterions

Real water samples contain various ionic species which might influence the adsorption of the hardness causing agents. To achieve this, a simulation study employed the use of sodium sulfate, potassium nitrate, sodium chloride and analytical grade calcium sulphate to mimic a real water sample with different metal ion concentrations. Figure 4.15 demonstrates the effect of counterions on the adsorption of Ca(II) ions by various polymeric membranes. According to these results, in the presence of the counterions the adsorption uptake of Ca(II) ions was 96.53%, 95.63%, 96.01% for the 3% PVDF-HFP/CA, 1% N-MWCNTs/CA, and 1% N-MWCNTs/3% PVDF-HFP/CA composite membranes, respectively. It can be noticed that the counterions did not affect the adsorption efficiency of Ca (II) ions significantly. These results are better as compared to a study which was conducted by Sepehr et al., [33]. In their study of removal of hardness constituents, calcium, and magnesium by natural and alkaline modified pumice stones in single and binary systems, the removal efficiency of 53% and 61% for natural and modified adsorbents were recorded, respectively. Interestingly, the removal efficiency of Ca (II) for all the polymeric membranes remained above 90% in the presence of the counterions, as compared to the removal efficiency of natural and modified adsorbent in the presence of counterions. This can be attributed to a

competition between the counterions with the hardness causing agents for occupying the active sites leading to a faster saturation of the adsorbents by the counterions in the presence of the hardness agents [33]. Furthermore, other membranes were also studied, and the results are presented on appendix 6.

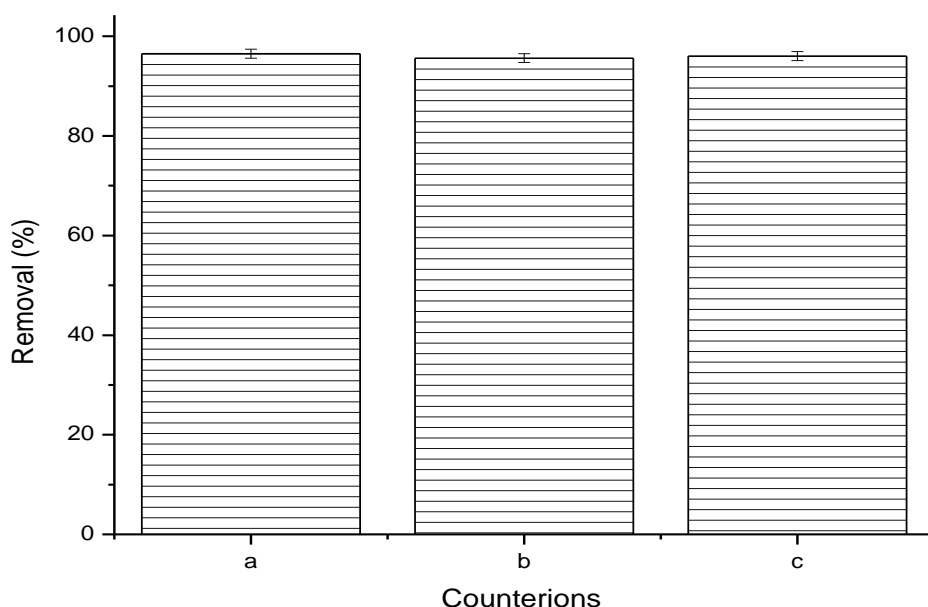


Figure 4.15: Effect of counterions on the adsorption of Ca (II) by (a) 3% PVDF-HFP/CA, (b) 1% N-MWCNTs/CA, (c) 1% N-MWCNTs/3% PVDF-HFP/CA composite membranes.

4.2.1.11 Effect of binary system on the adsorption of Ca (II)

To study the interfering effect of Mg(II) ions and Ca(II) metal ions one another, adsorption experiments were carried out in the optimal conditions using a mixture of Mg (II) and Ca (II) cations at 120 mg/L each (figure 4.16). Cationic uptake was 91.27%, 90.15%, and 91.12% for the 3% PVDF-HFP/CA, 1% N-MWCNTs/CA, and 1% N-MWCNTs/3% PVDF-HFP/CA composite membranes, respectively. It can be observed that the removal efficiencies in binary system for all the polymeric membranes are slightly lower as compared to the values recorded in single ion adsorption tests. This can be ascribed to the competition between the two cationic species for occupying the active sites on the membrane surfaces leading to a rapid saturation of the membrane surfaces in the simultaneous presence of Mg(II) and Ca(II) metal ions. Similar trend of

results was observed by Sepehr et al., [33], and Swelam et al., [34]. Furthermore, other membranes were also studied, and the results are presented on appendix 7.

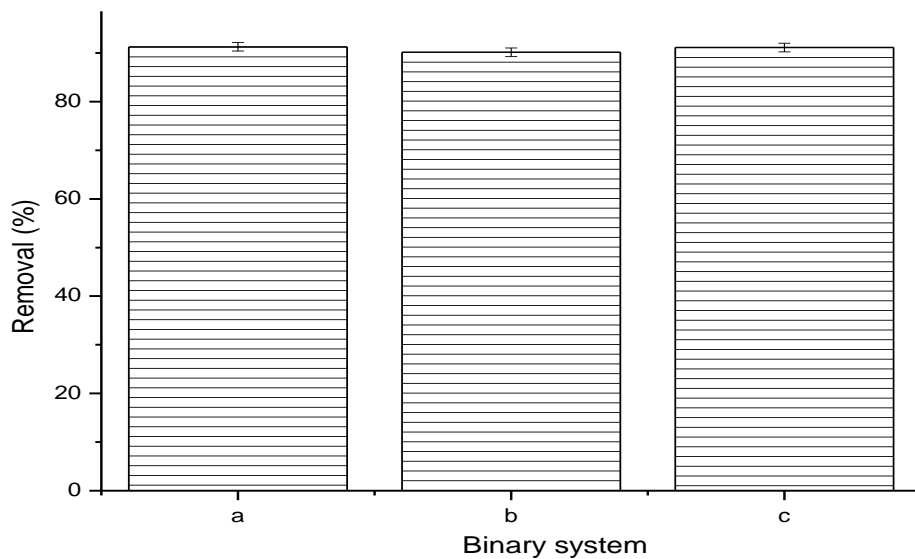


Figure 4.16: Effect of the binary system on the adsorption of Ca (II) by PVDF-HFP blend membranes

4.2.1.12 Recycling of polymeric membranes

Reusability experiments were carried out to study the regeneration of the spent membranes, which is an important parameter in terms of economic feasibility of the developed method. A solution of sodium hydroxide was used to carry out the reusability of the spent PVDF-HFP composite membranes. Figure 4.17 shows the reusability percentages of the spent membranes versus the number of cycles. The removal efficiency from the first to the third cycle reduced from 94.98 to 94.64%, 91.38 to 90.0%, and 90.65 to 90.13 % for the (a) 3 % PVDF-HFP/CA, (b) 1% N-MWCNTs/CA and (c) 1 % N-MWCNTs/3% PVDF-HFP/CA composite membranes. The 3% PVDF-HFP composite membrane had the least adsorption loss as compared to the other five polymeric membranes. Interestingly, the adsorption efficiency for all the polymeric membranes remained above 90 % after the successive three cycles, which indicates that the PVDF-HFP based membranes can be recycled for Ca(II) ions adsorption. The results for the 3% PVDF-HFP/CA after the three-adsorption cycle were 0.34% as

compared to 20% adsorption loss observed by Muqet et.al [19]. Furthermore, other membranes were also studied, and the results are presented on appendix 8.

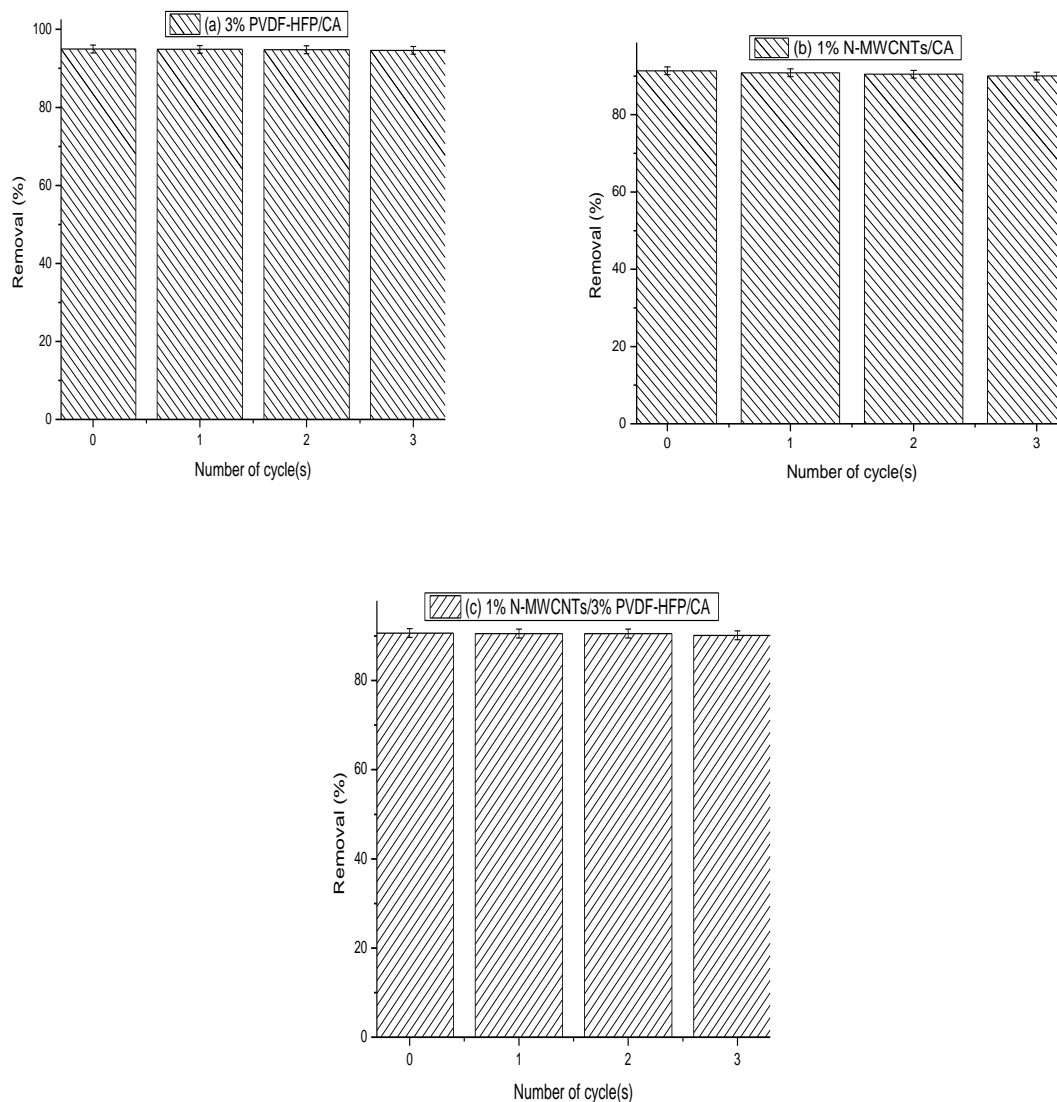


Figure 4.17: Effect of recycling of (a) 3% PVDF-HFP/CA, (b) 1% N-MWCNTs/CA, and (c) 1% N-MWCNTs/3% PVDF-HFP/CA composite membranes on the adsorption efficiency of Ca (II) metal ions.

Figure 4.18, 4.19 and table 4.5 presents the XRD, TGA and ICP-MS results of the best performing membrane (i.e., 3% PVDF-HFP composite membrane). Figure 4.18 a and b presents the diffraction patterns of the recycled and unspent 3% PVDF-HFP/CA composite membranes respectively [9]. The intensity of the characteristic peaks at 22.2° and 34.8° 2θ , for the recycled 3% PVDF-HFP/CA based membranes in figure 4.18 has reduced after three successive adsorption cycles. The TGA profile of the

recycled 3% PVDF-HFP/CA based membranes in figure 4.19 b shows an initial weight loss of 60 % at around 300 to 400 °C, this is due to the evaporation of the remaining residual solvents and moisture in the polymer matrix [8]. However, between the temperature intervals of about 350 °C – 450 °C, there is a 10 % weight loss which can be associated with the carbonization of the decomposed matter to ash. Similar results were reported by Das et al., [9]. The TGA profile of the unspent 3% PVDF-HFP/CA composite membrane in figure 4.19 a also shows similar results. This shows that the 3% PVDF-HFP composite membrane can be recycled for the Ca(II) metal ions.

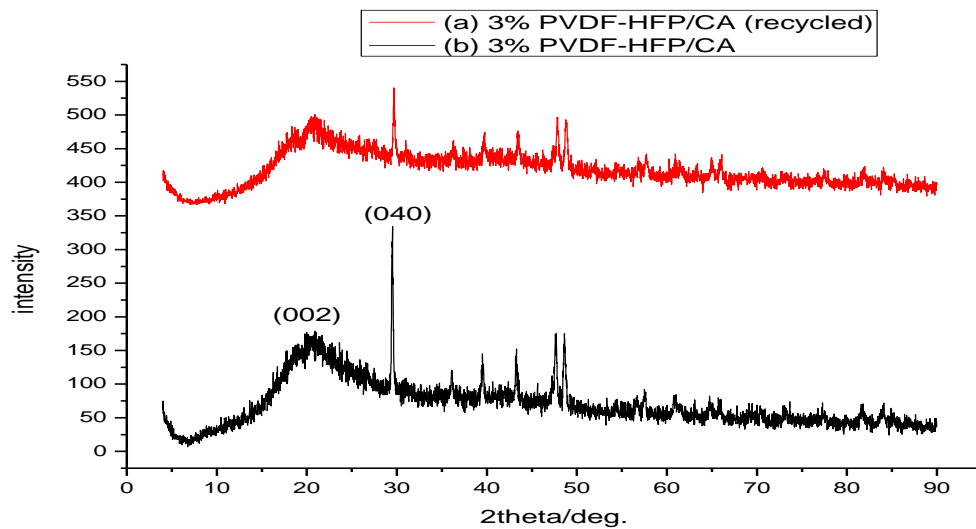


Figure 4.18: XRD of 3 % PVDF-HFP/CA after recycling the composite membrane at least 3 times for Ca (II) ions

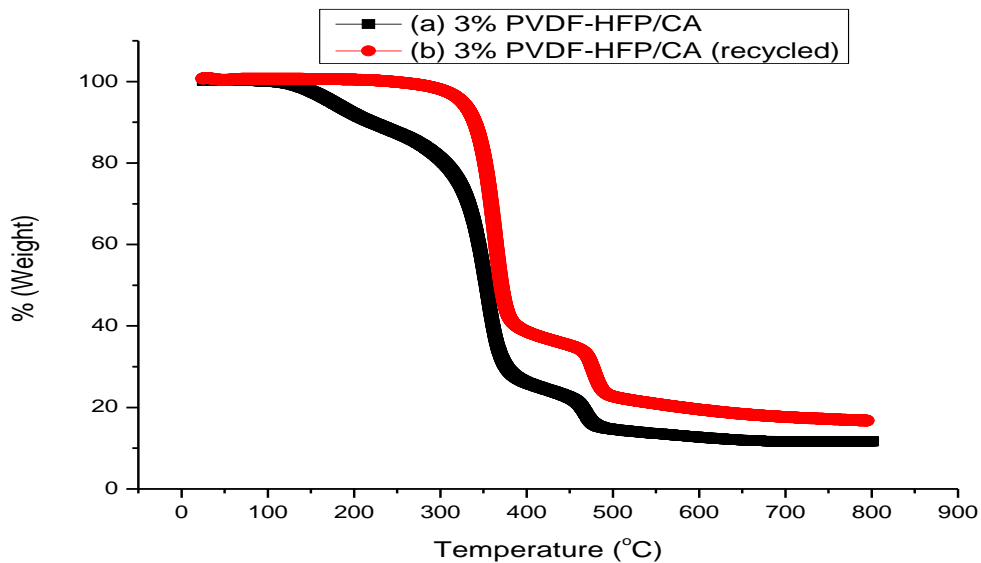


Figure 4.19: TGA profile of 3% PVDF-HFP/CA after recycling the composite membrane at least 3 times for Ca (II) ions

Table 4.5: ICP-MS spectrometry results of 3% PVDF-HFP composite membranes

Metal (mg/kg)	Ca	Mg
	15	50
% Accuracy on internal QC	102.00	110.80
3% PVDF-HFP/CA	131.50	BDL
Recycled 3% PVDF-HFP/CA	354.50	BDL

BDL stands for Below Detection Limit

The analysis of trace elements within the unspent and recycled 3% PVDF-HFP composite membrane was carried out using the inductively coupled plasma-plasma mass (ICP-MS) spectrometry. Firstly, the 3% PVDF-HFP/CA composite membrane was digested using a membrane digester, followed by the analysis of Ca (II) in the membrane sample. As it can be seen in table 4.5, that the quantity of Ca (II) metal ions in all the membranes exceeds the quantity of Mg (II) ions. The amount of Ca (II)

in the recycled 3% PVDF-HFP/CA membrane is 354.5 mg/kg, this value is higher than 131.5 mg/kg for the unspent 3% PVDF-HFP/CA based membrane. This means that the Ca (II) hardness ions were strongly adsorbed onto the membrane surface even after three successive adsorption cycles.

4.2.2 Batch adsorption studies of Magnesium (II) ions

4.2.2.1 Effect of pH on Mg (II) ions removal by PVDF-HFP membrane

The solution pH is regarded as an essential factor that affects the metal adsorption process, due to its impact on the degree of ionization of the adsorbent surface charge and the metal species [35]. Figure 4.20 presents the initial pH of Mg(II) solutions which were varied from 5 to 7.5. During this study, the data reveals that at lower pH intervals the membrane surface is surrounded by hydrogen ions (H^+) which prevents the adsorption of Mg(II) metal ions onto the binding sites of the membrane through the repulsive forces. In the basic media, the removal efficiency of the polymeric membrane also decreased because the Mg(II) ions start to precipitate because of metal hydroxide bonds. Highest removal efficiency was observed at pH of 7. This is because when the solution pH was increased to 7, the competition between the hydroxonium ions, H_3O^+ , and the hardness causing agent decreased. Similar results were observed by Muqet et al. [19] and Rolence et al., [20]. The pH value of 7 was chosen for the remaining tests.

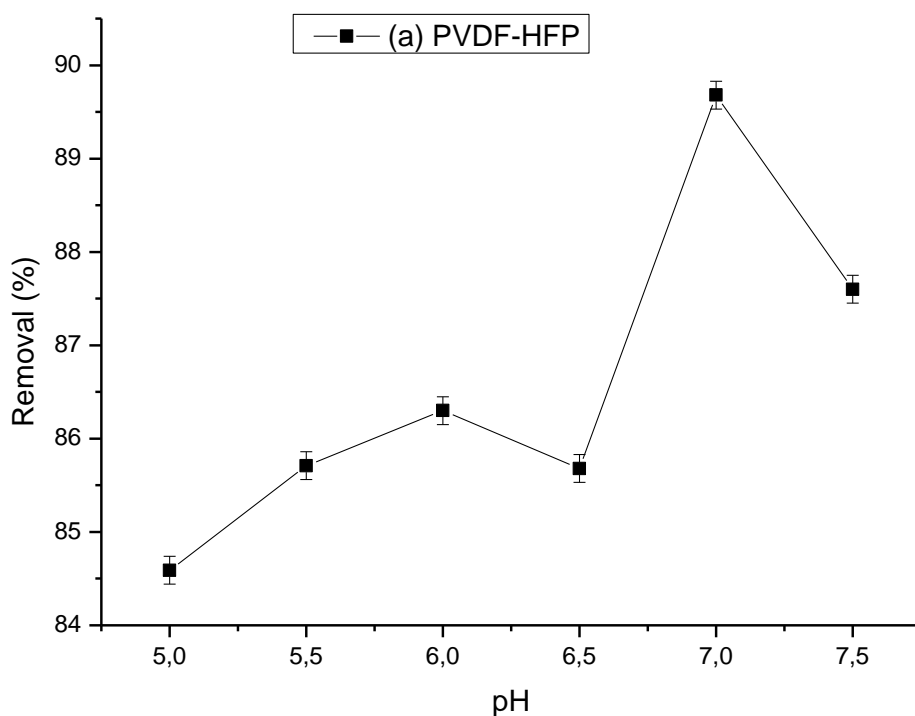


Figure 4.20: Effect of pH on the removal of Mg (II) ions using PVDF-HFP membrane

4.2.2.2 Effect of adsorbent dosage

Figure 4.21 presents the effect of membrane adsorbent dosage on the removal of Mg(II) ions by PVDF-HFP composite membranes. During this study, it was observed that from 0.1 – 0.3 mg/L dose there was an increase on the adsorption uptake of Mg(II) ions for all the membranes. These increases in the sorption of the amounts of metal ions are due to the existence of larger surface area as well as larger number of active binding sites for the ions [35]. The highest removal efficiency is observed at 0.5 mg/L dose, then immediately after 0.5 mg/L dose (i.e., 0.5 - 0.7 mg/L) the metal uptake starts to decrease. These results demonstrate that CA membrane alone gave the lowest Mg(II) ions removal, with approximately 83% followed by PVDF-HFP membrane. Interestingly, a slight increase on the Mg(II) removal was observed when CA was added on PVDF-HFP. The highest adsorption of approximately 87% was observed on 3% PVDF-HFP/CA composite membrane, better than the adsorption percentage reported in literature [21]. According to a study which was conducted by Chakrabarty and Sarma [36], it was observed that after a certain adsorbent dosage the maximum adsorption is attained and hence the number of ions remain constant even with further addition of dose of adsorbent [36].

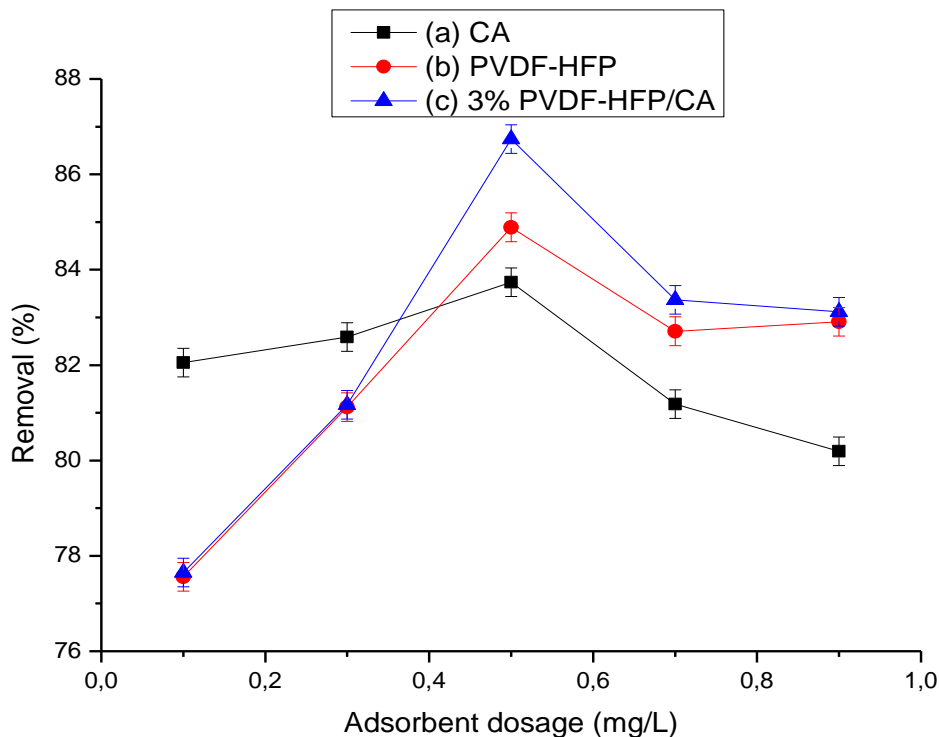


Figure 4.21: Effect of membrane adsorbent dosage on Mg(II) ions adsorption onto PVDF-HFP composite membranes

4.2.2.3 Effects of contact time on adsorption efficiency of Mg(II) by composite membranes

The effect of contact time on the removal of Mg(II) ions by various polymeric membranes is shown in figure 4.22. The results show an exponential growth on the adsorption uptake of Mg(II) ions by 1% N-MWCNTs/CA composite membrane during the first three hours of adsorption (30 – 180 mins) (figure 4.10 b). This is due to the available active sites on the membrane surface for the adsorption process. The highest adsorption of approximately 91.6% was observed on 1% N-MWCNTs /CA composite membrane at 150 mins, which exceeds the rest of the other 2 membranes presented in figure 4.22 a and c [20]. Figure 4.22 a and c shows an increase in Mg(II) removal during the first two hours (i.e., 120 minutes) of adsorption then further increase of contact time did not show any significant change in the hardness removal. This is because, there are many vacant surface sites available for the adsorption during the initial stage and with the passage of time. After a certain period, repulsive forces between solute molecules on solid phase and liquid phase create difficultness for the solute molecules to occupy remaining vacant surface sites. Similar trend of results was observed elsewhere [37, 38]. Furthermore, other membranes were also studied, and the results are presented in appendix 9.

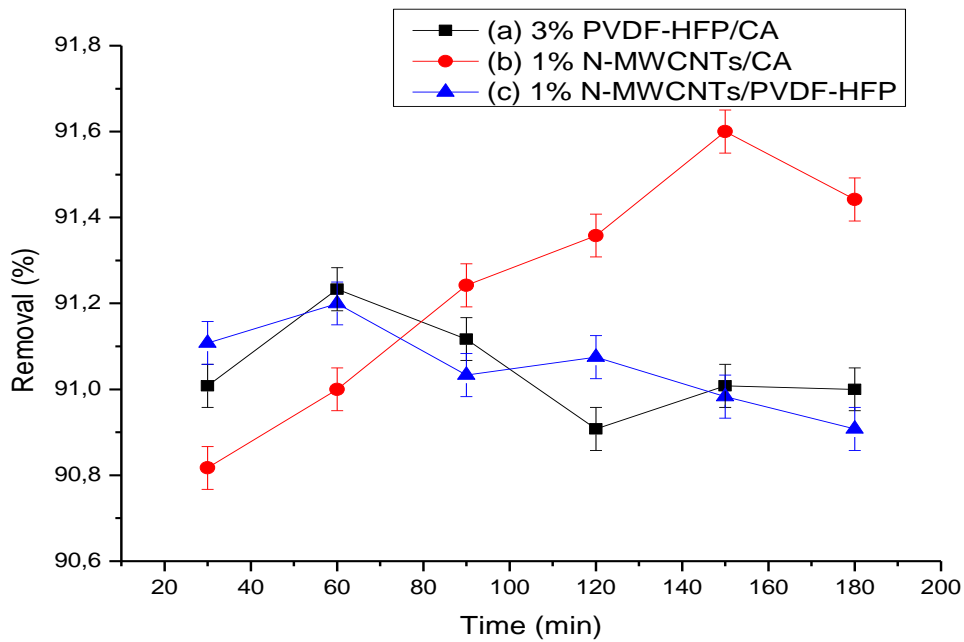
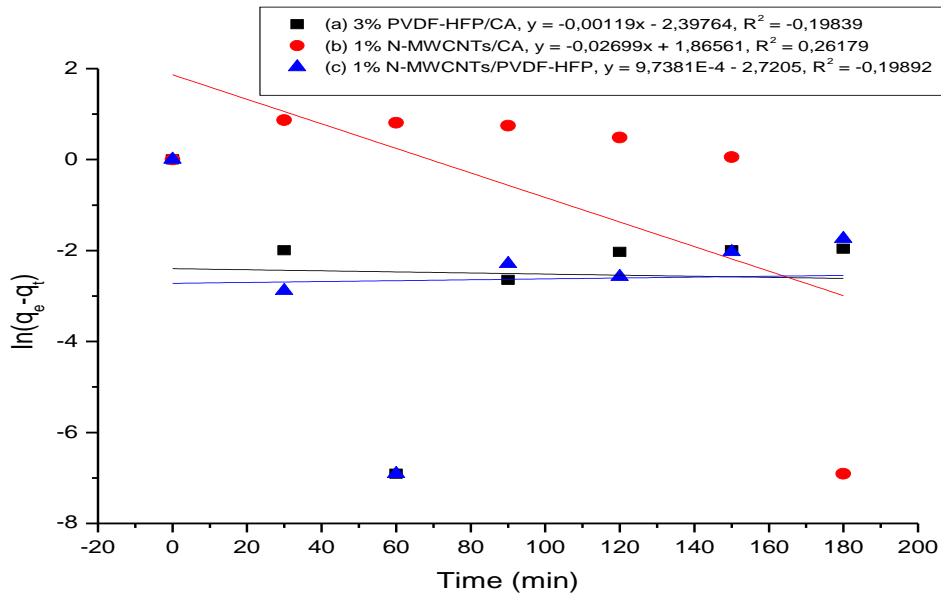


Figure 4.22: Effect of contact time on adsorption efficiency of Mg (II) ions on (a) 3% PVDF-HFP/CA, (b) 1% N-MWCNTs/CA, and (c) 1% N-MWCNTs/PVDF-HFP composite membranes

4.2.2.4 Adsorption kinetics of Mg(II) metal ions removal by polymeric membranes

The data presented in figure 4.23 shows the pseudo-first and second order kinetic model for the adsorption of Mg(II) ions onto the polymeric membranes. In table 4.6, the rate constant for the pseudo-second order kinetic model are higher than the values for the pseudo-first order model. Furthermore, the correlation coefficients, R^2 , values for the theoretical and experimental values for the pseudo-first order are lower as compared to the ones for the second-order kinetic model. This data shows that the pseudo-second order yields a better fit than the pseudo-first order kinetic model [37]. Furthermore, other membranes were also studied, and the results are presented in appendix 10.

A



B

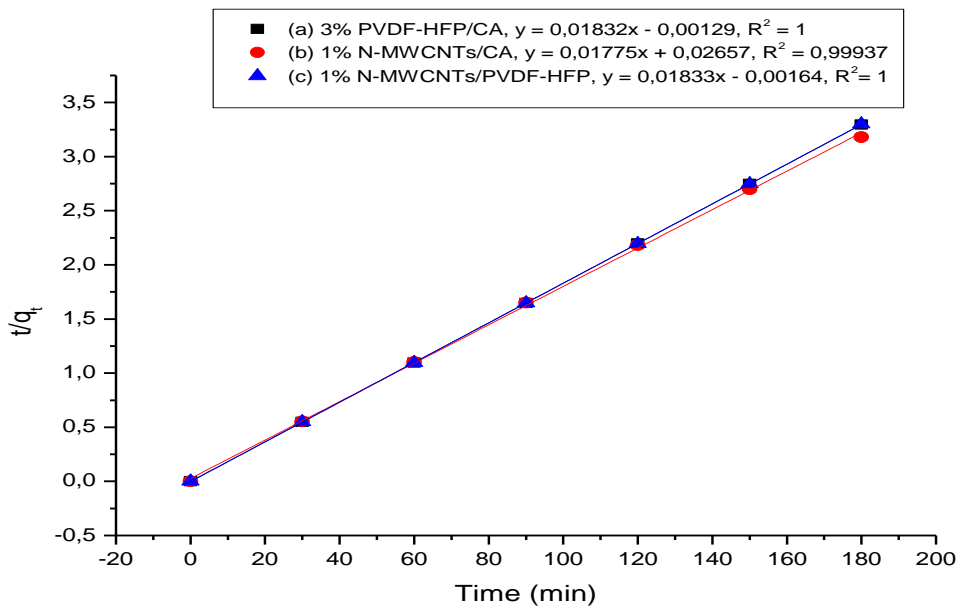


Figure 4.23: Pseudo-first order (A) and Pseudo-second order (B) kinetic model for adsorption of Mg (II) ions onto (a) 3% PVDF-HFP/CA, (b) 1% N-MWCNTs/CA, and (c) 1% N-MWCNTs/PVDF-HFP composite membranes.

Table 4.6: Kinetic parameters for Mg (II) adsorption onto PVDF-HFP based membrane

Membrane	q _e (mg/g)	Pseudo-first order Kinetic model			Pseudo-second order Kinetic model		
		K ₁ (min ⁻¹)	q _e (mg/g)	R ²	K ₂ (g/mg.mi n)	q _e (mg/g)	R ²
3% PVDF-HFP/CA	54.741	0.00119	0.0909	-0.19839	-0.2602	54.585	1

1% N-MWCNTs/CA	56.631	0.02699	6.4598	0.26179	0.0119	56.338	0.99937
1% N-MWCNTs/PVDF-HFP	54.721	-9.7381E-4	0.0658	-0.19892	-0.2049	54.555	1

4.2.2.5 Effect of initial metal ion concentration on the adsorption of Mg(II) by PVDF-HFP based membranes.

The concentration effect on the removal of Mg(II) hardness by various polymeric membranes is presented in figure 4.24. The data presents a rapid exponential growth of Mg(II) removal when the concentration was increased from 100 - 300 mg/L for all the composite membranes. The removal efficiency of Mg(II) by 1% N-MWCNTs/CA composite membrane increased from approximately 93.00 to 99.00% when the concentration was increased from 100 to 300 mg/L (figure 4.24 a), which exceeds the rest of the other composite membranes presented in figure 4.24 b and c. The surface saturation for all the membranes was achieved approximately at 600 - 1200 mg/L, at this stage the removal efficiency of Mg(II) was constant for all the membranes. These results are better as compared to a study which was conducted by Werkneh et al., [21]. In their study of removal of water hardness causing constituents using alkali modified sugarcane bagasse and coffee husk at Jigjiga city, Ethiopia, their highest removal efficiency of 90.80% and 93.30% was observed at an initial Mg(II) ion concentration of 120 ppm. Accordingly, for initial metal concentration of 60 to 120 mg/L the adsorption efficiency reduced to 88% and 89.50% respectively. Furthermore, their adsorption efficiency of Mg(II) hardness was improved by increasing the contact time and decreased by increasing the initial ions concentration from 60 - 120 mg/L. Furthermore, other membranes were also studied, and the results are presented in appendix 11.

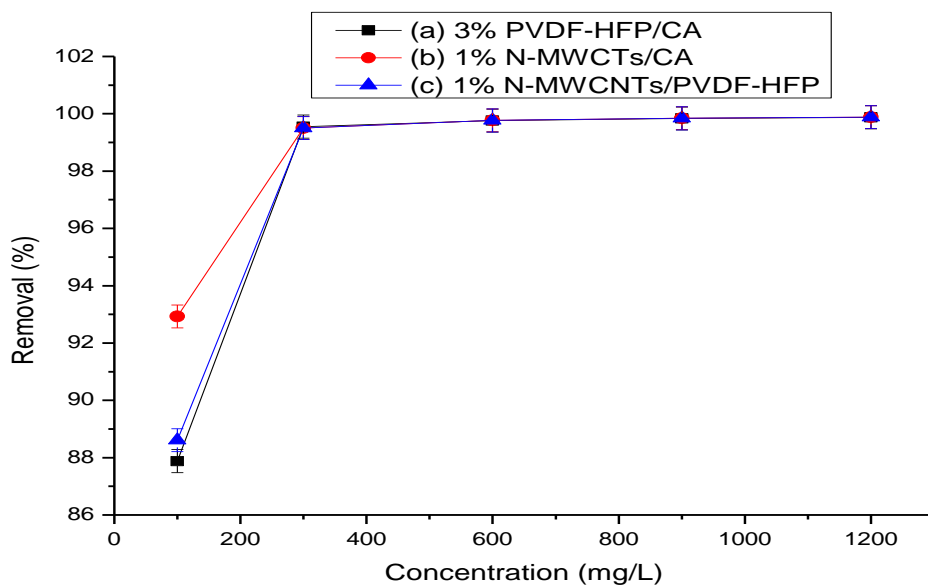


Figure 4.24: Effect of initial metal ion concentration on the adsorption efficiency of Mg (II) ions on (a) 3% PVDF-HFP/CA, (b) 1% N-MWCNTs/CA, and (c) 1% N-MWCNTs/PVDF-HFP composite membranes

4.2.2.6 Effect of temperature

Effect of temperature on the adsorption of Mg(II) metal ions onto PVDF-HFP composite membranes was studied by conducting different set of experiments at 20 °C, 25 °C ,30 °C and 35 °C and the results are presented in figure 4.25. Temperature plays an important role on the adsorption of metals onto the membrane surface and has two major effects on the adsorption process; increase in the temperature increases the rate of adsorbate diffusion across the external boundary layer and in the internal pores of the adsorbate particles as the liquid viscosity decreases with increase in temperature and the other affects the equilibrium capacity of the adsorbate. It can be observed that increasing temperature favours the removal of the hardness causing agents. This may be attributed to the increase in ion mobility to the sorbent materials. Temperature affects the interaction between the metal ions and the sorbent which influences the stability of the metal–sorbent complex. Higher temperature intervals (i.e 35 °C) enhance sorption due to the increased surface activities and kinetic energy of the solute [39]. Furthermore, other membranes were also studied, and the results are presented in appendix 12.

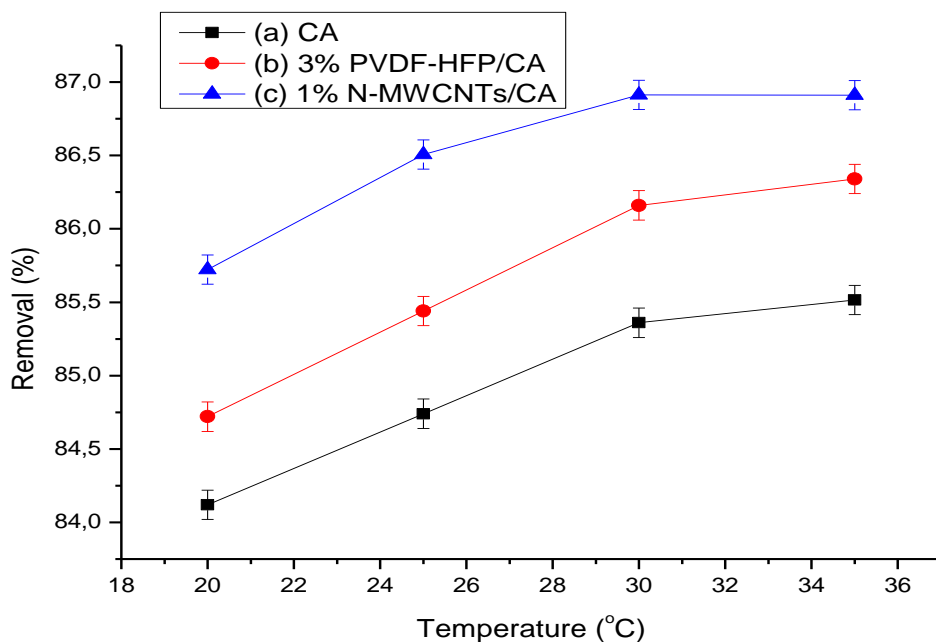
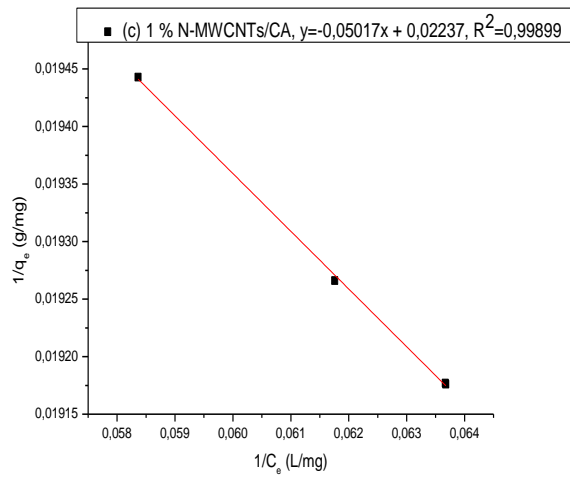
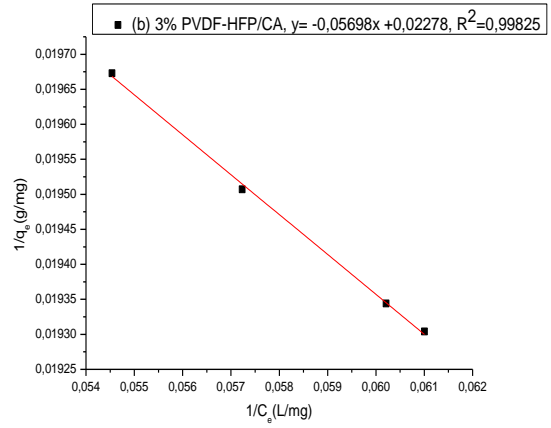
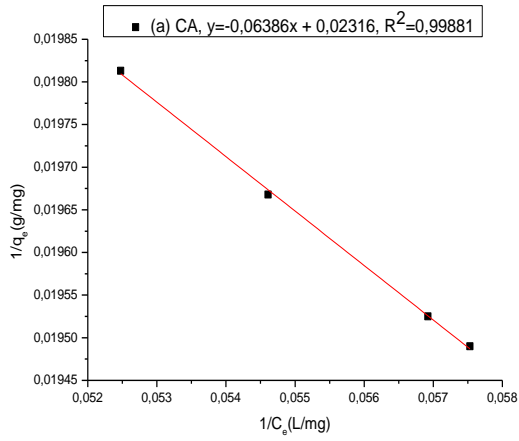


Figure 4.25: Effect of temperature on adsorption efficiency of Mg (II) ions on (a) CA, (b) 3% PVDF-HFP/CA, (c) 1% N-MWCNTs/CA membranes.

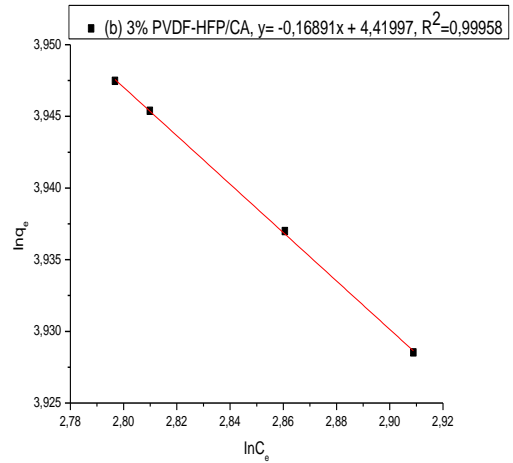
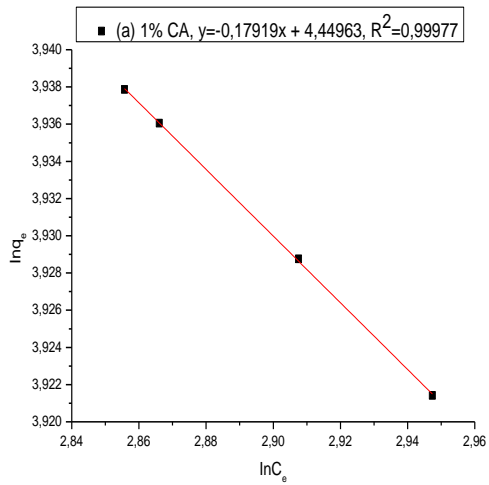
4.2.2.7 Adsorption isotherm models

The plots of Langmuir and Freundlich isotherms (figure 4.25 (i) and (ii)) along with their intercepts and slopes were used to calculate the adsorption constants as shown in table 4.7. The obtained isotherm data reveals that the R^2 values for Freundlich isotherm ($R^2 = 0.99958 - 0.99978$) are higher as compared to the Langmuir isotherm model ($R^2 = 0.99825 - 0.99899$). The Langmuir isotherm assumes a monolayer adsorption and elaborates that no further adsorption of metals can take place once the active sites are fully occupied [39]. The maximum adsorption capacity (i.e q_{max}), from the Langmuir isotherm model for the 1% N-MWCNTs/CA composite membrane was 45 mg/g at 298.15 K. This value exceeds the ones reported elsewhere, [25, 26, 37, 38, 39, 40, 41, 42]. The equilibrium parameter (i.e., R_L) values for all the membranes are below 1, indicating a favourable adsorption as recorded in this literature [20, 22]. Furthermore, other membranes were also studied, and the results are presented in appendix 13.

(i) Langmuir isotherm



(ii) Freundlich isotherm



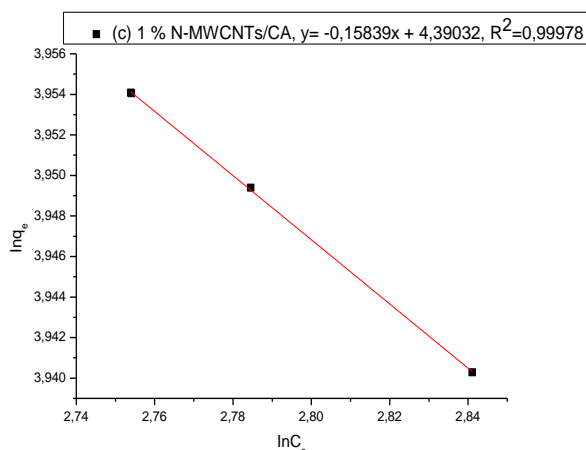


Figure 4.26: Effect of the Langmuir and Freundlich isotherm on adsorption efficiency of Mg (II) ions on (a) CA, (b) 3% PVDF-HFP/CA, (c) 1% N-MWCNTs/CA, composite membrane.

Table 4.7: Langmuir and Freundlich isotherm parameters for Mg (II) ions adsorption onto PVDF-HFP composite membranes

Membrane	q_{max} (mg/g)	Langmuir model			Freundlich model		
		b (L/mg)	R^2	R_L	K_f (mg/g)	n	R^2
CA	43.178	-0.363	0.99881	-0.02350	28159.828	-5.581	0.99977
3% PVDF-HFP/CA	43.898	-0.400	0.99825	-0.02128	26300.863	-5.920	0.99958
1% N-MWCNTs/CA	44.703	-0.446	0.99899	-0.01904	24565.183	-6.313	0.99978

Table 4.8: Comparison of Mg (II) adsorption capacity by various materials

Table 4.8 summarises the list of previously reported adsorption capacities of Ca(II) ions by some synthetic adsorbents, not only conventional adsorbents but also natural based adsorbents. The results shows that the 1% N-MWCNTs/CA membrane has the adsorption ability for Mg(II) ions better than the ones shown in table 4.8. Another advantage of the 1% N-MWCNTs/CA composite membrane is the availability of the raw material for fabrication of the membrane, it is easily regenerated, and it is environmentally friendly.

Adsorbent	Experimental Conditions	Max adsorption	% Removal	Refer
-----------	-------------------------	----------------	-----------	-------

1% N-MWCNTs/CA	pH =7 Temp = 298 K Dosage = 0.5 mg/L	45	99	this study
Surfactant modified bentonite adsorbent coating	Adsorbent: binder ratio (0.75:1.0 (w/w)) Hardness =120 mg/L	14.63	66.67	[25]
Modified Amorphophallus campanulas skin as a low-cost adsorbent	Dosage = 1.5 g/25 mL Hardness = 100 mg/L	1.79 and 20.10	85	[26]
Titan yellow supported on classic thiourea-formaldehyde resins	pH = 10.5 Dosage = 0.05 g/20 mL Temp = 298 K	19.45	-	[37]
Bentonite/ γ -alumina nanocomposite	pH = 7.8 Dosage = 20 g/L Temp = 293 K	3.48	-	[38]
Zeolite	pH = 6.5 Dosage = 2.5 g/50 mL	15.70	22.50 to 81.40	[39]
Melon (<i>Citrullus lanatus</i>) husk as natural adsorbent	pH = 7 Dosage = 0.5 g/0.04 dm ³	1.00	-	[40]
Ion-exchange method	pH = 3 Mass of resin = 10 g Ratio of resin to solution = 1g/100 mL	12	70	[41]
Pistacia vera shell	pH = 8 Adsorbent mass = 1.5 g	2.19	-	[42]

4.2.2.8 Thermodynamics of adsorption

The parameters of enthalpy (ΔH°) and entropy (ΔS°) were calculated from the slope and the intercept of the linear plot of $\ln K_c$ vs $1/T$. Figure 4.27 presents the thermodynamic plot and the related parameters are displayed in Table 4.9. The values of ΔH° were positive for all the Mg-PVDF-HFP composite membranes; meaning that the adsorption reaction was endothermic in nature whereas the positive values of ΔS° indicates a higher degree of randomness at the solid-solute interface during the adsorption of Mg(II) [40]. The negative values of ΔG° decreased with an increase in temperature, indicating that the sorption of Mg(II) onto the membranes was spontaneous in nature and higher temperatures favoured the adsorption process [30]. In addition, the more the negative values of ΔG° , this implies an increased driving force of sorption, resulting in higher adsorption capacity [31]. This data demonstrates that the adsorption process of Mg(II) ions by PVDF-HFP based membrane is spontaneous, endothermic, and mainly physical in nature [29, 32]. Furthermore, other membranes were also studied, and the results are presented in appendix 14.

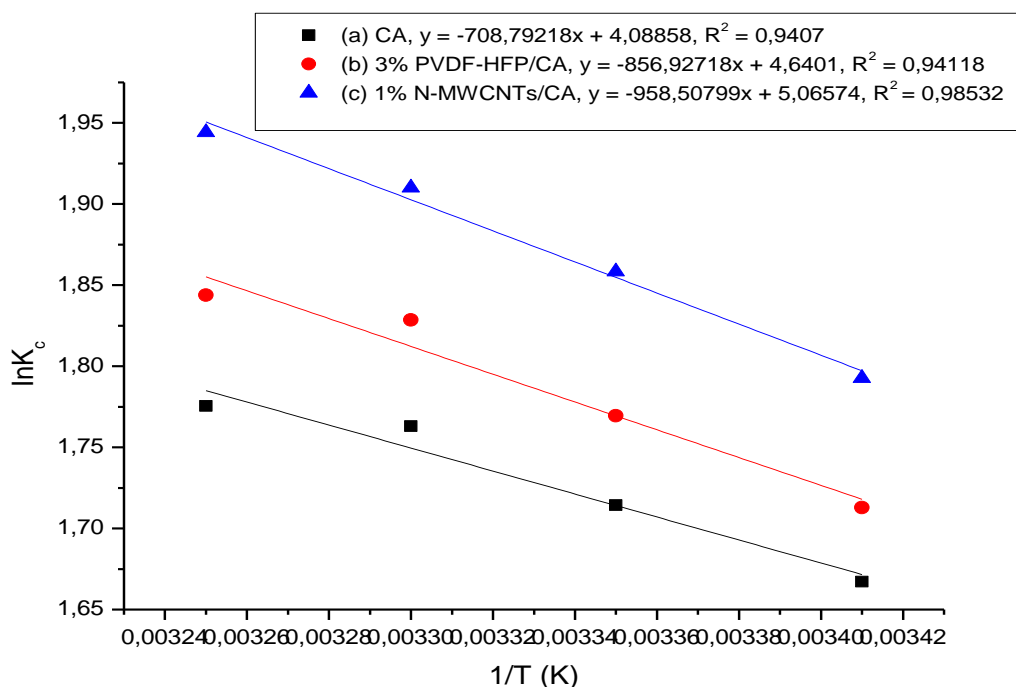


Figure 4.27: Thermodynamic parameters of Mg (II) ions onto (a) CA, (b) 3% PVDF-HFP/CA, (c) 1% N-MWCNTs/CA, composite membranes.

Table 4.9: Thermodynamic parameters for Mg(II) (120 mg/L) adsorption by PVDF-HFP composite membranes

Membrane	Temperature (K)	Thermodynamic parameters		
		ΔG (KJ/mol)	ΔH (KJ/mol)	ΔS (J.mol/K)
CA	293.15	-4063.342	85.253	0.492
	298.15	-4249.570		
	303.15	-4443.749		
	308.15	-4723.794		
3% PVDF-HFP/CA	293.15	-4174.537	103.070	0.558
	298.15	-4386.360		
	303.15	-4608.892		
	308.15	-4980.983		
1% N-MWCNTs/CA	293.15	-4369.216	115.288	0.609
	298.15	-4606.399		
	303.15	-4813.932		
	308.15	-4980.983		

4.2.2.9 Effect of counterions

A simulation study employed the use of analytical grade magnesium sulphate, potassium nitrate, sodium sulfate and sodium chloride to mimic a real water sample and the results are presented in figure 4.28. The observations reveal that about 97% removal efficiency of Mg (II) in the presence of the counterions is achieved for all the polymeric membranes. This results correlate with the ones in the single ion adsorption tests, meaning that the presence of counterions did not influence the adsorption of the hardness causing agent. This results are better as compared to a study which was conducted by Sepehr [33]. Furthermore, other membranes were also studied, and the results are presented in appendix 15.

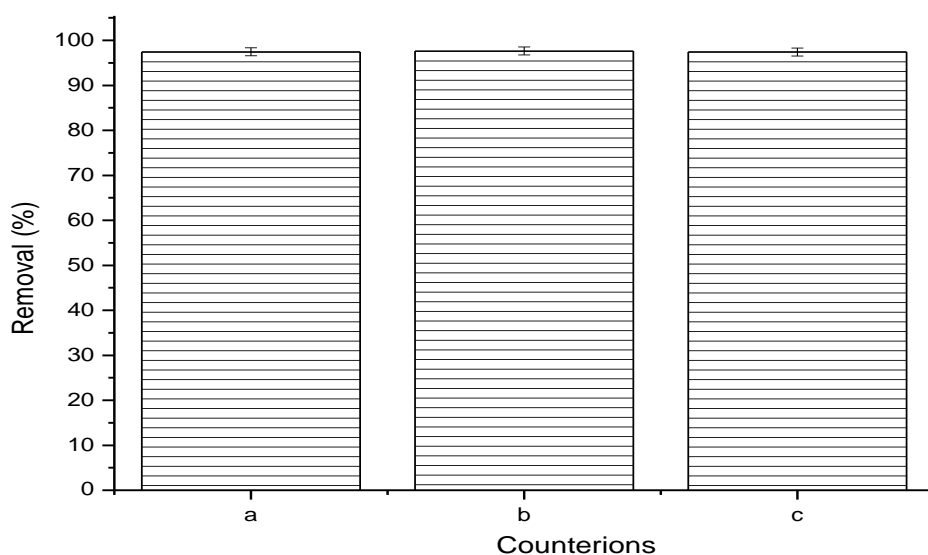


Figure 4.28: Effect of counterions on the adsorption of Mg (II) by (a) 3% PVDF-HFP/CA, (b) 1% N-MWCNTs/CA, (c) 1% N-MWCNTs/PVDF-HFP composite membranes

4.2.2.10 Effect of binary system

The study of the interfering effect of Mg(II) and Ca(II) ions on one another was conducted in the optimal conditions using a mixture of Mg(II) and Ca(II) (120 ppm each) and the results are presented in figure 4.29. The Mg (II) uptake was 94.48%, 95.17% and 94.56% for (a) 3% PVDF-HFP/CA, (b) 1% N-MWCNTs/CA, and 1 % N-MWNCTs/PVDF-HFP composite membranes respectively. It can be noticed that the equilibrium time and adsorption efficiency were not lower compared to the values

observed in the single system. The results are better as compared to the ones reported in this literature [34]. In their study of removal of Ca (II) and Mg (II) from Aqueous-Organic Solutions on Strong Cation-Exchange of ResinexTMK-8H, the results for Mg(II) uptake were lower in the binary as compared to the ones in the single adsorption tests. The reason was that there was a competition between the two cationic species for occupying the active sites leading to a faster saturation of the adsorbent in the simultaneous presence of calcium and magnesium [33, 34]. Furthermore, other membranes were also studied, and the results are presented in appendix 16.

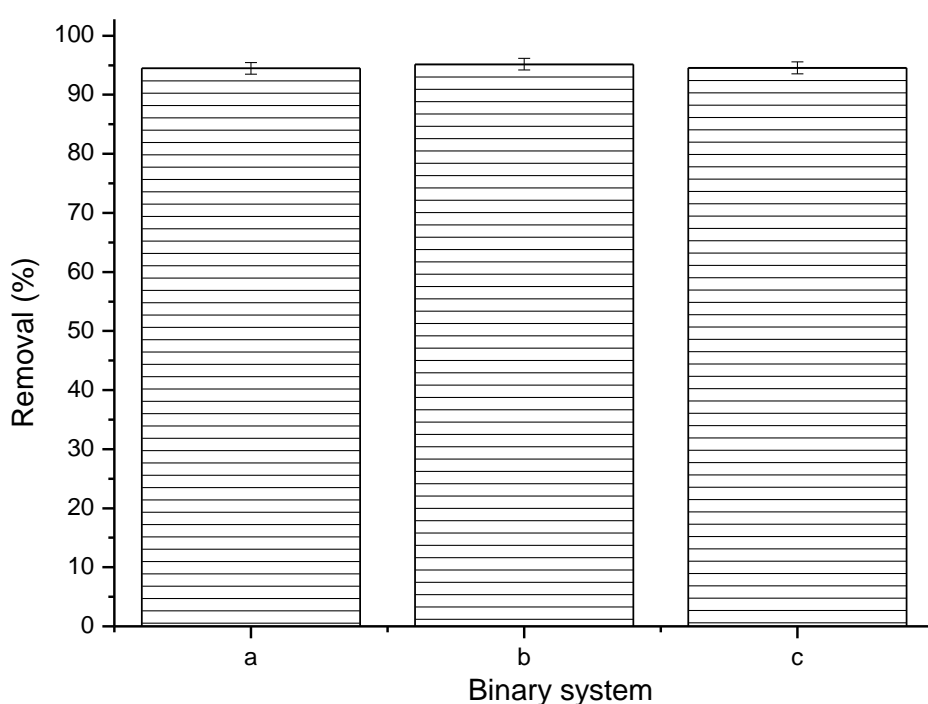


Figure 4.29: Effect of the binary system on the adsorption of Mg (II) by (a) 3% PVDF-HFP/CA, (b) 1% N-MWCNTs/CA, (c) % N-MWCNTs/PVDF-HFP composite membranes

4.2.2.11 Recycling of the PVDF-HFP composite membranes

Figure 4.30 shows the reusability of the spent membranes versus the number of adsorption cycles. The 1% N-MWCNTs/CA membrane had the least adsorption loss as compared to the other five polymeric membranes. Interestingly, the adsorption

efficiency for all the polymeric membranes remained above 90% after the three adsorption cycles, which indicates that the PVDF-HFP based membranes can be recycled for Mg(II) ions adsorption. The results for 1% N-MWCNTs/CA composite membrane after the three-adsorption cycle was 1.02% as compared to 45% adsorption loss observed by Muqet et.al [19]. Furthermore, other membranes were also studied, and the results are presented in appendix 17.

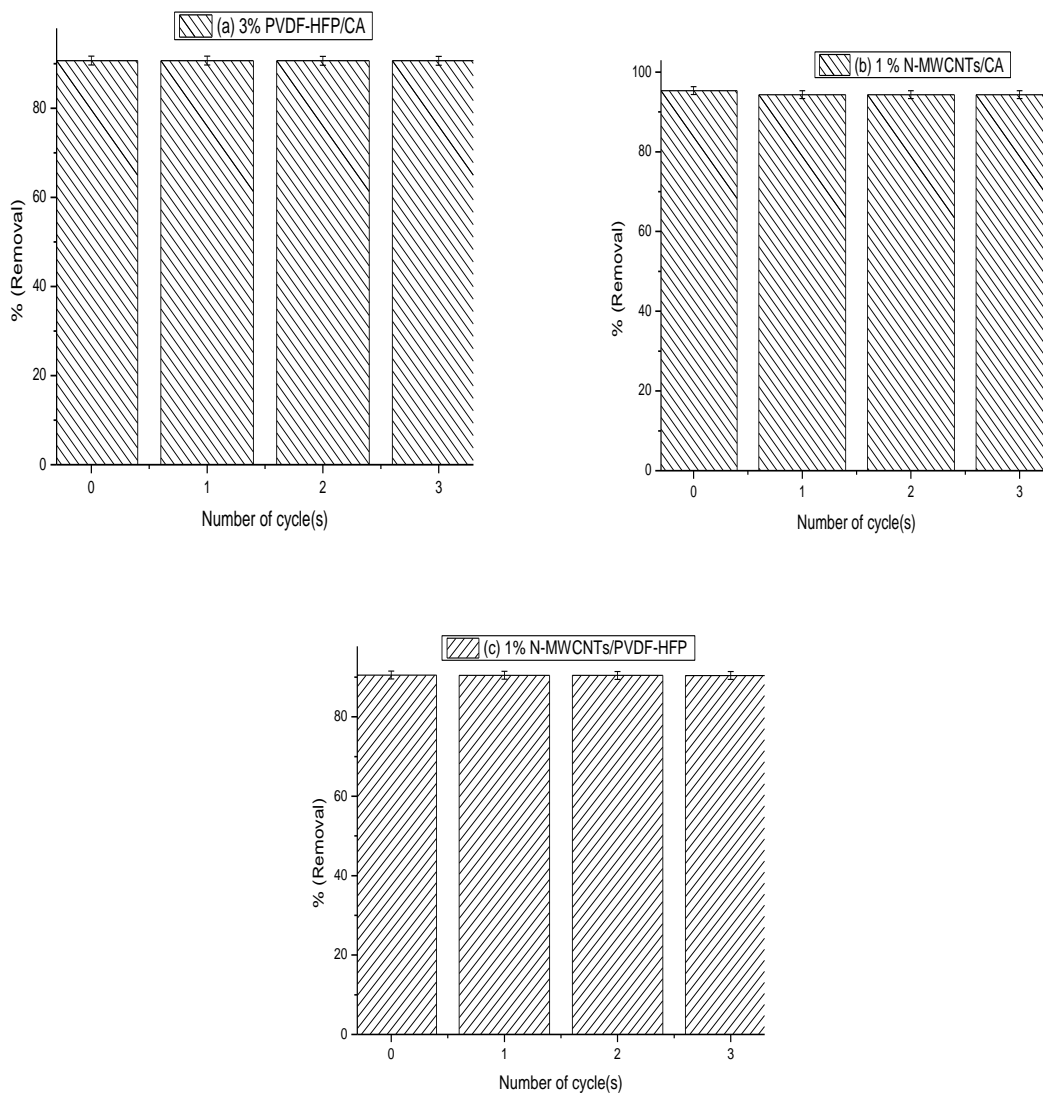


Figure 4.30: Effect of reusability on the adsorption of Mg (II) ions onto (a) 3% PVDF-HFP/CA, (b) 1% N-MWCNTs/CA, and (c) 1% N-MWCNTs/PVDF-HFP composite membranes.

4.3 REAL WATER APPLICATIONS

Tables 4.10 to 4.13 shows the results of real water samples from various sampling sites in the Limpopo province in summer season (February 2021) before and after membrane adsorption at 25 and 30 °C. These results demonstrate that within the borehole water samples the Ca(II) concentrations decreased as follows: Bergendal > Sekonye > Mokomene > Ga-Phasha > Ga-Machaba > My Darling. The concentration of calcium hardness is affected by the borehole depth; higher electrical conductivity means higher total dissolved solids (TDS) [20]. Borehole water samples had high Ca(II) ion concentration as compared to Mg (II) ions. This is because groundwater is in contact with the minerals that contain Ca(II) (e.g CaSO₄ or CaCl₂) present in the rocks and soil, and as water percolates through these minerals are dissolved. The TDS is directly proportional to the electrical conductivity of water, this can be ascribed to all the inorganic salts present in the water samples [26]. The WHO has defined the permissible limit for water hardness as 120 mg/L of CaCO₃. [43,44,45]. All the water samples were less than 120 ppm except for Bergendal which contains hard water of 130.25 mg/L for Ca(II) before membrane adsorption. All the water samples with the Mg(II) concentration were within the permissible limit before membrane adsorption. Interestingly, after membrane adsorption using the 3% PVDF-HFP/CA and 1% N-MWCNTs/CA for both metal ions the concentrations were all within the range of soft water [44,45]. It can be observed that the pH and the electrical conductivity of the water samples were within the acceptable limits as recommended by the WHO [46].

The results recorded in table 4.12 presents the adsorption of Ca(II) and Mg(II) by 3% PVDF-HFP and 1% N-MWCNTs/CA membranes at 25 °C, respectively. It can be observed that the adsorption of the metals by the membranes is lower at 25 °C, this is because the pH=7 of the water samples was not adjusted. There is a higher concentration of the protons in the acidic medium (results from the acidification of the water samples) which hinders the adsorption of the metals of interest hence the concentrations of the metal ions after adsorption are low. Table 4.13 shows the results of Ca(II) and Mg(II) removal by 3% PVDF-HFP and 1% N-MWCNTs/CA membranes at 30 °C, respectively. The pH = 7 was adjusted in this case, hence the concentration of the metal ions after adsorption is higher as compared to the results recorded at 25

°C. The optimum temperature and pH of the solution plays a vital role on the adsorption of the metal of interest. High temperature (i.e., 30 °C) causes the thermal energy of the adsorbing material to increase hence more adsorption of the metal ions onto the surface of the membranes [22]. The solution pH plays an important role on the sorption of the adsorbate by the adsorbent; this creates an electrostatic interaction between the positively charged metal ions with the negatively charged membrane surface [19].

Table 4.10: Physicochemical analysis of real water samples before membrane adsorption process at 25 °C.

Sampling sites and borehole depths (m)	Physical parameters (25 °C)	Chemical parameters (25 °C)		
	Conductivity (mS/m)	pH	Calcium (mg/L)	Magnesium (mg/L)
SANS 241 Standards	≤ 170	≤ 5 to 9.7	0 to 60	0 to 60
WHO Standards	≤ 250	≥ 6.5 to 8.5	0 to 60	0 to 60
Sekonye (40)	58	8.13	87.74	12.72
Mokomene (70)	36	7.58	67.91	12.51
Ga-Phasha (100)	22	7.13	61.73	13.02
My Darling (50)	47	7.45	40.87	12.62
Bergendal (33)	17	6.86	130.25	13.44
Ga-Machaba (60)	22	7.13	66.78	13.03

Table 4.11: Physicochemical analysis of real water samples before membrane adsorption process at 30 °C.

Sampling sites and borehole depths (m)	Physical parameters (30 °C)	Chemical parameters (30 °C)		
	Conductivity (mS/m)	pH	Calcium hardness (mg/L)	Magnesium hardness (mg/L)
SANS 241 Standards	≤ 170	≤ 5 to 9.7	0 to 60	0 to 60
WHO Standards	≤ 250	≥ 6.5 to 8.5	0 to 60	0 to 60
Sekonye (40)	9	7.01	73.99	12.54
Mokomene (70)	12	7.05	55.51	12.30
Ga-Phasha (100)	13	7.07	46.49	12.80
My Darling (50)	14	7.09	31.40	12.42
Bergendal (33)	10	7.02	91.49	13.15
Ga-Machaba (60)	11	7.03	36.66	12.72

Table 4.12: Chemical analysis of real water samples after membrane adsorption process at 25 °C.

Sampling sites and borehole depths (m)	Chemical parameters (25 °C)			
	Calcium hardness concentration after treatment with 3% PVDF-HFP/CA membrane (mg/L)	Calcium hardness concentration after treatment with 1% N-MWCNTs/CA membrane (mg/L)	Magnesium hardness concentration after treatment with 3% PVDF-HFP/CA membrane (mg/L)	Magnesium hardness concentration after treatment with 1% N-MWCNTs/CA membrane (mg/L)
SANS 241 Standards	120	120	120	120
WHO Standards	120	120	120	120
Sekonye (40)	80.58	82.93	11.73	11.67
Mokomene (70)	63.27	62.41	11.57	11.46
Ga-Phasha (100)	60.53	61.07	12.13	11.97
My Darling (50)	39.21	38.77	11.66	11.58
Bergendal (33)	126.80	127.45	12.41	12.35
Ga-Machaba (60)	58.37	58.92	12.02	11.90

Table 4.13: Chemical analysis of real water samples after membrane adsorption process at 30 °C.

Sampling sites and borehole depths (m)	Chemical parameters (30 °C)			
	Calcium hardness concentration after treatment with 3% PVDF-HFP/CA membrane (mg/L)	Calcium hardness concentration after treatment with 1% N-MWCNTs/CA membrane (mg/L)	Magnesium hardness concentration after treatment with 3% PVDF-HFP/CA membrane (mg/L)	Magnesium hardness concentration after treatment with 1% N-MWCNTs/CA membrane (mg/L)
SANS 241 Standards	120	120	120	120
WHO Standards	120	120	120	120
Sekonye (40)	6.50	7.24	1.12	1.22
Mokomene (70)	4.79	5.34	1.02	1.13
Ga-Phasha (100)	3.34	4.50	1.00	1.09
My Darling (50)	2.22	3.39	1.00	1.10
Bergendal (33)	6.22	9.24	1.10	1.19
Ga-Machaba (60)	3.48	4.17	1.12	1.17

4.3.1 Effect of membrane reusability on real hard water samples

Reusability of the spent adsorbent is important to reduce the environmental degradation. Figure 4.31 to 4.34 presents the reusability of 3% PVDF-HFP/CA and 1% N-MWCNTs/CA composite membranes in Sekonye and Bergendal water samples.

The adsorption capacity of Ca (II) from the first to the third cycle reduced from 91.12 to 91.04% and 93.23 to 93.13% while the adsorption capacities of Mg(II) decreased from 91.00 to 90.91% and 91.6 to 91.57% for Sekonye and Bergendal water samples using the 3% PVDF-HFP/CA composite membranes. When the 1% N-MWCNTs composite membranes were used, the adsorption uptake of Ca(II) from the first to the third cycle reduced from 90.32 to 90.13% and 89.95 to 89.85% while Mg(II) decreased from 90.31 to 89.83% and 90.87 to 90.38% for Sekonye and Bergendal water samples. The 3% PVDF-HFP/CA composite membrane showed the highest adsorption loss as compared to the 1% N-MWCNTs/CA composite membranes. Interestingly, the adsorption loss from the first until the third cycle for the two composite membranes remained above 80%, which indicates that the PVDF-HFP based membranes can be recycled for the hardness causing agents. The adsorption loss for the 3% PVDF-HFP/CA and 1% N-MWCNTs/CA after the three cycles was $\leq 0.10\%$ and 0.50% , respectively. These results are better as compared to the adsorption loss of 10% which was recorded elsewhere [19].

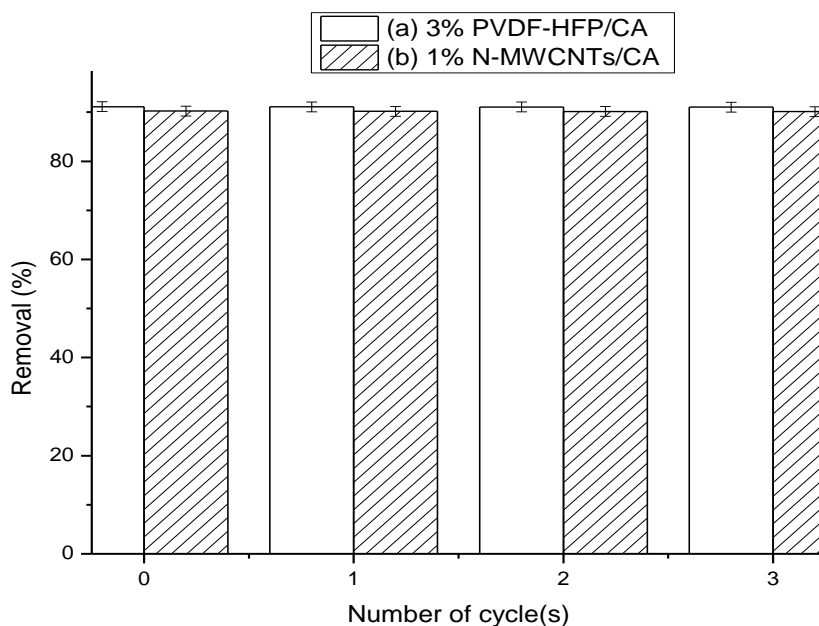


Figure 4.31: Effect of membrane reusability on the removal of calcium hardness using 3% PVDF-HFP/CA and 1% N-MWCNTs/CA from Sekonye water samples. (Concentration 73.99 mg/L, dosage 0.5 mg/L, pH 7, time 90 minutes, temperature = 30 °C, 200 rpm agitation speed).

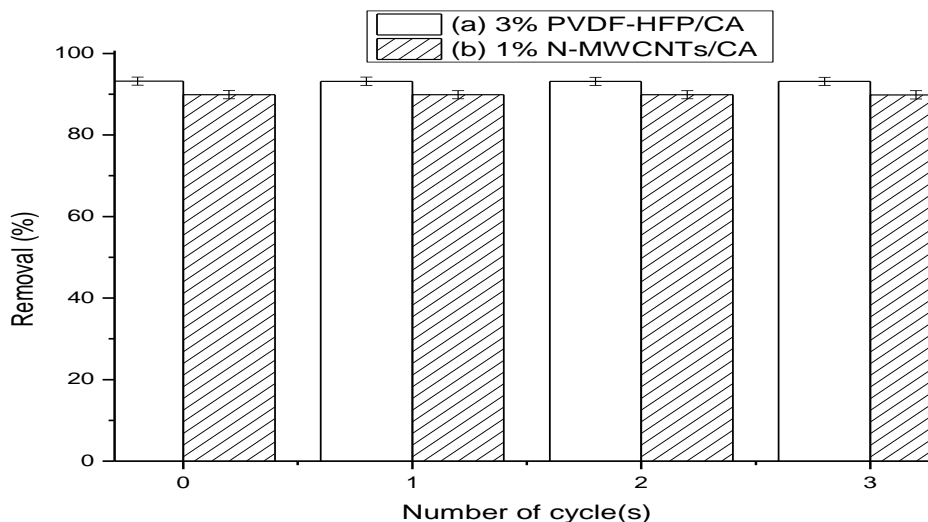


Figure 4.32: Effect of membrane reusability on the removal of calcium hardness using 3% PVDF-HFP/CA and 1% N-MWCNTs/CA from Bergendal water samples. (Concentration 91.49 mg/L, dosage 0.5 mg/L, pH 7, time 90 minutes, temperature = 30 °C, 200 rpm agitation speed)

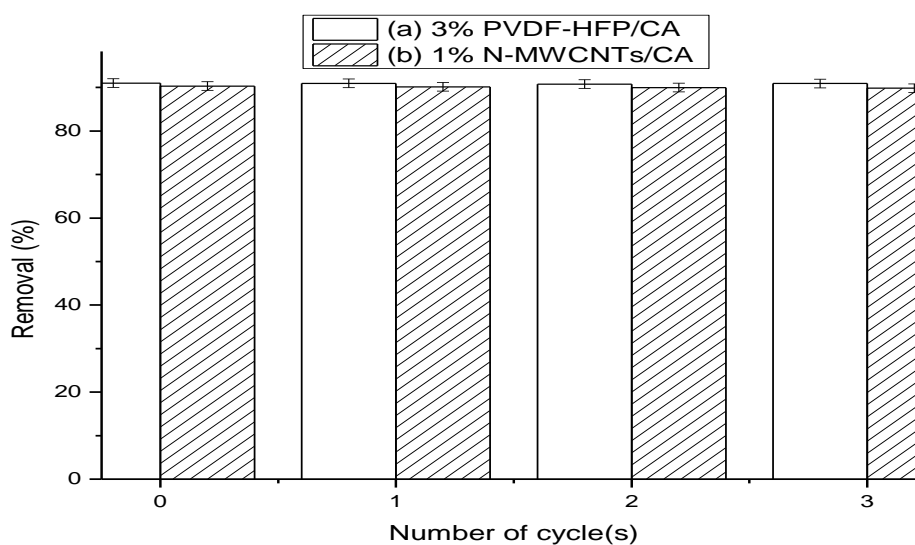


Figure 4.33: Effect of membrane reusability on the removal of magnesium hardness using 3% PVDF-HFP/CA and 1% N-MWCNTs/CA from Sekonye water samples. (Concentration 12.535 mg/L, dosage 0.5 mg/L, pH 7.00, time 90 minutes, temperature = 30 °C, 200 rpm agitation speed)

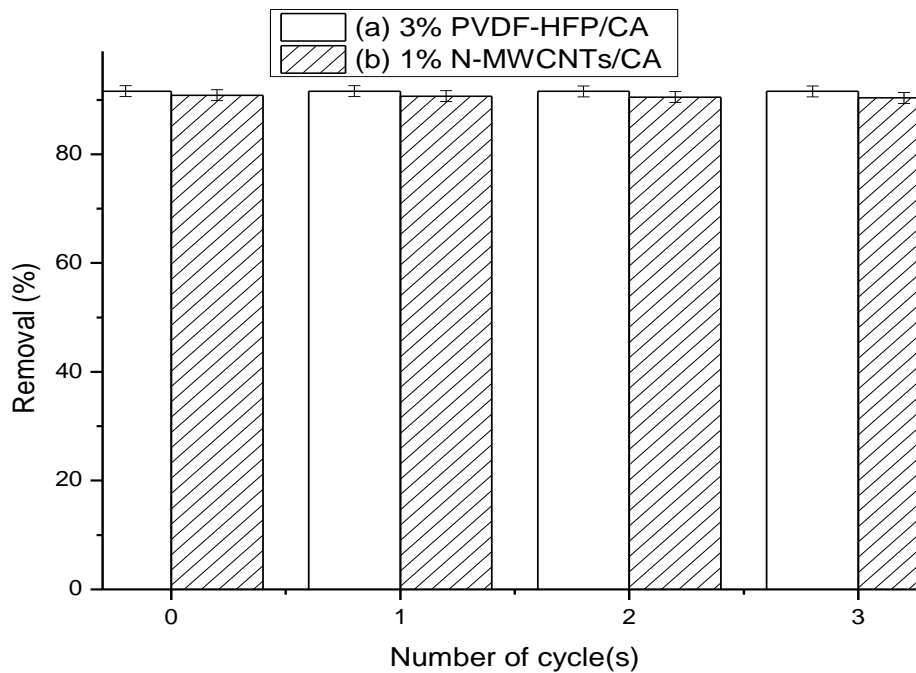


Figure 4.34: Effect of membrane reusability on the removal of magnesium hardness using 3% PVDF-HFP/CA and 1% N-MWCNTs/CA from Bergendal water samples. (Concentration 13.145 mg/L dosage 0.5 mg/L, pH 7.00, time 90 minutes, temperature = 30 °C, 200 rpm agitation speed.

REFERENCES

- [1] Ritter, U., Tsierkezos, N.G., Prylutsky, Y.I., Matzui, L.Y., Gubanov, V.O., Bilyi, M.M. and Davydenko, M.O., 2012. Structure–electrical resistivity relationship of N-doped multi-walled carbon nanotubes. *Journal of Materials Science*, 47(5), pp.2390-2395.
- [2] Dognani, G., Hadi, P., Ma, H., Cabrera, F.C., Job, A.E., Agostini, D.L. and Hsiao, B.S., 2019. Effective chromium removal from water by polyaniline-coated electrospun adsorbent membrane. *Chemical Engineering Journal*, 372, pp.341-351.
- [3] Yadav, A., Sharma, P., Panda, A.B. and Shahi, V.K., 2021. Photocatalytic TiO₂ incorporated PVDF-co-HFP UV-cleaning mixed matrix membranes for effective removal of dyes from synthetic wastewater system via membrane distillation. *Journal of Environmental Chemical Engineering*, p.105904.

- [4] El-Gendi, A., Abdallah, H., Amin, A. and Amin, S.K., 2017. Investigation of polyvinylchloride and cellulose acetate blend membranes for desalination. *Journal of Molecular Structure*, 1146, pp.14-22.
- [5] Asghar, M.R., Zhang, Y., Wu, A., Yan, X., Shen, S., Ke, C. and Zhang, J., 2018. Preparation of microporous Cellulose/Poly (vinylidene fluoride-hexafluoropropylene) membrane for lithium-ion batteries by phase inversion method. *Journal of Power Sources*, 379, pp.197-205.
- [6] Asghar, M.R., Anwar, M.T., Xia, G. and Zhang, J., 2020. Cellulose/Poly (vinylidene fluoride hexafluoropropylene) composite membrane with titania nanoparticles for lithium-ion batteries. *Materials Chemistry and Physics*, 252, p.123122.
- [7] Yu, C., Wang, Y., Liu, Y., Guo, C. and Hu, Y., 2013. Facile growth of ZnO nanocrystals on nitrogen-doped carbon nanotubes for visible-light photodegradation of dyes. *Materials Letters*, 100, pp.278-281.
- [8] Tripathi, M., Bobade, S.M. and Kumar, A., 2019. Preparation of polyvinylidene fluoride-co-hexafluoropropylene-based polymer gel electrolyte and its performance evaluation for application in EDLCs. *Bulletin of Materials Science*, 42(1), p.27.
- [9] Das, A.M., Ali, A.A. and Hazarika, M.P., 2014. Synthesis and characterization of cellulose acetate from rice husk: Eco-friendly condition. *Carbohydrate polymers*, 112, pp.342-349.
- [10] Rajesh, S., Maheswari, P., Senthilkumar, S., Jayalakshmi, A. and Mohan, D., 2011. Preparation and characterisation of poly (amide-imide) incorporated cellulose acetate membranes for polymer enhanced ultrafiltration of metal ions. *Chemical Engineering Journal*, 171(1), pp.33-44.
- [11] Salam, M.A. and Burk, R., 2017. Synthesis and characterization of multi-walled carbon nanotubes modified with octadecylamine and polyethylene glycol. *Arabian Journal of Chemistry*, 10, pp. S921-S927.
- [12] Shin, J., Nho, Y.C., seon Hwang, I., Fei, G., Kim, A.R. and Nahm, K.S., 2010. Irradiated PVdF-HFP-tin oxide composite membranes for the applications of direct methanol fuel cells. *Journal of Membrane Science*, 350(1-2), pp.92-100.

- [13] Steinmetz, M., Lima, D., Machado, R.R.L., Sundararaj, U., Arjmand, M., da Silva, A.B., Santos, J.P., Pessoa, C.A. and Wohnrath, K., 2020. Nitrogen-doped carbon nanotubes towards electrochemical sensing: Effect of synthesis temperature. *Diamond and Related Materials*, 110, p.108093.
- [14] Ameli, A., Arjmand, M., Pötschke, P., Krause, B. and Sundararaj, U., 2016. Effects of synthesis catalyst and temperature on broadband dielectric properties of nitrogen-doped carbon nanotube/polyvinylidene fluoride nanocomposites. *Carbon*, 106, pp.260-278.
- [15] Santos, J.P.F., Arjmand, M., Melo, G.H.F., Chizari, K., Bretas, R.E.S. and Sundararaj, U., 2018. Electrical conductivity of electrospun nanofiber mats of polyamide 6/polyaniline coated with nitrogen-doped carbon nanotubes. *Materials & Design*, 141, pp.333-341.
- [16] Elias, M., Uddin, M., Saha, J.K., Hossain, M., Sarker, D.R., Akter, S., Siddiquey, I.A. and Uddin, J., 2021. A highly efficient and stable photocatalyst; N-doped ZnO/CNT composite thin film synthesized via simple sol-gel drop coating method. *Molecules*, 26(5), p.1470.
- [17] Iqhrammullah, M., Marlina, M., Khalil, H.P.S., Kurniawan, K.H., Suyanto, H., Hedwig, R., Karnadi, I., Olaiya, N.G., Abdullah, C.K. and Abdulmadjid, S.N., 2020. Characterization and performance evaluation of cellulose acetate–polyurethane film for lead II ion removal. *Polymers*, 12(6), p.1317.
- [18] Zhao, D., Yu, Y. and Chen, J.P., 2016. Treatment of lead contaminated water by a PVDF membrane that is modified by zirconium, phosphate and PVA. *Water research*, 101, pp.564-573.
- [19] Muqeet, M., Khaliq, A., Qureshi, U.A., Mahar, R.B., Ahmed, F., Khatri, Z., Kim, I.S. and Brohi, K.M., 2018. Aqueous hardness removal by anionic functionalized electrospun cellulose nanofibers. *Cellulose*, 25(10), pp.5985-5997.
- [20] Rolence, C., Machunda, R. and Njau, K.N., 2014. Water hardness removal by coconut shell activated carbon. *International Journal of Science, Technology and Society*, 2(5), pp.97-102.

- [21] Werkneh, A.A., Abay, A.K. and Senbeta, A.M., 2015. Removal of water hardness causing constituents using alkali modified sugarcane bagasse and coffee husk at Jigjiga city, Ethiopia: A comparative study. *world*, 1, p.2.
- [22] Magadzu, T., Moganedi, K. and Macevele, L., 2021. Adsorption of Cadmium (II) Ions from Aqueous Solutions using Poly (Amidoamine)/Multi-Walled Carbon Nanotubes Doped Poly (Vinylidene Fluoride-Co-Hexafluoropropene) Composite Membrane. *Journal of Membrane Science and Research*, 7(3), pp.152-165.
- [23] Gafoor, A., Ali, N., Kumar, S., Begum, S. and Rahman, Z., 2020. Comparative and optimization studies of PE and PVP binder with different graphene electrodes for the reduction of hardness. *Materials Today: Proceedings*, 37, pp.453-458.
- [24] Bibiano-Cruz, L., Garfias, J., Salas-García, J., Martel, R. and Llanos, H., 2016. Batch and column test analyses for hardness removal using natural and homoionic clinoptilolite: breakthrough experiments and modeling. *Sustainable Water Resources Management*, 2(2), pp.183-197.
- [25] Ab Kadir, N.N., Shahadat, M. and Ismail, S., 2017. Formulation study for softening of hard water using surfactant modified bentonite adsorbent coating. *Applied Clay Science*, 137, pp.168-175.
- [26] Lestari, A.Y.D., Malik, A., Ilmi, M.I. and Sidiq, M., 2018. Removal of calcium and magnesium ions from hard water using modified *Amorphophallus campanulatus* skin as a low-cost adsorbent. In *MATEC Web of Conferences* (Vol. 154, p. 01020). EDP Sciences.
- [27] Çalgan, E. and Ozmetin, E., 2019. Optimization of hardness removal using response surface methodology from wastewater containing high boron by Bigadic clinoptilolite. *Desalination and Water Treatment*, 172, pp.281-291.
- [28] Soliman, E.M., Ahmed, S.A. and Fadl, A.A., 2020. Microwave-enforced green synthesis of novel magnetic nano composite adsorbents based on functionalization of wood sawdust for fast removal of calcium hardness from water samples. *Water Environment Research*, 92(12), pp.2112-2128.

- [29] Lima, R.R., de Lima, P.D.S., Greati, V.R., de Sousa, P.B. and Medeiros, G.V., 2019. Sodium-Modified Vermiculite for Calcium Ion Removal from Aqueous Solution. *Industrial & Engineering Chemistry Research*, 58(22), pp.9380-9389.
- [30] Han, R., Zhang, J., Han, P., Wang, Y., Zhao, Z. and Tang, M., 2009. Study of equilibrium, kinetic and thermodynamic parameters about methylene blue adsorption onto natural zeolite. *Chemical Engineering Journal*, 145(3), pp.496-504.
- [31] Chen, G.C., Shan, X.Q., Zhou, Y.Q., Shen, X.E., Huang, H.L. and Khan, S.U., 2009. Adsorption kinetics, isotherms, and thermodynamics of atrazine on surface oxidized multiwalled carbon nanotubes. *Journal of Hazardous Materials*, 169(1-3), pp.912-918.
- [32] Yang, S., Li, L., Pei, Z., Li, C., Lv, J., Xie, J., Wen, B., and Zhang, S., 2014. Adsorption kinetics, isotherms, and thermodynamics of Cr (III) on graphene oxide. *Colloids and Surfaces A: Physicochemical and Engineering Aspects*, 457, pp.100-106.
- [33] Sepehr, M.N., Zarrabi, M., Kazemian, H., Amrane, A., Yaghmaian, K., and Ghaffari, H.R., 2013. Removal of hardness agents, calcium, and magnesium, by natural and alkaline modified pumice stones in single and binary systems. *Applied Surface Science*, 274, pp.295-305.
- [34] Swelam, A., Awad, M. and Salem, A., 2014. Removal of Ca (II) and Mg (II) from Aqueous-Organic Solutions on Strong Cation Exchange of ResinexTMK-8H. *International Journal of Environment*, 3(3), pp.161-171.
- [35] Saeed, A.M. and Hamzah, M.J., 2013. New approach for removal of total hardness (Ca²⁺, Mg²⁺) from water using commercial polyacrylic acid hydrogel beads, study, and application. *International journal of advanced biological and biomedical research*, 1(9), pp.1142-1156.
- [36] Chakrabarty, S. and Sarma, H.P., 2012. Defluoridation of contaminated drinking water using neem charcoal adsorbent: kinetics and equilibrium studies. *International Journal of ChemTech Research*, 4(2), pp.511-516.
- [37] Elwakeel, K.Z., 2020. Magnesium sorption onto titan yellow supported on classic thiourea-formaldehyde resin. *Aswan University Journal of Environmental Studies*, 1(2), pp.125-136.

- [38] Pourshadlou, S., Mobasherpour, I., Majidian, H., Salahi, E., Bidabadi, F.S., Mei, C.T. and Ebrahimi, M., 2020. Adsorption system for Mg²⁺ removal from aqueous solutions using bentonite/ γ -alumina nanocomposite. *Journal of colloid and interface science*, 568, pp.245-254.
- [39] Aragaw, T.A. and Ayalew, A.A., 2019. Removal of water hardness using zeolite synthesized from Ethiopian kaolin by hydrothermal method. *Water Practice and Technology*, 14(1), pp.145-159.
- [40] Mustapha, S., Ndamitso, M.M., UM, M., NO, A. and Idris, M., 2016. Study on activated from melon (*Citrullus lanatus*) husk as natural adsorbent for removal of hardness in water. *Advances in Analytical Chemistry*, 6(1), pp.1-9.
- [41] Cetin, G., 2014. Removal of hardness of earth alkaline metals from aqueous solutions by ion exchange method. *International Scholarly Research Notices*, 2014.
- [42] Pratomo, U., Anggraeni, A., Lubis, R.A., Pramudya, A., Farida, I.N., 2015. Study of softening hardwater using *Pistacia vera* shell as adsorbent for calcium and magnesium removal. *Procedia Chem.* 16, 400–406.
- [43] Guecciaa, R., Alhadidib, A.M.M., Cipollinaa, A. and Micala, G., 2020. Donnan dialysis for tap-water softening. *Desalination and Water Treatment*, 192, pp.19-32.
- [44] Campbell, J. and Peterson, D., 2010. Determination of water hardness from common water sources using flame atomic absorbance spectrometry. *Concordia College Journal of Analytical Chemistry*, 1, pp.4-8.
- [45] Soliman, E.M., Ahmed, S.A. and Fadl, A.A., 2020. Microwave-enforced green synthesis of novel magnetic nano composite adsorbents based on functionalization of wood sawdust for fast removal of calcium hardness from water samples. *Water Environment Research*, 92(12), pp.2112-2128.
- [46] WHO., 2018. Water health and human rights, World water day 2001. Available online at [\(http://www.worldwaterday.org/thematic/hmnrights.html#n4\)](http://www.worldwaterday.org/thematic/hmnrights.html#n4). (accessed 10 June 2021)

CONCLUSIONS AND RECOMMENDATIONS

5.1 CONCLUSIONS

Softening of hard water by removing Ca(II) and Mg(II) cations was studied using PVDF-HFP based membranes as adsorbents. The composite membranes were prepared successfully using the phase inversion method and consisted of various composition such as CA, PVDF-HFP, 3% PVDF-HFP/CA, 1% N-MWCNTs/CA, 1% N-MWCNTs/PVDF-HFP and 1% N-MWCNTs/3% PVDF-HFP/CA. Fourier transform infrared (FTIR) spectroscopy confirmed the formation of the functional groups on the membrane surfaces.

X-ray diffraction (XRD) results have confirmed the hexagonal graphite structures of the pristine N-MWCNTs, and the semi-crystalline nature of the neat PVDF-HFP membrane as well as the amorphous region of the cellulose chains present in the CA membrane.

Thermogravimetric analysis (TGA) results demonstrated that the thermal stability of the pure N-MWCNTs did not show any weight loss. The TGA thermograms of PVDF-HFP and 1% N-MWCNTs/PVDF-HFP composite membranes showed a distinct single step weight loss with an increase in temperature shoulder, while the TGA thermograms of CA, 3% PVDF-HFP/CA, 1% N-MWCNTs/CA and 1% N-MWCNTs/3% PVDF-HFP/CA composite membranes started to decompose at low temperature intervals between 300 and 400 °C.

Scanning electron microscopy (SEM) images have depicted the formation of small pores distributed uniformly on the surface of PVDF-HFP, upon the addition of CA, and N-MWCNTs into the PVDF-HFP casting solution, a solidified and dense skin layer was observed.

Transmission electron microscopy (TEM) confirmed the formation of bamboo-like structure and the presence of very defective and less aligned parts in the walls of N-MWCNTs, which results from the nitrogen atoms, bringing about drastic local distortions within the hexagonal graphitic-based structure.

The concentration of Ca(II) and Mg(II) cations in synthetic water samples was investigated in batch studies wherein parameters such as pH, time, temperature, and adsorbent dosage were optimised. The highest adsorption of 99 % was observed on 3% PVDF-HFP and 1% N-MWCNTs/CA composite membranes for Ca(II) and Mg(II), respectively.

The maximum adsorption efficiency of 56 mg/g and 45 mg/g evaluated by Langmuir isotherm for Ca(II) and Mg(II) ions was achieved at an optimum pH of 7 and adsorption dosage of 0.5 mg/L for the 3% PVDF-HFP/CA and 1% N-MWCNTs/CA based membranes. The adsorption kinetics and isotherm models were all consistent with the pseudo-second order and Freundlich isotherm models for all the membranes suggesting that the sorption process met heterogeneous adsorption. Furthermore, the thermodynamic parameters indicated that the adsorption is physical and endothermic in nature.

Reusability studies showed that all the PVDF-HFP based membranes can be recycled at least 3 times for Ca(II) ions with an adsorption loss of only 0.35% for 3% PVDF-HFP/CA composite membrane and the results were further confirmed by XRD, TGA and ICP-MS spectrometry. Regeneration studies of the PVDF-HFP composite membranes were also performed on Mg (II) ions. The 1% N-MWCNTs/CA composite membrane showed an adsorption loss of 1.02 % from the first adsorption cycle to the third cycle. Thus, the findings from this study have shown that the PVDF-HFP based membranes could provide valuable material for hardness removal to acceptable level.

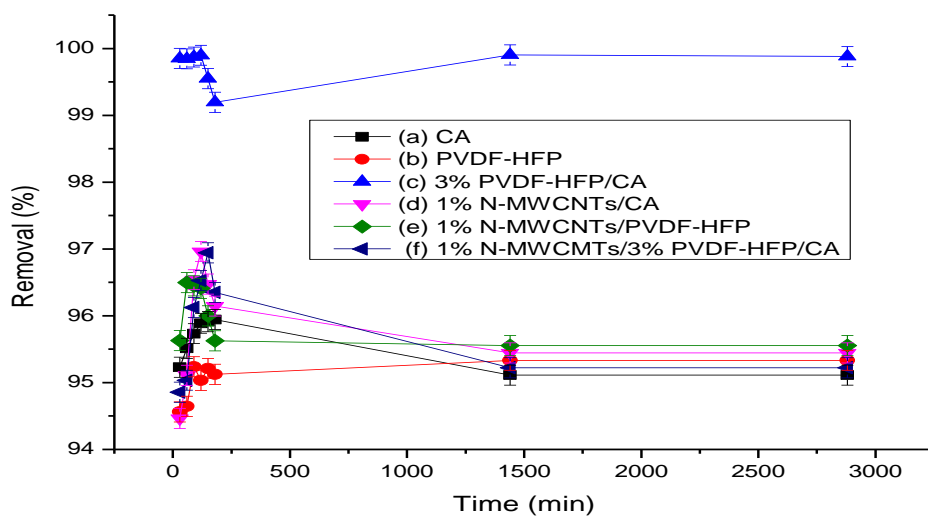
Real water samples from various sampling sites in the Limpopo village were analysed before and after membrane adsorption. The results demonstrated that borehole water samples from Bergendal contained hard water of 130.25 ppm for Ca(II) ions. Calcium concentration levels reduced from 130.25 ppm to 6.22 ppm and 9.24 ppm, after

membrane adsorption with 3% PVDF-HFP/CA and 1% N-MWCNTs/CA composite membranes, respectively. It was observed that the composite membranes can soften hard water to acceptable as recommended by the WHO. The ultimate composite membrane is the 3% PVDF-HFP/CA, because the reusability studies of the real water samples also showed that the 3% PVDF-HFP/CA can be reused at least 3 times with adsorption loss of $\leq 0.1\%$ as compared to 0.5% for 1% N-MWVCNTs/CA composite membrane.

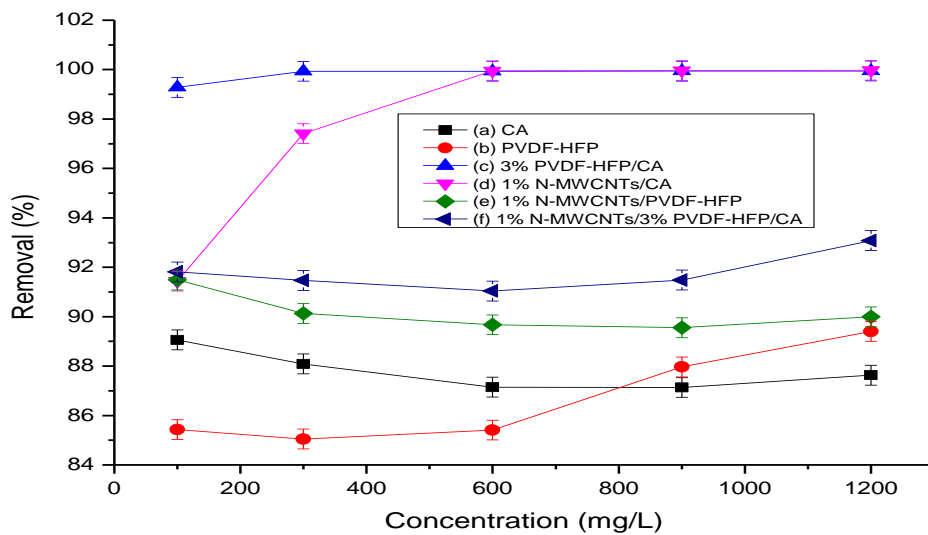
5.2 RECOMMENDATIONS

This study was aimed at preparing alternative highly adsorptive and cost-effective PVDF-HFP composite membranes for removal of hardness causing ions from aqueous solutions. In future, Brunauer Emmett-Teller (BET) will be used to determine surface area of the PVDF-HFP based membranes. Modification of the PVDF-HFP composite membranes using various methods/materials such as metal organic fragments (MOF) can be carried out to enhance the removal of other water pollutants. Furthermore, membrane filtration studies should be conducted to investigate the removal of hardness constituents and other water pollutants such as heavy metals.

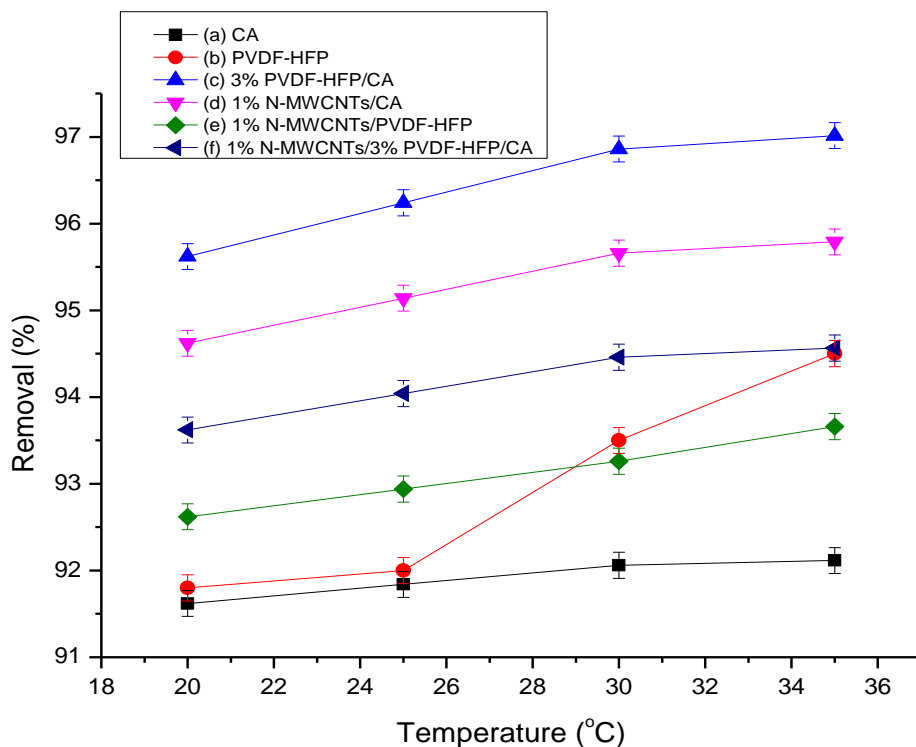
1.2 5.3 APPENDICES



Appendix 1: Effect of contact time on adsorption efficiency of Ca (II) ions onto (a) CA, (b) PVDF-HFP, (c) 3 % PVDF-HFP/CA, (d) 1 % N-MWCNTs/CA, (e) 1 % N-MWCNTs/PVDF-HFP and (f) 1% N-MWCNTs/3 % PVDF-HFP/CA composite membranes

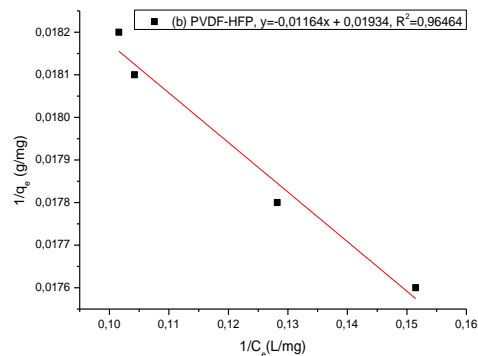
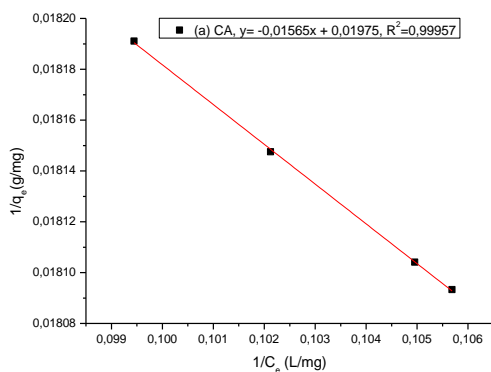


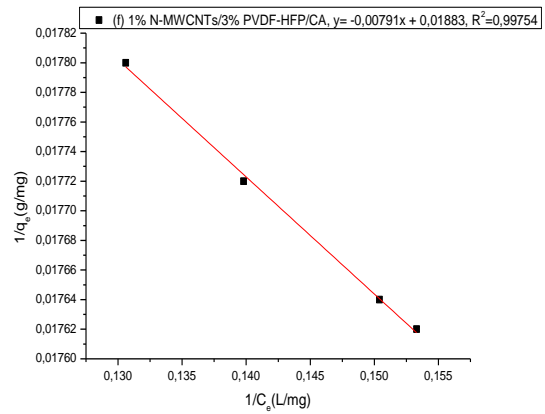
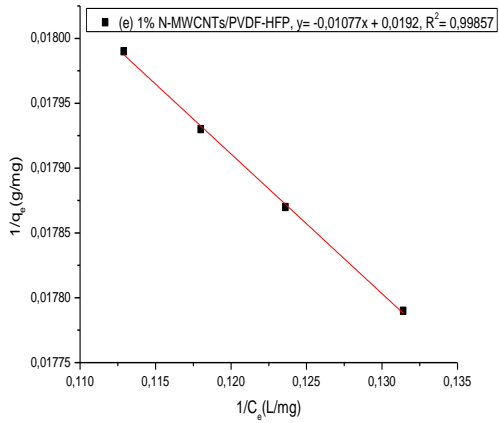
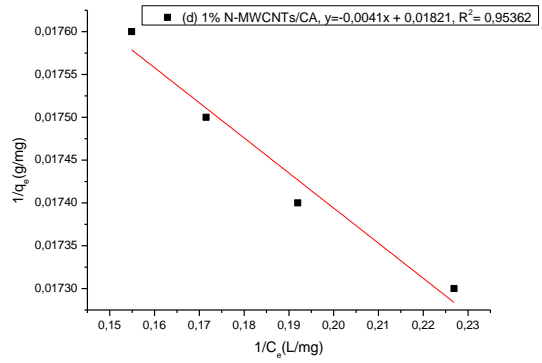
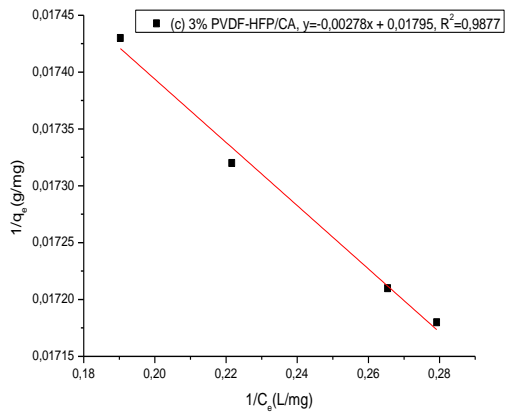
Appendix 2: Effect of initial metal ion concentration on the adsorption efficiency of Ca (II) ions onto (a) CA, (b) PVDF-HFP, (c) 3% PVDF-HFP/CA, (d) 1% N-MWCNTs/CA, (e) 1% N-MWCNTs/PVDF-HFP and 1% N-MWCNTs/3% PVDF-HFP/CA composite membranes



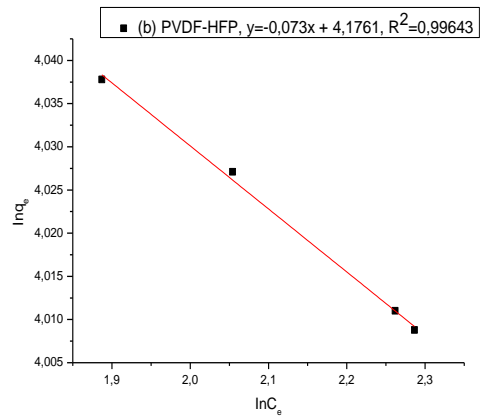
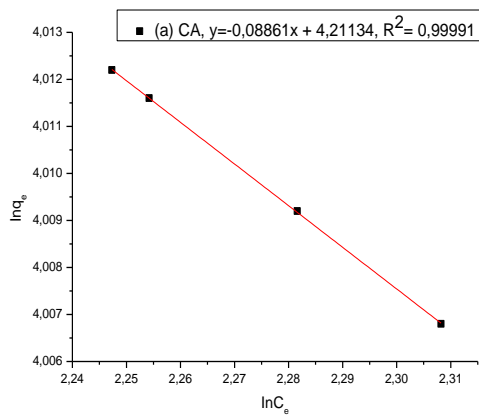
Appendix 3: Effect of temperature on adsorption efficiency of Ca (II) ions on (a) CA, (b) PVDF-HFP, (c) 3% PVDF-HFP/CA, (d) 1% N-MWCNTs/CA, (e) 1% N-MWCNTs/PVDF-HFP and 1% N-MWCNTs/3% PVDF-HFP/CA based membrane.

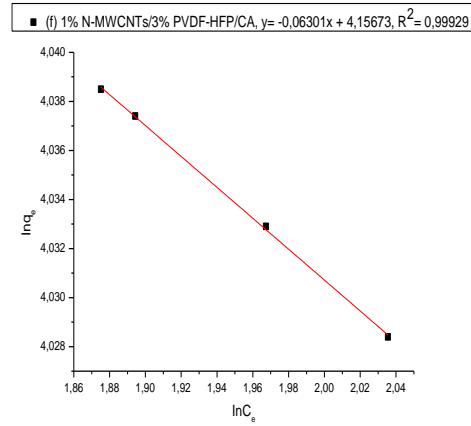
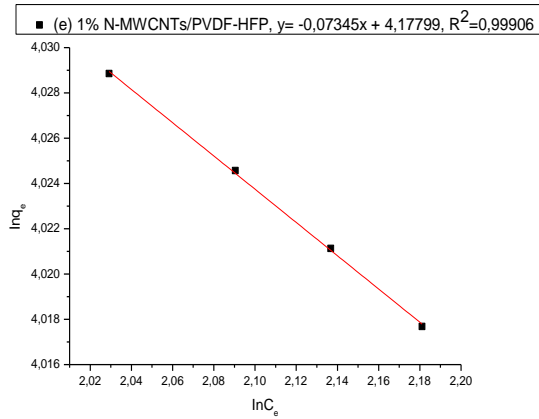
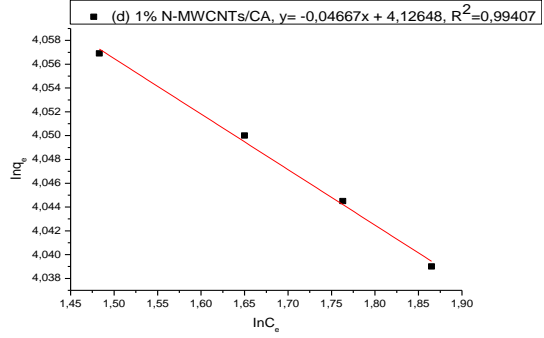
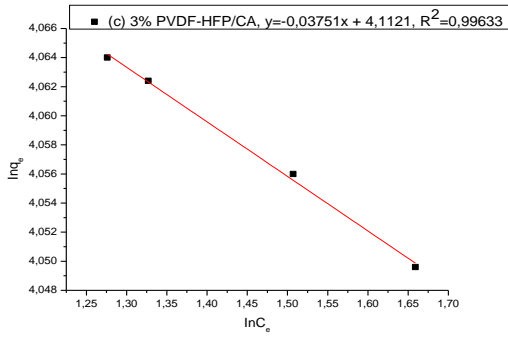
(i) Langmuir Isotherms





(i) Freundlich isotherm

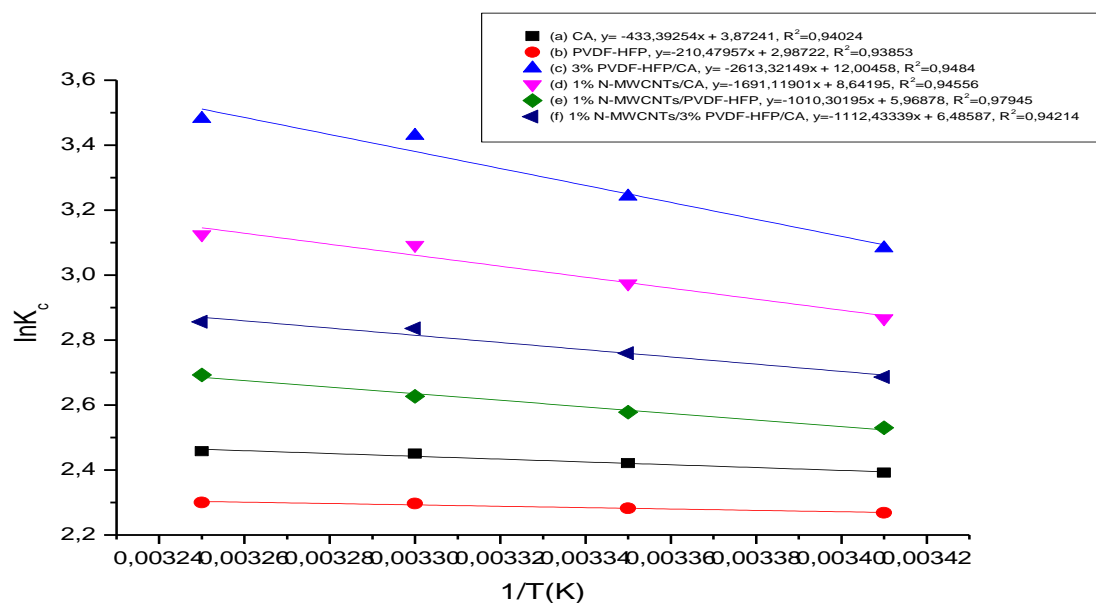




Appendix 4: (i) Langmuir isotherm and (ii) Freundlich isotherm for the adsorption of Ca (II) ions onto (a) CA, (b) PVDF-HFP, (c) 3% PVDF-HFP/CA, (d) 1% N-MWCNTs/CA, (e) 1% N-MWCNTs/PVDF-HFP and (f) 1% N-MWCNTs/3% PVDF-HFP/CA based membranes.

Table 5.3.1: Langmuir and Freundlich isotherm parameters for Ca (II) ions adsorption onto PVDF-HFP composite membranes.

Membrane	q _{max} (mg/g)	Langmuir model			Freundlich model		
		b (L/mg)	R ²	R _L	K _f (mg/g)	n	R ²
CA	50.633	-1.262	0.99957	-0.00665	16268.219	-11.285	0.99991
PVDF-HFP	51.706	-1.662	0.96464	-0.00504	15000.302	-13.699	0.99643
3% PVDF-HFP/CA	55.710	-6.457	0.9877	-0.00129	12944.939	-26.660	0.99633
1% N-MWCNTs/CA	54.915	-4.441	0.95362	-0.00188	13380.736	-21.427	0.99407
1% N-MWCNTs/PVDF-HFP	52.083	-1.783	0.99857	-0.00470	15065.724	-13.615	0.99906
1% N-MWCNTs/3% PVDF-HFP/CA	53.107	-2.381	0.99754	-0.00351	14345.973	-15.870	0.99929

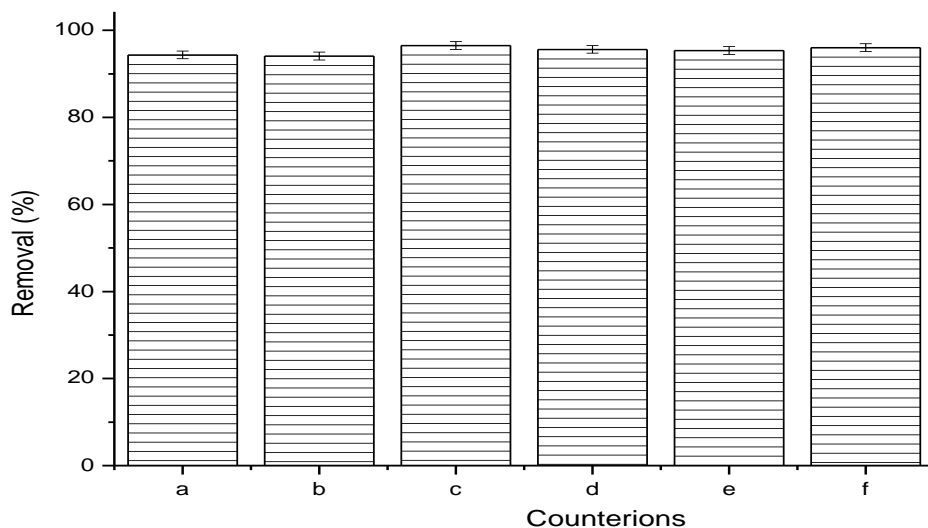


Appendix 5: Thermodynamic parameters of Ca (II) ions onto (a) CA, (b) PVDF-HFP, (c) 3% PVDF-HFP/CA, (d) 1% N-MWCNTs/CA, (e) 1% N-MWCNTs/PVDF-HFP and (f) 1% N-MWCNTs/3% PVDF-HFP/CA composite membranes.

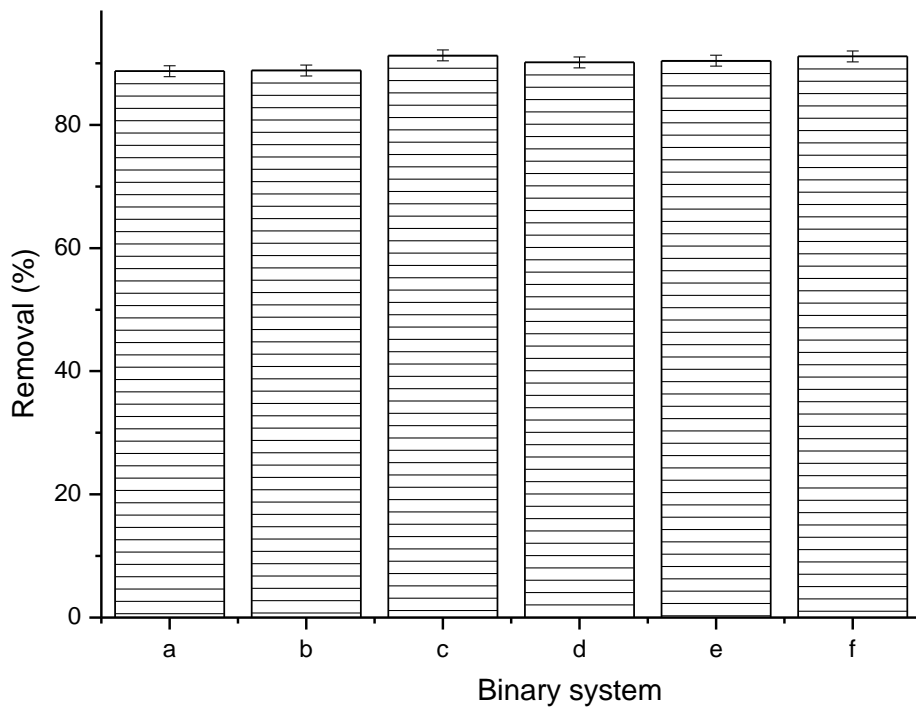
Table 5.3.2: Thermodynamic parameters for Ca (II) (120 ppm) adsorption by PVDF-HFP composite membranes

Membrane	Temperature (K)	Thermodynamic parameters		
		ΔG (KJ/mol)	ΔH (KJ/mol)	ΔS (J.mol/K)
CA	293.15	-5829.416	52.128	0.466
	298.15	-6000.735		
	303.15	-6176.282		
	308.15	-6297.489		
PVDF-HFP	293.15	-5527.913	25.316	0.359
	298.15	-5657.395		
	303.15	-5788.476		
	308.15	-5893.216		
3% PVDF-HFP/CA	293.15	-7514.851	314.328	1.444
	298.15	-8037.388		
	303.15	-8642.525		
	308.15	-8918.861		
1% N-MWCNTs/CA	293.15	-6988.033	203.406	1.0394
	298.15	-7372.779		
	303.15	-7795.377		
	308.15	-8005.342		
1% N-MWCNTs/PVDF-HFP	293.15	-6165.586	121.518	0.718
	298.15	-6389.179		
	303.15	-6621.897		

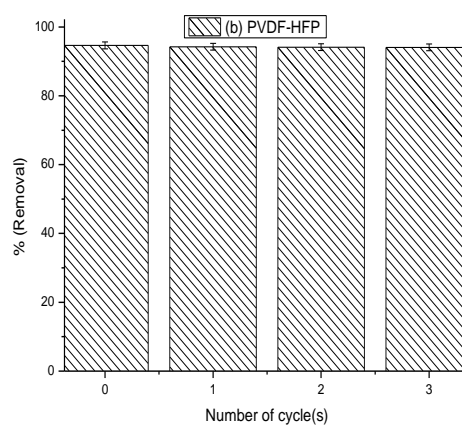
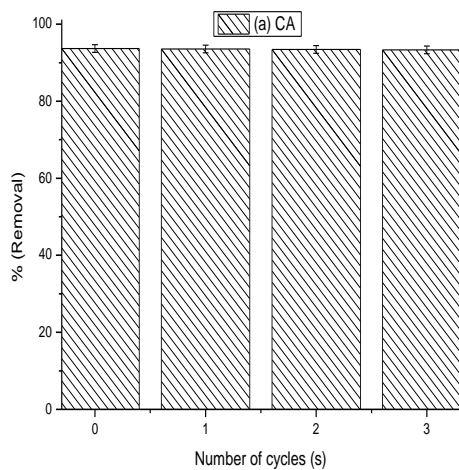
	308.15	-6898.824		
1% N-MWCNTs/3% PVDF-HFP/CA	293.15	-6546.636	133.802	0.780
	298.15	-6838.194		
	303.15	-7148.282		
	308.15	-7318.051		

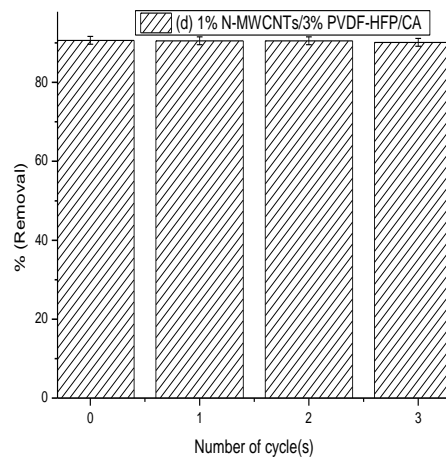
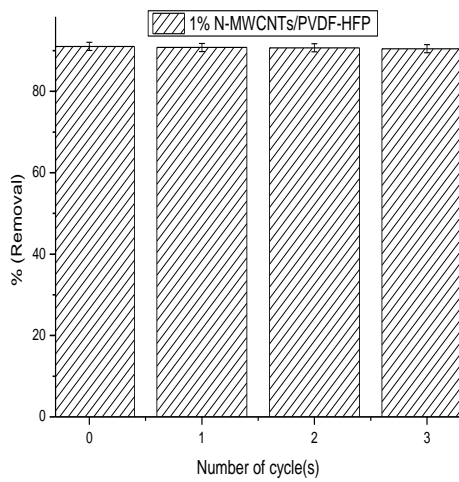
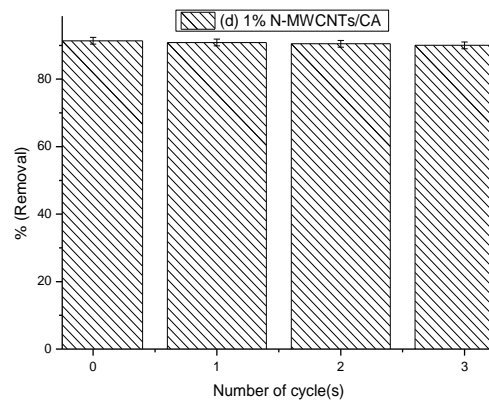
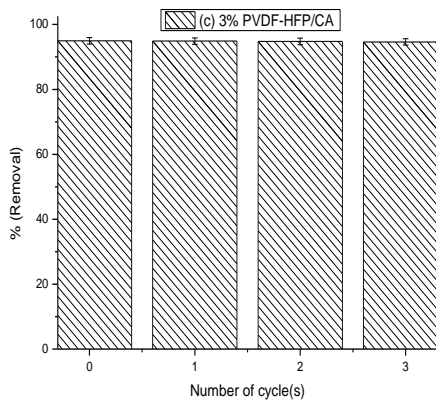


Appendix 6: Effect of counterions on the adsorption of Ca (II) ions onto (a) CA, (b) PVDF-HFP, (c) 3% PVDF-HFP/CA, (d) 1% N-MWCNTs/CA, (e) 1% N-MWCNTs/PVDF-HFP and (f) 1% N-MWCNTs/3% PVDF-HFP/CA composite membranes.



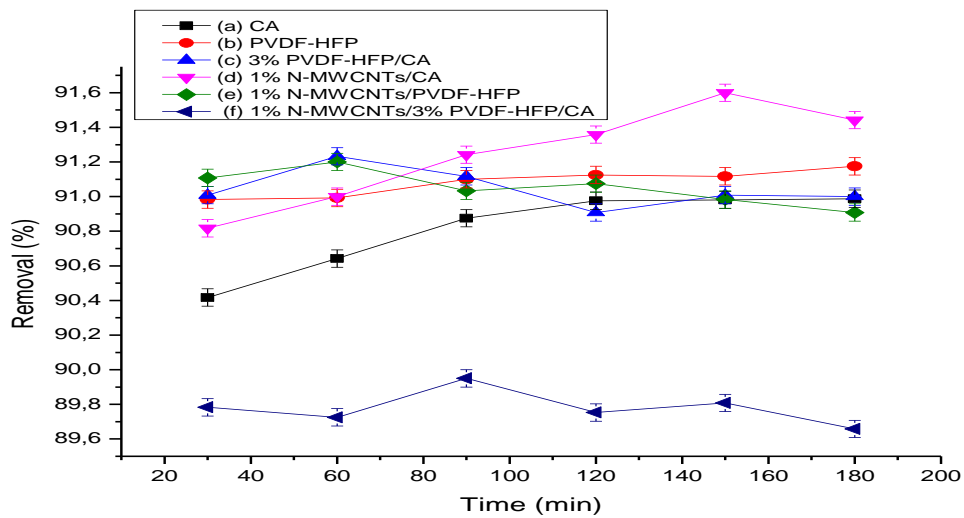
Appendix 7: Effect of the binary system on the adsorption of Ca (II) onto (a) CA, (b) PVDF-HFP, (c) 3% PVDF-HFP/CA, (d) 1% N-MWCNTs/CA, (e) 1% N-MWCNTs/PVDF-HFP and (f) 1% N-MWCNTs/3% PVDF-HFP/CA composite membranes.



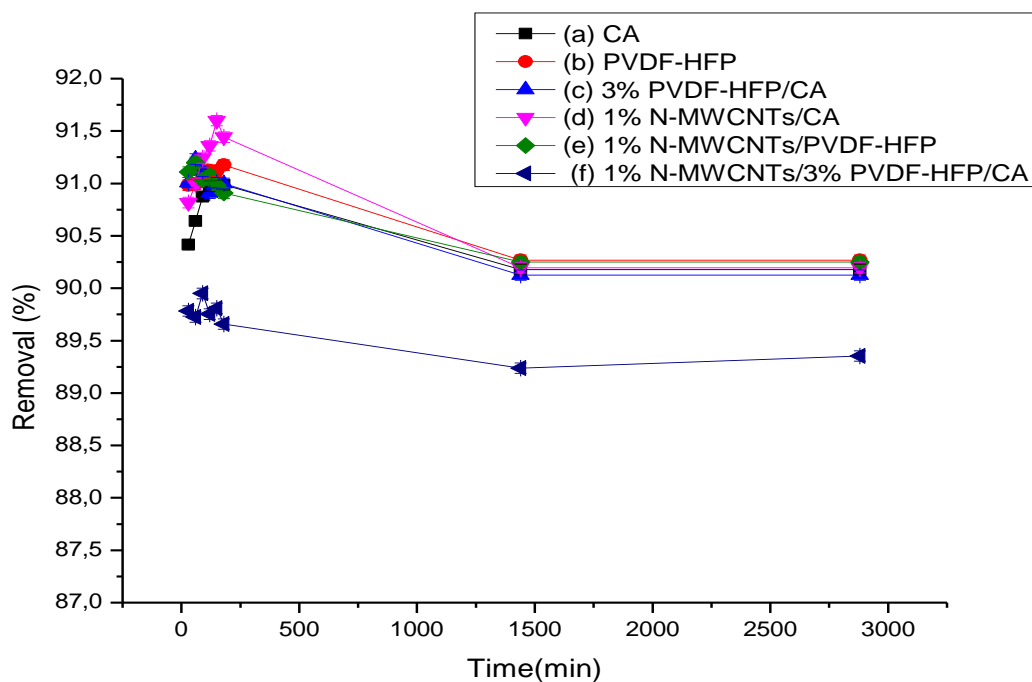


Appendix 8: Effect of recycling of (a) CA, (b) PVDF-HFP, (c) 3% PVDF-HFP/CA, (d) 1% N-MWCNTs/CA, (e) 1% N-MWCNTs/PVDF-HFP, and (f) 1% N-MWCNTs/3% PVDF-HFP/CA composite membranes for the adsorption efficiency of Ca (II) ions.

A

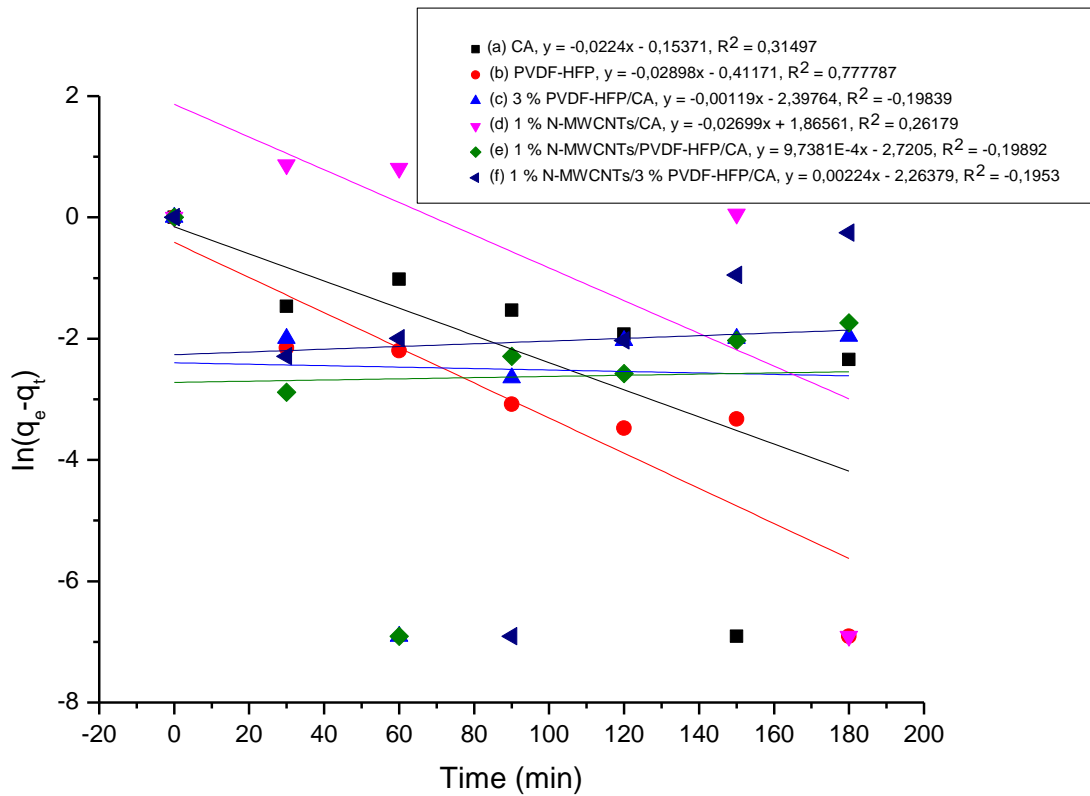


B

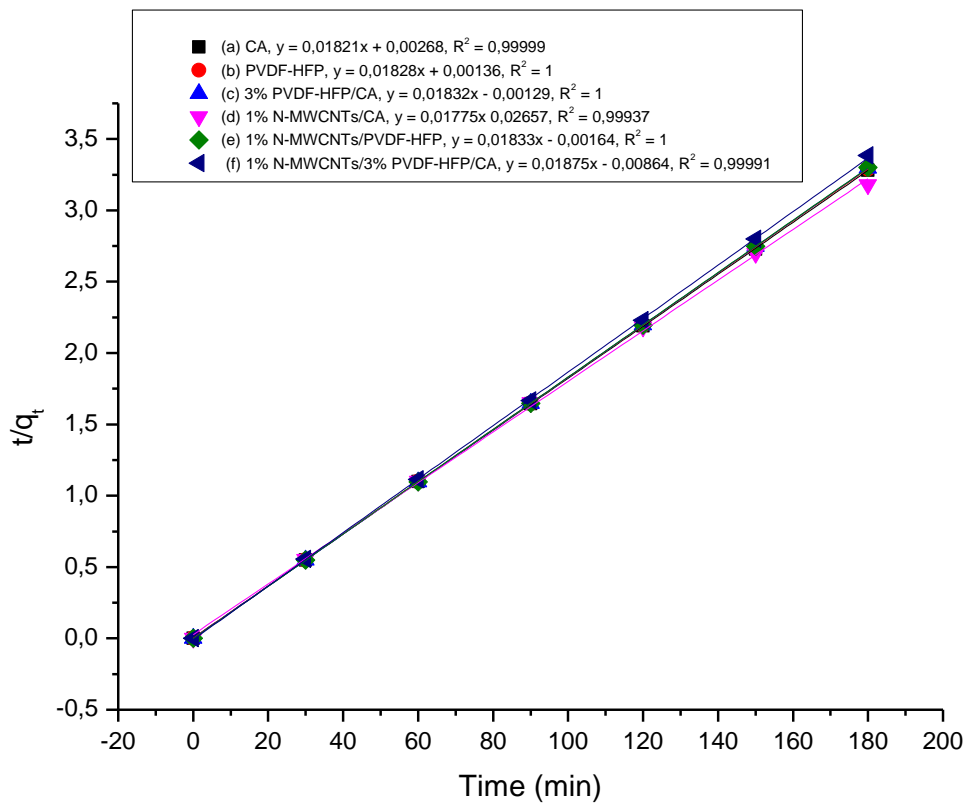


Appendix 9: Effect of contact time A (0 to 180 mins) and B (24 to 48 hours) on adsorption efficiency of Mg (II) ions onto (a) CA, (b) PVDF-HFP, (c) 3% PVDF-HFP/CA, (d) 1% N-MWCNTs/CA, (e) 1% N-MWCNTs/PVDF-HFP and (f) 1% N-MWCNTs/3% PVDF-HFP/CA composite membranes

A



B

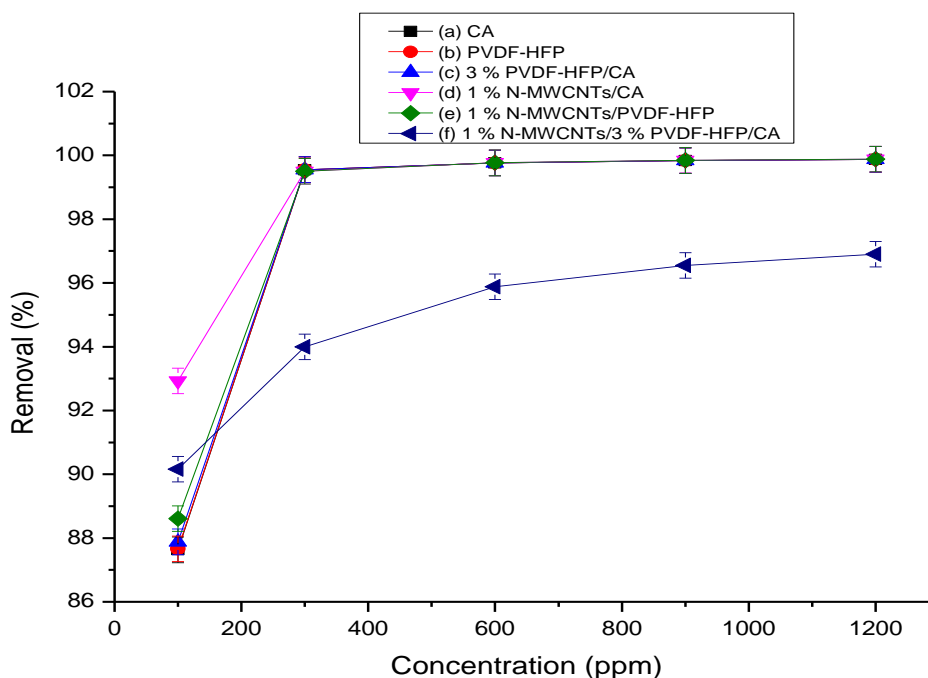


Appendix 10: Pseudo-first order (A) and Pseudo-second order (B) kinetic model for

adsorption of Mg (II) ions on (a) CA, (b) PVDF-HFP, (c) 3% PVDF-HFP/CA, (d) 1% N-MWCNTs/CA, (e) 1% N-MWCNTs/PVDF-HFP and (f) 1% N-MWCNTs/3% PVDF-HFP/CA composite membranes.

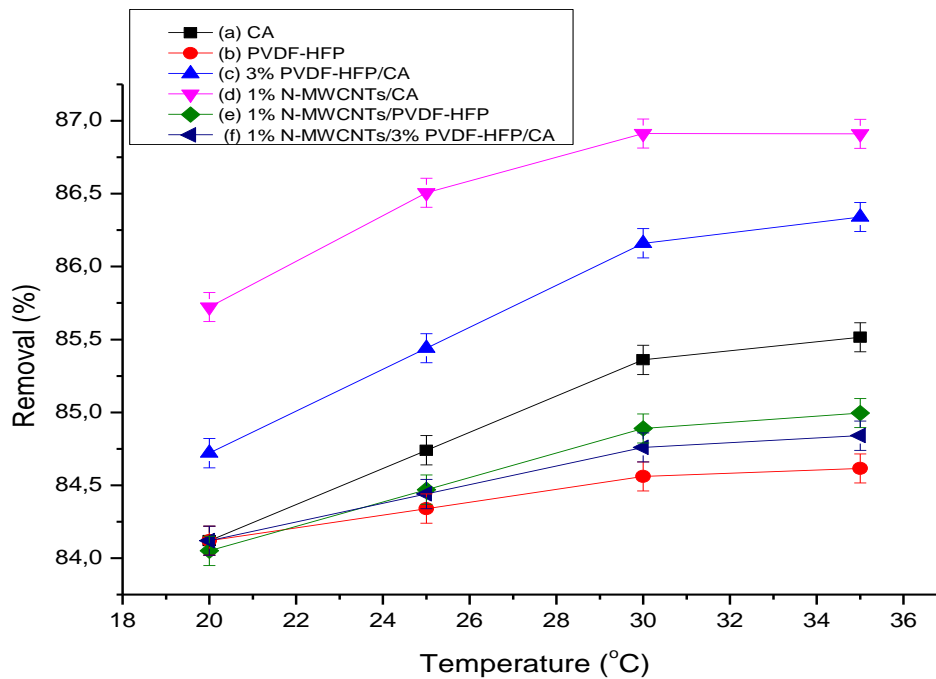
Table 5.3.3: Kinetic parameters for Mg (II) adsorption onto PVDF-HFP based membrane

Membrane	q_e (mg/g)	Pseudo-first order Kinetic model			Pseudo-second order Kinetic model		
		K_1 (min^{-1})	q_e (mg/g)	R^2	K_2 (g/mg.min)	q_e (mg/g)	R^2
CA	54.961	0.02240	0.8575	0.314970	0.1237	54.915	0.99999
PVDF-HFP	54.706	0.02898	0.6625	0.77787	0.2457	54.705	1
3% PVDF-HFP/CA	54.741	0.00119	0.0909	-0.19839	-0.2602	54.585	1
1% N-MWCNTs/CA	56.631	0.02699	6.4598	0.26179	0.0119	56.338	0.99937
1% N-MWCNTs/PVDF-HFP	54.721	-9.7381E-4	0.0658	-0.19892	-0.2049	54.555	1
1% N-MWCNTs/3% PVDF-HFP/CA	53.971	-0.00224	0.1039	-0.19530	-0.04069	53.333	0.99991



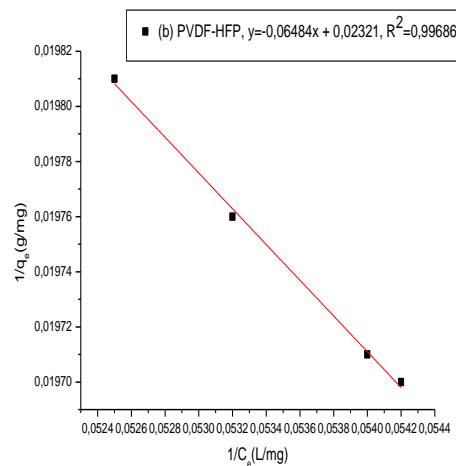
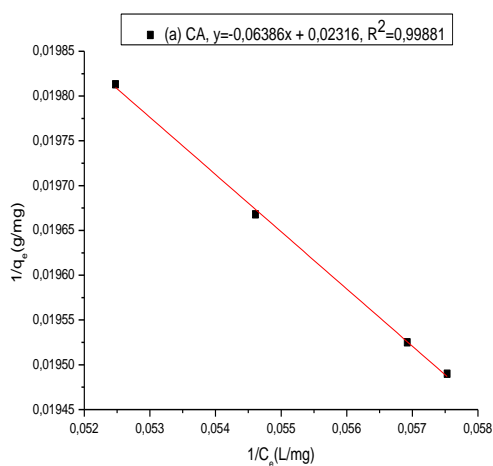
Appendix 11: Effect of initial metal ion concentration on the adsorption efficiency of Ca (II) ions on (a) CA, (b) PVDF-HFP, (c) 3% PVDF-HFP/CA, (d) 1% N-MWCNTs/CA,

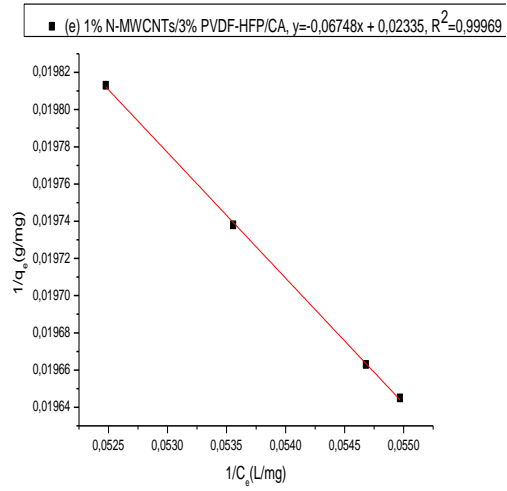
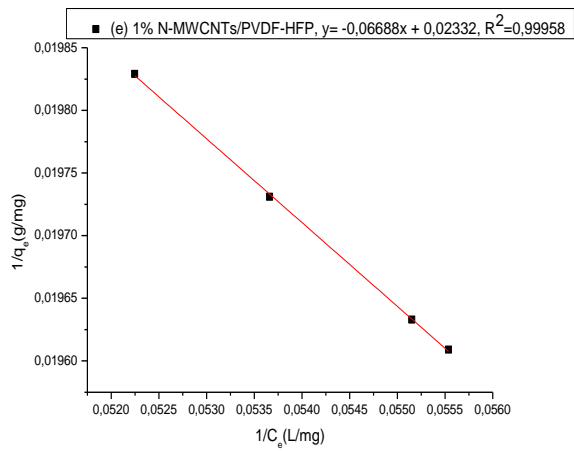
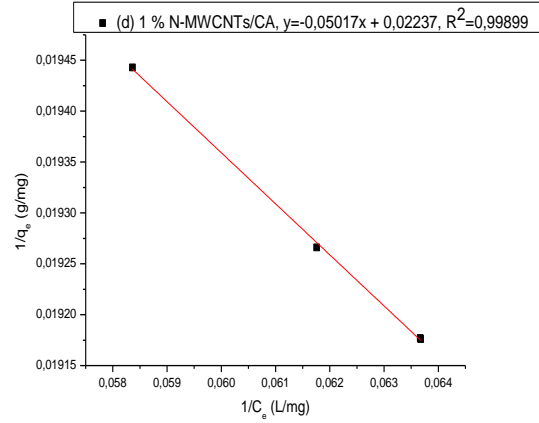
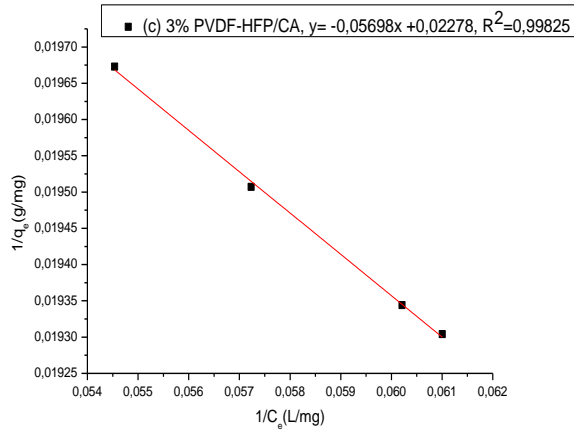
(e) 1% N-MWCNTs/PVDF-HFP and 1% N-MWCNTs/3% PVDF-HFP/CA composite membranes



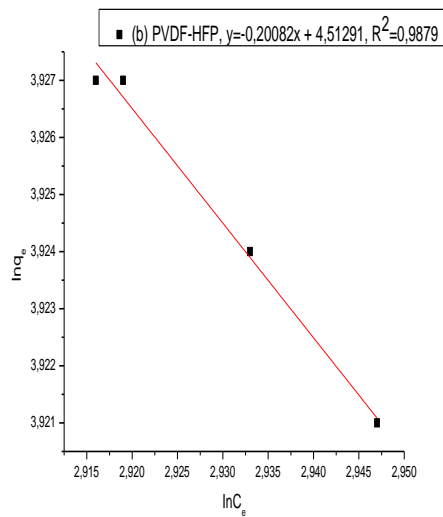
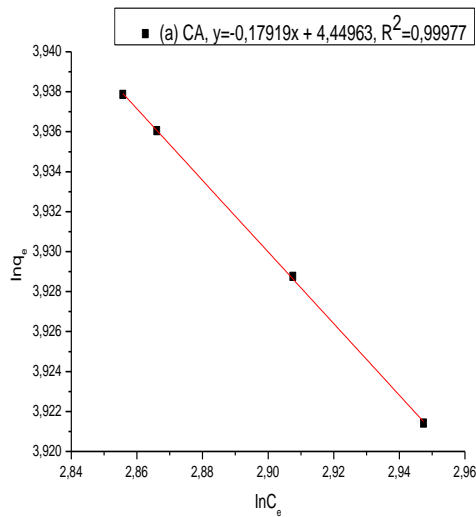
Appendix 12: Effect of temperature on adsorption efficiency of Mg (II) ions on (a) CA, (b) PVDF-HFP, (c) 3% PVDF-HFP/CA, (d) 1% N-MWCNTs/CA, (e) 1% N-MWCNTs/PVDF-HFP and 1% N-MWCNTs/3% PVDF-HFP/CA composite membrane.

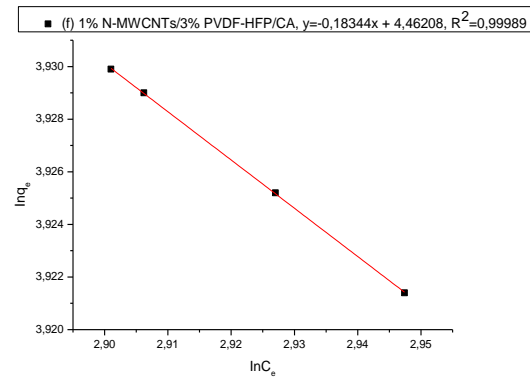
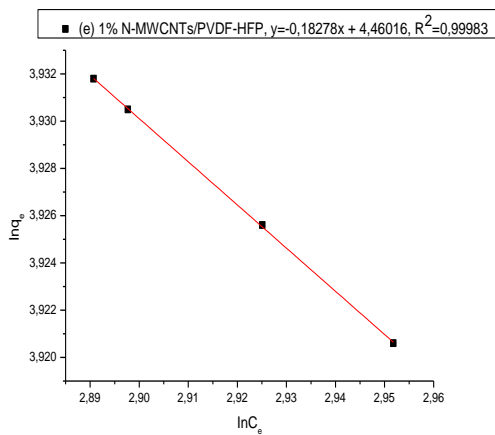
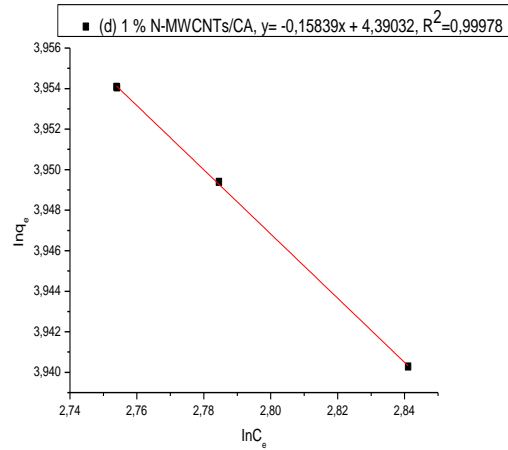
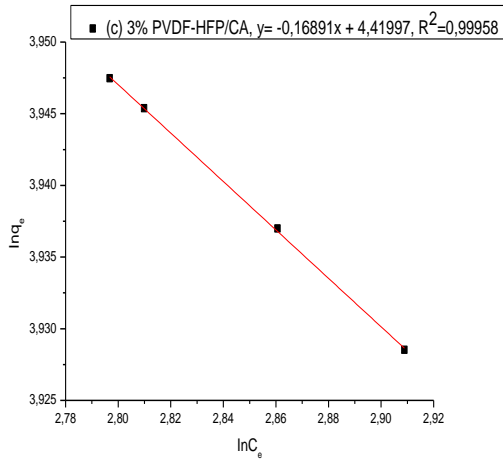
(i) Langmuir isotherm





(ii) Freundlich isotherm



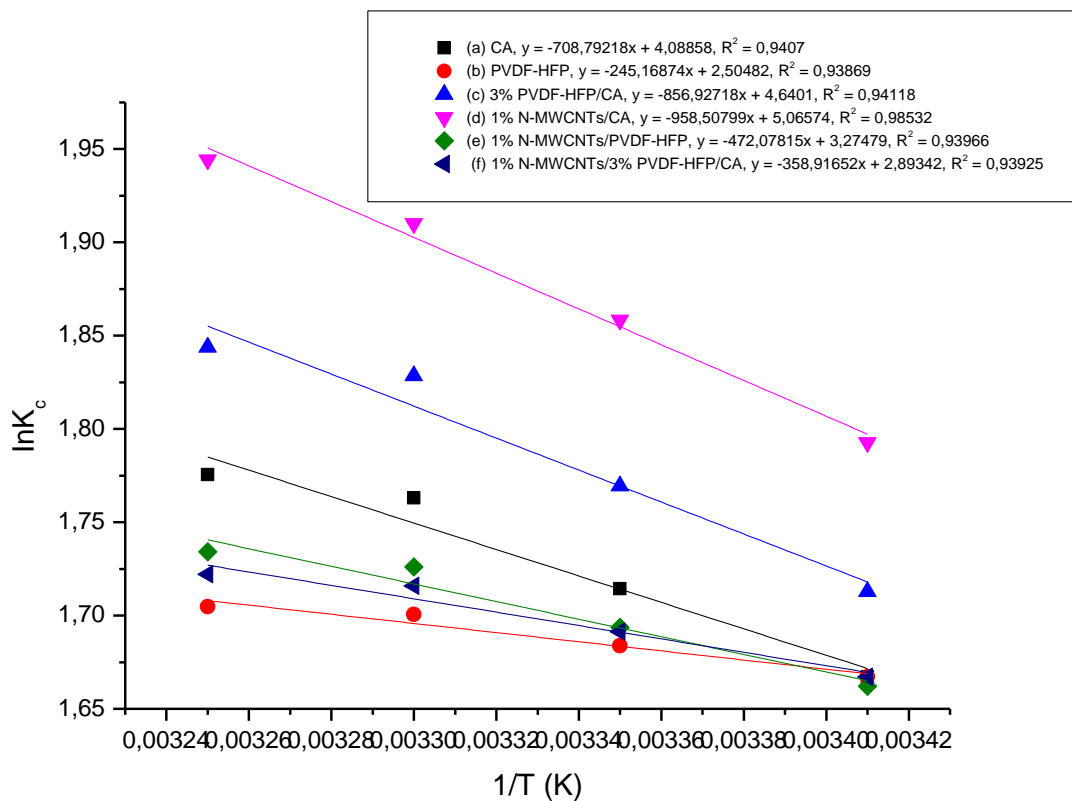


Appendix 13: Effect of the Langmuir and Freundlich isotherm on adsorption efficiency of Mg (II) ions on (a) CA, (b) PVDF-HFP, (c) 3% PVDF-HFP/CA, (d) 1% N-MWCNTs/CA, (e) 1% N-MWCNTs/PVDF-HFP and 1% N-MWCNTs/3% PVDF-HFP/CA composite membrane.

Table 5.3.4: Langmuir and Freundlich isotherm parameters for Mg (II) ions adsorption onto PVDF-HFP composite membranes.

Membrane	q _{max} (mg/g)	Langmuir model			Freundlich model		
		b (L/mg)	R ²	R _L	K _f (mg/g)	n	R ²
CA	43.178	-0.363	0.99881	-0.02350	28159.828	-5.581	0.99977
PVDF-HFP	43.085	-0.358	0.99686	-0.02383	32576.918	-4.980	0.98790
3% PVDF-HFP/CA	43.898	-0.400	0.99825	-0.02128	26300.863	-5.920	0.99958
1% N-MWCNTs/CA	44.703	-0.446	0.99899	-0.01904	24565.183	-6.313	0.99978
1% N-MWCNTs/PVDF-HFP	42.882	-0.349	0.99958	-0.02446	28850.942	-5.471	0.99983

1% N-MWCNTs/3% PVDF-HFP/CA	42.867	-0.346	0.99969	-0.02468	28978.773	-5.451	0.99989
----------------------------	--------	--------	---------	----------	-----------	--------	---------

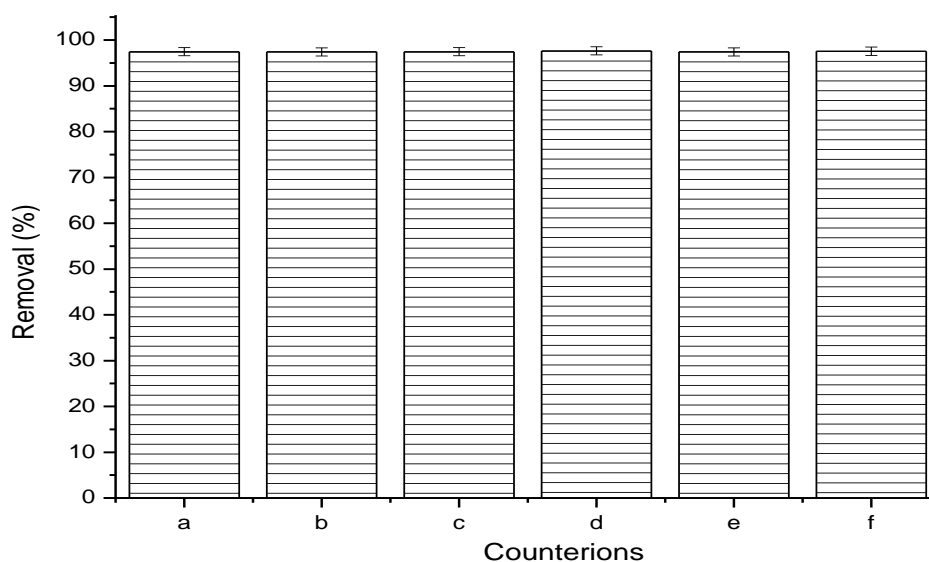


Appendix 14: Thermodynamic parameters of Mg (II) ions onto (a) CA, (b) PVDF-HFP, (c) 3% PVDF-HFP/CA, (d) 1% N-MWCNTs/CA, (e) 1% N-MWCNTs/PVDF-HFP and (f) 1% N-MWCNTs/3% PVDF-HFP/CA composite membranes.

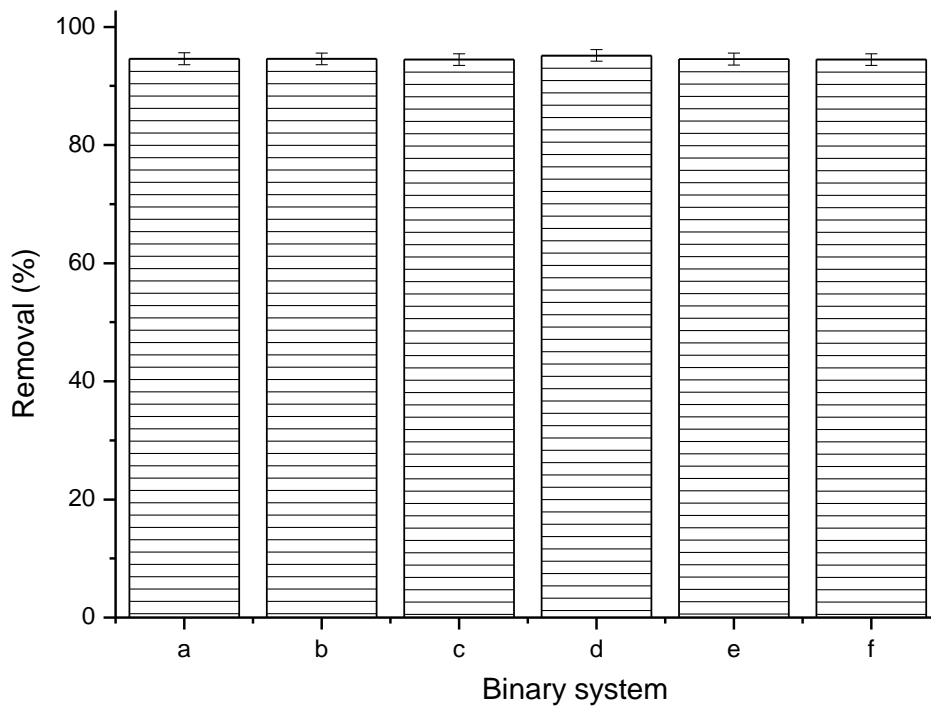
Table 5.3.5: Thermodynamic parameters for Mg (II) (120 ppm) adsorption by PVDF-HFP composite membranes

Membrane	Temperature (K)	Thermodynamic parameters		
		ΔG (KJ/mol)	ΔH (KJ/mol)	ΔS (J.mol/K)
CA	293.15	-4063.342	85.253	0.492
	298.15	-4249.570		
	303.15	-4443.749		
	308.15	-4548.959		
PVDF-HFP	293.15	-4063.342	29.489	0.301
	298.15	-4173.703		
	303.15	-4285.921		
	308.15	-4367.419		
3% PVDF-HFP/CA	293.15	-4174.537	103.070	0.558

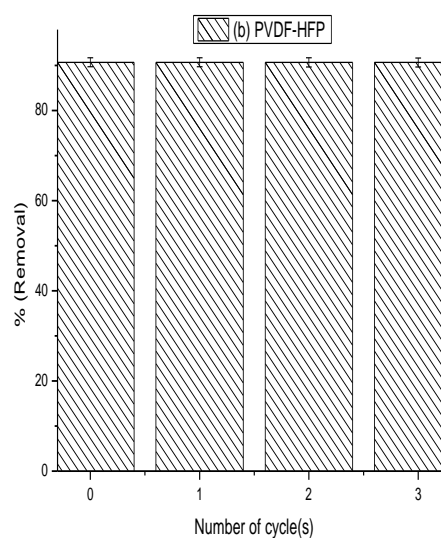
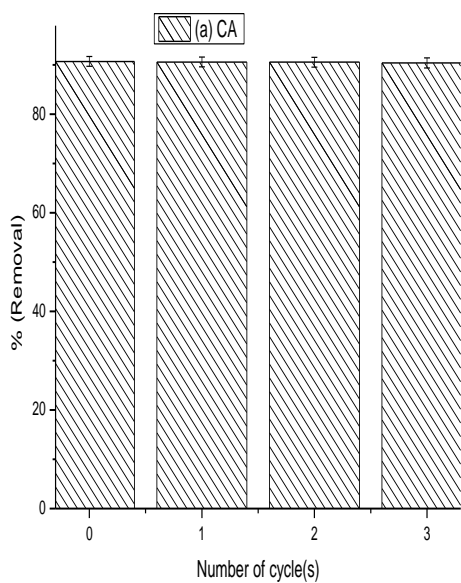
	298.15	-4386.360		
	303.15	-4608.892		
	308.15	-4723.794		
1% N-MWCNTs/CA	293.15	-4369.216	115.288	0.609
	298.15	-4606.399		
	303.15	-4813.932		
	308.15	-4980.983		
1% N-MWCNTs/PVDF-HFP	293.15	-4050.594	56.781	0.394
	298.15	-4198.185		
	303.15	-4350.190		
	308.15	-4442.972		
1% N-MWCNTs/3% PVDF-HFP/CA	293.15	-4063.342	43.170	0.348
	298.15	-4192.342		
	303.15	-4324.736		
	308.15	-4411.967		

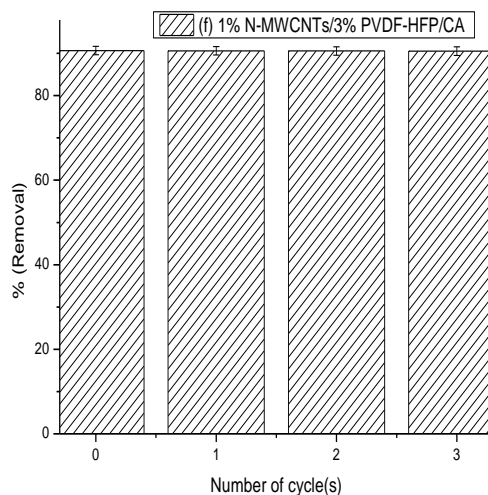
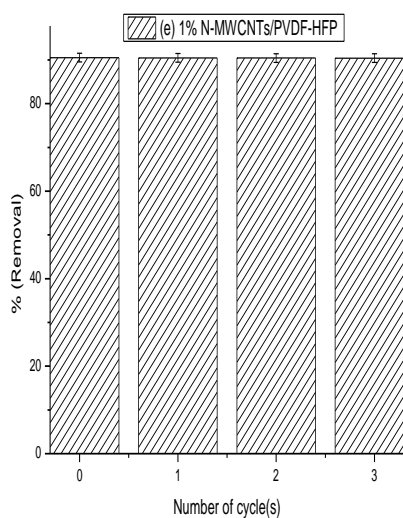
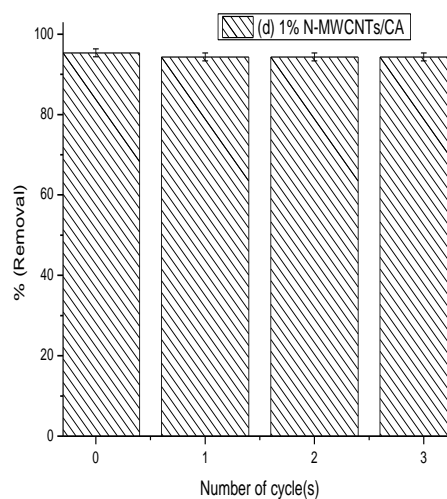
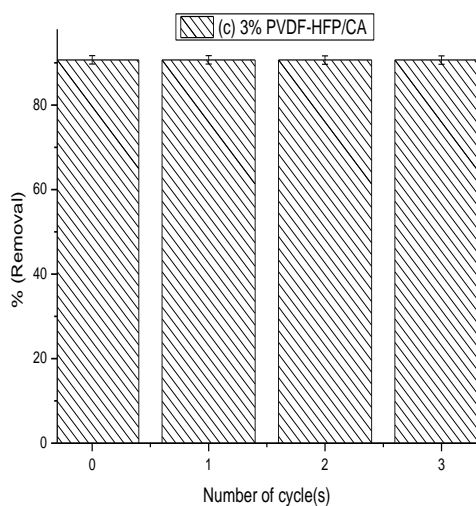


Appendix 15: Effect of counterions on the adsorption of Mg (II) by (a) CA, (b) PVDF-HFP, (c) 3% PVDF-HFP/CA, (d) 1% N-MWCNTs/CA, (e) 1% N-MWCNTs/PVDF-HFP and (f) 1% N-MWCNTs/3% PVDF-HFP/CA composite membranes



Appendix 16: Effect of the binary system on the adsorption of Mg (II) by (a) CA, (b) PVDF-HFP, (c) 3% PVDF-HFP/CA, (d) 1% N-MWCNTs/CA, (e) 1% N-MWCNTs/PVDF-HFP and (f) 1% N-MWCNTs/3% PVDF-HFP/CA composite membranes





Appendix 17: Effect of reusability on the adsorption of Mg (II) ions onto (a) CA, (b) PVDF-HFP, (c) 3% PVDF-HFP/CA, (d) 1% N-MWCNTs/CA, (e) 1% N-MWCNTs/PVDF-HFP and (f) 1% N-MWCNTs/3% PVDF-HFP/CA composite membranes.